CONTROLLING CAPILLARY PRESSURE IN CONCRETE TO PREVENT PLASTIC SHRINKAGE CRACKING

R.C. DEYSEL

Controlling cappillary pressure in concrete to prevent plastic shrinkage cracking

Renier Christiaan Deysel

A dissertation submitted in partial fulfilment of the requirements for the degree of

MASTER OF ENGINEERING (STRUCTURAL ENGINEERING)

in the

FACULTY OF ENGINEERING, BUILT-ENVIRONMENT AND INFORMATION TECHNOLOGY

UNIVERSITY OF PRETORIA

MAY 2022

DISSERTATION SUMMARY

CONTROLLING CAPILLARY PRESSURE IN CONCRETE TO PREVENT PLASTIC SHRINKAGE CRACKING

R.C. DEYSEL

Supervisor: Boshoff, William P
Co-Supervisor: Smit, Martha S
Department: Civil Engineering
University: University of Pretoria
Degree: Master of Engineering (Structural Engineering)

Plastic shrinkage cracking occurs in concrete members with large exposed surface areas, such as concrete pavements, bridge decks and floor slabs. Current research has shown that a notable increase in plastic shrinkage was observed in the engineering practice, leading to considerably more cracking problems than in the past. Plastic shrinkage cracking occurs when the plastic shrinkage of fresh concrete is restrained, leading to tensile stresses, which result in cracks when the tensile strength is exceeded. Plastic shrinkage is caused by negative capillary pressure build-up in fresh concrete. Controlling the negative capillary pressure build-up makes it possible to reduce the risk of plastic shrinkage cracking.

The aim of this study was to develop a model that uses live in-situ capillary pressure measurements in fresh concrete to control the capillary pressure build-up to prevent plastic shrinkage cracking at any evaporation rate. A model was developed that calculates a critical pressure limit for when an action is needed to prevent plastic shrinkage cracking. The model uses the negative capillary pressure build-up area between two crucial time points in plastic shrinkage to determine this limit.

The proposed model was tested and verified in two phases. The testing and verification of the model were conducted on a low bleed concrete having a water/cement ratio of 0.5 and a self-compacting concrete with a water/cement ratio of 0.4. Tensiometers were used to measure the capillary pressure build-up in concrete. The first phase consisted of determining the parameters required for the model.

The second phase used the determined parameters to test the model with the two concrete mixtures at various evaporation rates.

The results showed that the model could determine a critical pressure limit relevant to the concrete and evaporation rate. The proposed model proved to be a valuable tool in controlling the capillary pressure and preventing plastic shrinkage cracking in low bleed and self-compacting concrete.

DECLARATION

I, the undersigned hereby declare that:

- I understand what plagiarism is and I am aware of the University's policy in this regard;
- The work contained in this thesis is my own original work;
- I did not refer to work of current or previous students, lecture notes, handbooks or any other study material without proper referencing;
- Where other people's work has been used this has been properly acknowledged and referenced;
- I have not allowed anyone to copy any part of my thesis;
- I have not previously in its entirety or in part submitted this thesis at any university for a degree.

DISCLAIMER:

The work presented in this report is that of the student alone. Students were encouraged to take ownership of their projects and to develop and execute their experiments with limited guidance and assistance. The content of the research does not necessarily represent the views of the supervisor or any staff member of the University of Pretoria, Department of Civil Engineering. The supervisor did not read or edit the final report and is not responsible for any technical inaccuracies, statements or errors. The conclusions and recommendations given in the report are also not necessarily that of the supervisor, sponsors or companies involved in the research.

Renier Christiaan Deysel

15062890

26 May 2022

ACKNOWLEDGEMENTS

I would like to express my gratitude to the following organisations and persons who made this dissertation possible:

a) My Creator for blessing me with the talent, opportunity and ability to conduct this research.

b) The University of Pretoria for the use of the laboratory facilities at Engineering 4.0 and the Centrifuge laboratory during the research.

c) Professor W.P. Boshoff, my supervisor, and Doctor M.S. Smit, my co-supervisor, for their guidance and support throughout the study.

d) The following persons are gratefully acknowledged for their assistance during the course of the study:

   i) Mr A. Broekman

   ii) Mr D. Mostert

   iii) Mr J. Botha

   iv) Mr J. Scholtz

   v) Mr J. Vermaak

   vi) Professor S.W. Jacobsz

e) My family and friends for their encouragement and unconditional support during the study.

f) Lastly, our three dogs for always being happy to see me.

TABLE OF CONTENTS

LIST OF TABLES

LIST OF FIGURES

LIST OF ACRONYMS

Acronym	Description
ACC	Accelerator
ACI	American Concrete Institute
AEA	Air-Entraining Agent
ASTM	American Standard Testing Methods
CP	Capillary Pressure
MCC	Mobile Climate Chamber
EN	European Standard
ERL-x	Evaporation rate x for the Low Bleed Concrete (x = 1 to 6)
ERS-y	Evaporation rate y for the SCC (y = 1 and 2)
h	Hour
N	Newton
m	Meter
min	Minutes
Pa	Pascal
PS	Plastic Shrinkage
PSD	Particle Size Distribution
REF	Reference Concrete
SANS	South African National Standards
SCC	Self-Compacting Concrete
SD	Standard Deviation
SP	Superplasticisers
SRA	Shrinkage-Reducing Admixture
STB	Stabiliser
VMC	Volumetric Moisture Content
w/c	Water/Cement Ratio

LIST OF SYMBOLS

Symbol	Description	Unit
A_C	Area of the negative CP build-up curve with applied boundary	kPa.min
A_{NC}	Area of the no crack negative CP build-up curve	kPa.min
B	Total bleeding from the unit concrete surface	g
C_s	Severity of PS cracking	kg.h/m^2
D_{av}	Average diameter of the aggregate	cm
E	Total evaporation from the unit concrete surface	g
ER	Evaporation rate	kg/m^2/h
$f(t)$	The function of the no crack negative CP build-up curve	kPa
$g(t)$	The function of the negative CP build-up curve of the sample concrete	kPa
P	Negative CP	Pa
PC	PS cracking area	cm^2/m
P_{iset}	The negative CP value at the initial setting time of the concrete	kPa
P_B	The negative CP value of the critical pressure limit	kPa
r	Radius of the meniscus	m
R	Restraining factor	%
RH	Relative humidity	%
T_a	Air temperature	°C
T_c	Concrete (water surface) temperature	°C
t_{DC}	Drying time of the sample curve	min
t_{DNC}	Drying time of the no crack negative CP build-up curve	min
t_{iset}	Initial setting time	min or h
t_B	Time correlating to the critical pressure limit value	min
T_{RC}	The Trapezoidal rule estimate for the area of $g(t)$	kPa.min
T_{RNC}	The Trapezoidal rule estimate for the area of $f(t)$	kPa.min
V	Wind velocity	km/h
V_p	Paste volume	m^3/m^3
w_c	The w/c ratio	-
W_{bl}	Total bleed water	kg/m^2
σ_t	Surface tension	N/m

1 INTRODUCTION

1.1 BACKGROUND

Plastic shrinkage cracking is a problem commonly experienced in concrete members with large exposed surface areas, such as concrete pavements, bridge decks and floor slabs (Qi, 2003; Kwak and Ha, 2006). It is an early-age characteristic of concrete, occurring within the first 3 to 8 hours after casting. Plastic shrinkage cracking occurs when fresh concrete is restrained from deforming, leading to the formation of tensile stresses in the concrete and causing cracking. These tensile stresses in concrete result from the negative capillary pressure that develops in concrete. These plastic shrinkage cracks tend to be more severe when the concrete members have large surface areas or are exposed to harsh climatic conditions. Once cracks occur, there are several long-lasting durability challenges for the future of the life of the concrete structure, such as steel reinforcement corrosion and carbonation. (Qi, 2003; Otieno *et al*., 2010).

The negative capillary pressure build-up in concrete is one of the main driving forces for plastic shrinkage (Wittmann, 1976; Slowik *et al*., 2008; Slowik *et al*., 2014). Investigating the capillary pressure behaviour in fresh concrete can help improve the understanding of plastic shrinkage in concrete. Capillary pressure in fresh concrete is usually measured using electrical pressure sensors or capillary pressure sensors, but in this research, tensiometers are used for capillary pressure measurement. A tensiometer is a device used on-site to measure the direct negative pressure (suction) in the soil with the ability to measure high negative pressure values before cavitation. (Raviv and Lieth, 2008; Toll *et al*., 2013).

1.2 PROBLEM STATEMENT

Plastic shrinkage cracking in concrete structures can be a significant concern in the construction industry because these cracks compromise aesthetics, serviceability, and durability (Dao *et al*., 2010). Plastic shrinkage cracking is a common early-age problem in the construction industry worldwide, which occurs when drying fresh concrete is restrained from deforming in the plastic state. Plastic shrinkage cracks are more severe on concrete structures with large surface areas (for instance, highway pavement, bridges, decks and slabs) or when the concrete is exposed to harsh drying climatic conditions, typical of the South African climate.

In the current research, a notable increase in plastic shrinkage was observed in the engineering practice (when high strength concrete was used), leading to considerably more cracking problems than in the past (Huang *et al*., 2019). Once these cracks occur, harmful chemicals and water can easily penetrate the concrete and corrode the steel reinforcement in the concrete

structure, which can cause the structure to fail. Therefore, these cracks can pose several long-lasting durability challenges for the future of the service life of the concrete structure (Qi, 2003).

The purpose of this research is to utilise the capillary pressure behaviour of concrete to develop an empirical model. The model will determine a critical pressure limit for when an action is needed to prevent plastic shrinkage cracking. Preventing these cracks will improve the service life and reduce additional construction and maintenance costs.

1.3 OBJECTIVES OF THE STUDY

The research aims to develop a model that uses live in-situ capillary pressure measurements in fresh concrete to control the capillary pressure build-up to prevent plastic shrinkage cracking at any evaporation rate. Two hypotheses are made for this study:

1. A negative capillary pressure build-up in concrete over time exist, where no plastic shrinkage cracks will form.

2. Plastic shrinkage cracks can be prevented by maintaining a similar or lower pressure-time area as the negative capillary pressure build-up where no crack will form.

The hypotheses can be rejected or verified by achieving the following objectives:

- Provide a fundamental understanding of plastic shrinkage cracking and how the negative capillary pressure build-up and critical pressure limit influence the plastic shrinkage cracking in fresh concrete,
- Shed light on determining the critical pressure limit in fresh concrete mixtures,
- Determining whether tensiometers can measure the negative capillary pressure in fresh concrete and if tensiometers can be used to minimise or prevent plastic shrinkage cracks from forming by monitoring the negative capillary pressure behaviour in fresh concrete,
- Present an empirical model that helps prevent plastic shrinkage cracking in fresh concrete for different concrete mix designs on-site or in a laboratory.

1.4 SCOPE OF THE STUDY

The research focuses on the capillary pressure mechanism in fresh concrete and how this mechanism can be controlled to help prevent plastic shrinkage cracks from forming. The research was limited to the following:

- A low bleeding conventional concrete mix with a water/cement ratio of 0.5 for testing the model and a self-compacting concrete mix with a water/cement ratio of 0.4 for the verification of the empirical model.
- Concrete specimens were exposed to various evaporation rates that could be created in the different climate rooms available at the time.

1.5 METHODOLOGY

The following methodology was utilised to achieve the objectives of the study.

- A comprehensive literature review on plastic shrinkage cracking was done to understand this phenomenon occurring in concrete. The literature involved investigating the capillary pressure mechanisms, factors affecting plastic shrinkage cracking, and current methods and models used for preventing these cracks.
- The reviewed literature was used to develop an empirical model that shows when specific actions are to be taken to reduce the negative capillary pressure and prevent plastic shrinkage cracking.
- In preparation for the experimental work, an additional climate chamber was designed and built. The climate chamber had to control the air temperature, relative humidity, and wind speed to such an extent that it could simulate any harsh climatic environment possible in South Africa. Tensiometers were also built to measure the capillary pressure in fresh concrete.
- A procedure for the experimental work was established to verify the proposed model. The experimental work consisted of two phases:
    - In the first phase, the plastic shrinkage cracking characteristics of a low bleed and self-compacting concrete mixture in several evaporation rates was investigated. The characteristics were investigated to obtain the parameters required for the proposed model.
    - The second phase consisted of testing the proposed model with the low bleed concrete at various evaporation rates. The model was also tested with self-compacting concrete at several evaporation rates to verify the model.
- The results from the experimental work were analysed to evaluate the performance of the proposed model and identify any limitations. The model was then calibrated accordingly to provide an empirical model that helps engineers prevent plastic shrinkage cracking in fresh concrete.

1.6 ORGANISATION OF THE REPORT

The dissertation consists of the following chapters and appendices:

- Chapter 1 serves as an introduction to the report providing background and outlining the objectives and scope of the research.
- Chapter 2 is a comprehensive review of the literature on plastic shrinkage cracking to provide a fundamental understanding of plastic shrinkage cracking in fresh concrete.
- Chapter 3 shows the development of the empirical model from the literature.
- Chapter 4 provides an in-depth description of the experimental work done throughout the study.
- Chapter 5 provides the design process and details of the mobile climate chamber used during the experimental work.
- Chapters 6 & 7 present the results obtained during the experimental work from the low bleed concrete (Chapter 6) and self-compacting concrete (Chapter 7) and a detailed discussion of the results.
- Chapter 8 provides the model verification results and the limitations and calibration of the model.
- Chapter 9 provides the conclusions drawn from the results and recommendations for future research.
- Chapter 10 contains the list of references used throughout the dissertation.
- Appendices A to D consists of the additional information referenced throughout the study.

2 LITERATURE REVIEW

2.1 INTRODUCTION

This chapter presents a comprehensive review of the phenomenon in fresh concrete known as Plastic Shrinkage (PS) and PS cracking. The literature review aim to establish how the Capillary Pressure (CP) mechanism contributes to the PS cracking and the current state of methods and empirical models used to prevent PS cracking in concrete.

The literature review starts by defining PS and PS cracking in fresh concrete—followed by an overview of the factors that influence PS and PS cracking. The factors are grouped under the movement of mixture constituents in fresh concrete and the hardening of fresh concrete. Subsequently, the mechanisms causing PS cracking are addressed. This section is followed by a review of PS crack prevention measures and the recent literature on methods and models used to prevent PS cracking. Previous CP sensors and tensiometers are then reviewed and discussed. Lastly, the chapter is concluded by summarising the literature findings.

2.2 PLASTIC SHRINKAGE CRACKING

Concrete is in a plastic state before it has hardened and set. Concrete in a plastic state is referred to as fresh concrete. PS occur in fresh concrete. Shrinkage in fresh concrete results from water loss from the concrete through bleeding, surface evaporation, and water consumption through cement hydration (Neville, 1995; Lamond and Pielert, 2006). The amount of PS in fresh concrete is mainly controlled by the bleeding and surface evaporation of the water in the concrete. When the cumulative amount of evaporation exceeds the cumulative amount of bleeding of the concrete, PS occurs (Lamond and Pielert, 2006; Soutsos and Domone, 2017).

As the cumulative evaporation exceeds the bleeding of the concrete, tensile strains occur near the surface of the concrete. If the concrete is restrained, tensile stresses are induced. When fresh concrete has not developed enough strength to resist these tensile stresses, PS cracks can occur, as illustrated in Figure 2-1 (Lamond and Pielert, 2006; Soutsos and Domone, 2017). The strength to resist the tensile stresses is not covered by the hydration of the cement particles in the concrete but due to the CP and internal cohesion forces between the particles. The figure demonstrates how bleed water moves to the surface and evaporates. It also shows how the tensile strains act and PS cracks form in fresh concrete. The severity of these PS cracks increases when the concrete is exposed to elevated temperature and wind, leading to higher evaporation rates (Boshoff and Combrinck, 2013; Kayondo *et al.*, 2019). The PS cracking severity refers to how extreme the condition of the crack is.

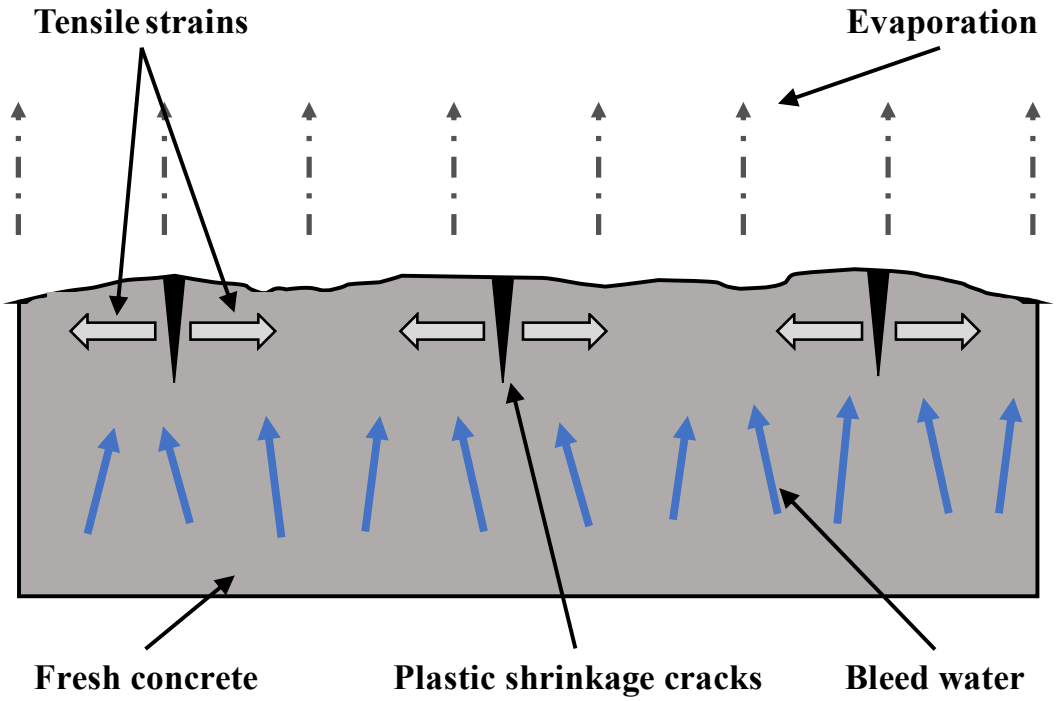

Figure 2-1: PS cracking formation in fresh concrete adapted from Soutsos and Domone (2017)

PS cracks can occur in three distinct patterns in reinforced and unreinforced concrete namely, diagonal, mapped or parallel. These cracks can have widths of up to 3 mm wide and lengths between 50 mm and 3 m. Depending on climatic conditions, cracks can reach a tampered depth of between 20 and 50 mm. In some cases, these cracks can be aggravated even further by dry shrinkage and extend these cracks through the entire depth of the slabs (Uno, 1998; Lamond and Pielert, 2006).

The diagonal crack pattern appears at approximately 45 ° in the direction in which the concrete is cast. These cracks are parallel to each other, and the distance between the cracks can be as large as 1 to 2 m. PS cracks can randomly form, known as a mapped crack pattern (Lamond and Pielert, 2006). The last crack pattern is the parallel crack pattern, which forms parallel to the top reinforcement in the concrete. Figure 2-2 a) and b) show two of the three types of PS cracking (not scaled).

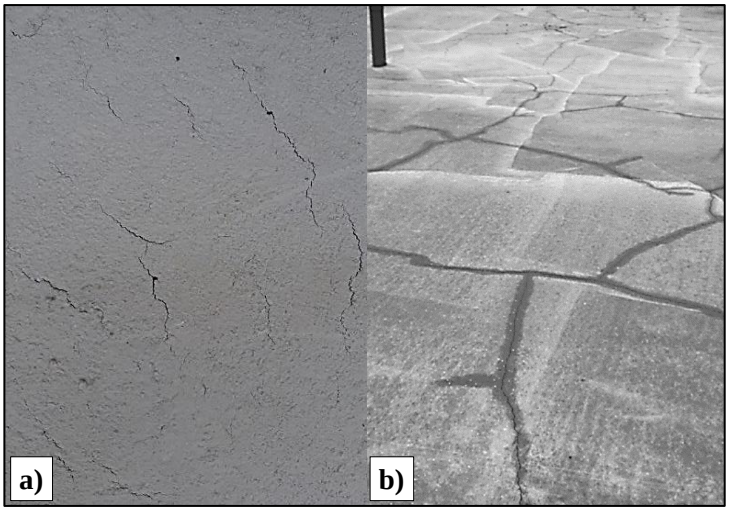

Figure 2-2: a) Diagonal and b) Mapped (Slowik *et al.*, 2008) PS cracking pattern

For the purpose of this discussion, the factors influencing PS cracking are discussed in two sections. Bleeding, evaporation, drying time and plastic settlement are discussed under "movement of mixture constituents in fresh concrete", and initial and final set are discussed under "hardening of fresh concrete".

2.3 MOVEMENT OF MIXTURE CONSTITUENTS IN FRESH CONCRETE

PS cracking is influenced by water movement in and from fresh concrete. Bleeding and evaporation are the phenomena that drive the movement of water from concrete. Drying time is when the cumulative amount of bleed water is equal to the cumulative amount of evaporated water, and the surface of the fresh concrete starts to dry. Plastic settlement occurs due to bleeding and particle settlement and adds to the volume reduction in fresh concrete.

2.3.1 Bleeding

Bleeding and segregation in concrete are early-age mechanisms that occur after casting fresh concrete. Bleeding is the upward migration of the mix-water to the surface of the fresh concrete. This migration occurs because water has the lowest specific gravity of all the constituents in the concrete mixture. While water moves upwards, the solid particles settle downwards. The downward settlement of the solid particles in concrete is known as segregation. The particle settlement will continue until the concrete is viscous(stiffen) enough to restrict the downwards settlement induced by gravity or when the particles interlock (Soutsos and Domone, 2017).

Figure 2-3 illustrates how bleeding and segregation in fresh concrete occur. The figure shows the upwards migration of water as well as the settlement of the solid particles (cement and aggregate). The figure also illustrates the two problems that arise from bleeding in concrete. The formation of a surface laitance and water-rich pockets in the concrete. A surface laitance

forms when bleed water migrates upwards and enriches the layer below the top surface of the concrete with water. The upward migration of the bleed water can also cause some of the water to become trapped under solid aggregate particles. Resulting in water-rich pockets forming below the solid particles. When the concrete absorbs the water in these pockets, air voids are left. These voids cause an enhanced local weakening of the interface zone between the paste and aggregate and reduce the strength of the concrete (Soutsos and Domone, 2017).

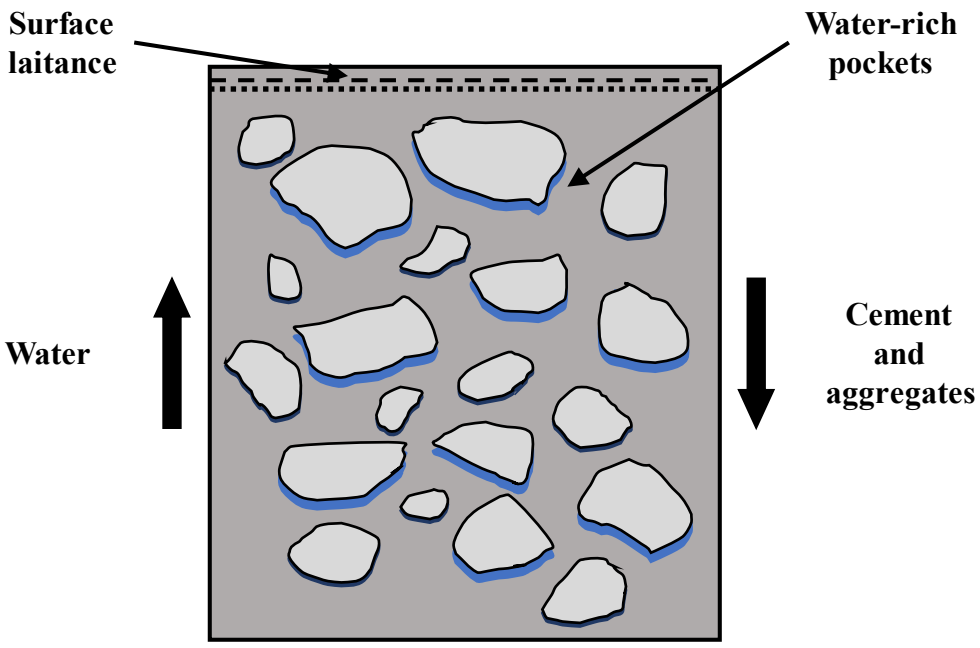

Figure 2-3: Bleeding and segregation in freshly cast concrete adapted from Soutsos and Domone (2017)

Bleeding occurs during the dormant period, around an hour (in conventional concrete without admixtures) when the cementitious material has little to no reaction (Lamond and Pielert, 2006). All types of concrete mixtures bleed to an extent. In some cases, the bleeding for some concrete mixtures might not be visible to the naked eye (Soutsos and Domone, 2017). In addition, bleeding will not be visible when the bleed water is continuously evaporated in harsh climatic conditions.

The accumulation of bleed water at the surface occurs through two types of bleeding such as normal bleeding or channel bleeding. Normal bleeding is a slow, uniform seepage over the entire surface of the concrete. In comparison, channel bleeding is bleeding through localised channels transporting the water to the surface, which sometimes transports fine particles to the surface of the concrete. Channel bleeding typically occurs in concrete mixtures with high water

content, low cement content or mixtures with high bleeding properties (Lamond and Pielert, 2006).

Figure 2-4 illustrates the bleeding process from the moment the cement paste was placed and the setting of the paste. The process is simplified by the following three zones known as the clear water in the surface zone, the zone of constant water content, and the compression zone. The clear water surface zone is the zone where clear water forms at the top of the concrete surface. The constant water zone is where the water/cement (w/c) ratio and the density remain constant, although some of the water moves through this zone. The compressive zone is where the pastes stiffen and can be seen as a transition zone. As the paste stiffens, the w/c ratio is reduced, and the solid particles represent a lower volume than the initial volume cast. The stiffening continues until the paste stabilises as the bleeding and settling stops (Lamond and Pielert, 2006).

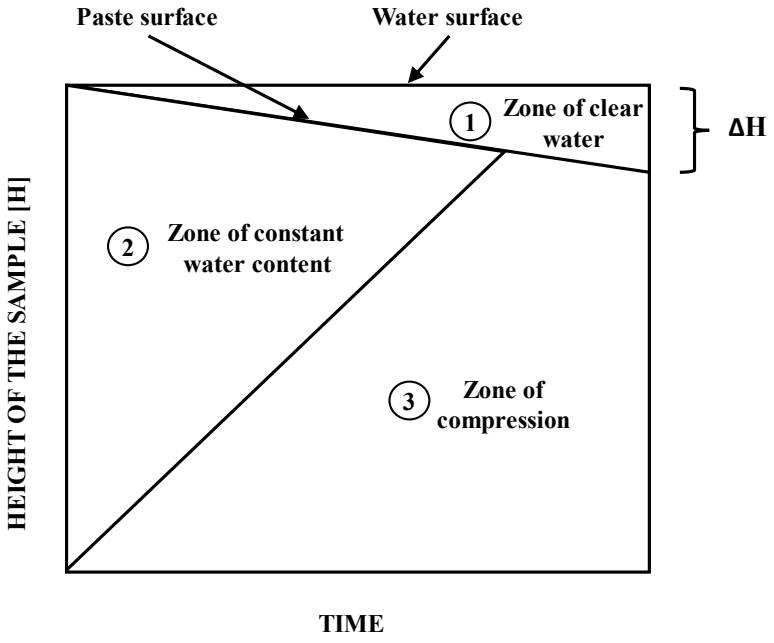

Figure 2-4: The bleeding process illustrated in cement paste adapted from Lamond and Pielert (2006)

In extreme bleeding situations, the bleed water layer forming on the concrete surface can be up to 2 % of the total depth of the concrete (Soutsos and Domone, 2017). Bleed water will either evaporate or be reabsorbed into the concrete with the continuing hydration. Evaporation of the bleed water aids in reducing the initial volume of the concrete (Soutsos and Domone, 2017). Bleeding in concrete also provides beneficial effects for fresh concrete, such as raising the amount of bleeding (water content) of the concrete surface when exposed to extreme weather conditions and helps mitigate PS cracking by restoring moisture to the concrete surface where

accelerated moisture loss (evaporation) occurred. As the bleed water on the surface continues to evaporate the concrete will continue to bleed (restoring the lost moisture), consequently increasing the w/c ratio of the concrete surface and decreasing the quality (Matalkah *et al*., 2019).

Klieger (1955) and Cheng (1994) identified two independent factors as the cause of bleeding in fresh concrete, namely gravity and negative CP. The negative CP build-up will only start when the cumulative evaporation exceeds the cumulative bleeding amount; once this occurs, no bleed water will be visible on the surface of the concrete. The movement of bleed water through the fresh concrete toward the surface of the concrete helps with the formation of the capillary pore network, which reduces the durability of the concrete (Matalkah *et al*., 2019). Meaning that a large amount of bleeding in the concrete will result in less durable concrete.

2.3.2 Evaporation

Evaporation is defined as how liquid transforms into a gas or vapour. Evaporation of a liquid typically occurs when heat energy is added, and the liquid absorbs this energy or when the pressure above the liquid surface is less than the pressure of the liquid; this will cause the active water molecules to escape from the liquid in the form of a vapour (Uno, 1998).

The evaporation rate of concrete is influenced by climatic conditions such as the relative humidity, concrete temperature, air temperature, wind velocity and solar radiation. Amplifying these climatic conditions increases the rate of evaporation, which consequently increases the drying of the concrete, which causes PS. Turcry and Loukili (2006) concluded that PS cracking would occur before or during the concrete setting when exposed to a moderate evaporation rate. However, when the concrete is exposed to a high evaporation rate, PS cracking will occur in the plastic state of the concrete.

The evaporation rate of water on the concrete surface is estimated using the following two ways: the American Concrete Institute (ACI) nomograph or the Uno evaporation rate formula (Uno, 1998; ACI, 1999). The ACI nomograph and the method used to estimate the evaporation rate are demonstrated in Figure 2-5. The nomograph requires the four parameters and starts with the air temperature, relative humidity, concrete temperature, and wind speed.

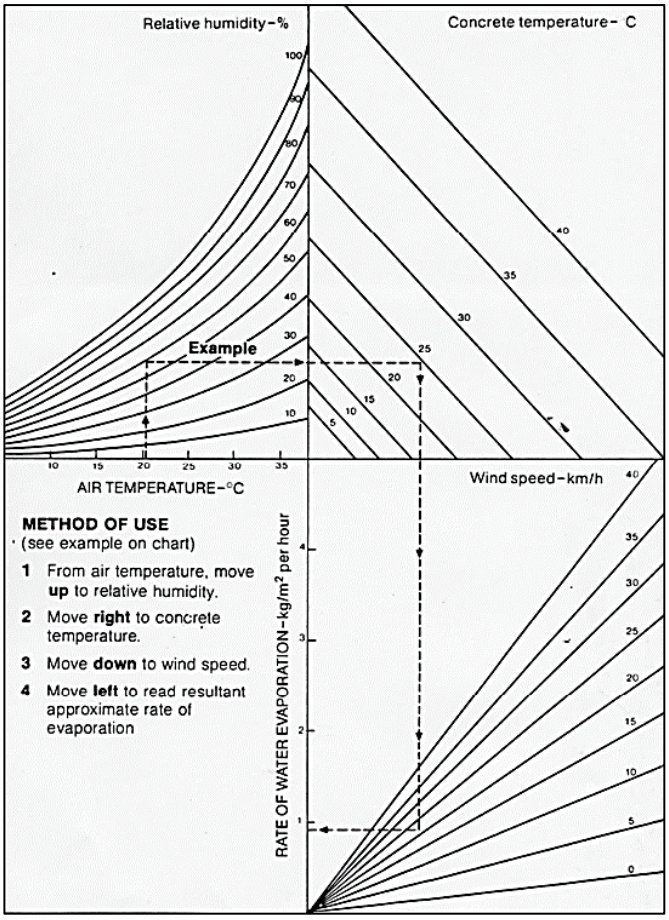

Figure 2-5: ACI nomograph used for estimating the evaporation rate of the surface moisture of concrete (Uno, 1998; ACI, 1999)

Uno (1998) developed the following equation to estimate the evaporation rate on the surface of the concrete by including all the main driving forces that influenced the evaporation rate of the concrete:

$$ER = 5([T_c + 18]^{2.5} - RH.[T_a + 18]^{2.5})(V + 4) \times 10^{-6} \quad (2.1)$$

with ER the evaporation rate [kg/m^2/h], T_c is the concrete (water surface) temperature [°C], RH is the relative humidity [%], T_a is the air temperature [°C] and V the wind velocity [km/h]. According to ACI (1999), PS cracks are likely to occur when concrete is exposed to an evaporation rate of 1 kg/m^2/h. Therefore, it is essential to take precautions when the evaporation rate approaches 1 kg/m^2/h.

The main driving forces identified by equation (2.1) for the evaporation rate of concrete are discussed as follows:

- **Relative Humidity.** The relative humidity is the ratio between the actual moisture present in a unit volume of air to the amount of moisture that air could hold at a certain temperature and is represented as a percentage. When the relative humidity reaches 100 %, the unit of air is fully saturated with moisture, and the evaporation will stop (meaning 0 $kg/m^2/h$) unless external forces such as wind replace the saturated air with non-saturated air (Uno, 1998).
- **Concrete Temperature.** The concrete temperature refers to the temperature measured on the surface of fresh concrete. The temperature of the concrete is influenced by the temperature of the individual materials added to the concrete mixture. Decreasing the temperature of the concrete when casting will significantly reduce evaporation.
- **Air Temperature.** The air temperature is defined as the ambient temperature of the area. Increasing the air temperature will increase the rate of evaporation (Kwak and Ha, 2006).
- **Wind Velocity.** Uno (1998) stated that wind velocity is one of the most crucial climatic elements affecting PS cracking in fresh concrete. The presence of wind accelerates the evaporation process by constantly removing the escaping water molecules. Therefore, decreasing the wind velocity reduces the evaporation rate effectively (Kwak and Ha, 2006).
- **Solar Radiation.** Solar radiation has an effective influence on the evaporation rate because it affects the ambient temperature and the temperature of the land mass (Uno, 1998). Research showed that solar radiation increases the evaporation rate by increasing the temperature on the concrete surface and accelerates the hydration of the cement, which results in strengthening the concrete surface. This phenomenon was examined when concrete slabs were cast in the shade and sunlight; the finding showed that the concrete slabs cast in the shade had more cracks than those cast in sunlight (Van Dijk and Boardman, 1971).

2.3.3 Drying Time

Drying time is the point where the cumulative amount of evaporation is equal to the cumulative amount of bleeding of the concrete, as defined by Kwak and Ha (2006). After this point, the cumulative evaporation exceeds the bleeding, and the negative CP builds up, causing PS in the concrete. The drying time in concrete is dependent on the evaporation rate and the bleeding rate of the concrete, as illustrated in Figure 2-6. The figure was adapted from the results found by Kwak and Ha (2006), which demonstrates that when maintaining the same amount of bleeding and increasing the evaporation rate, the drying time will decrease, resulting in an earlier occurrence of PS cracking. By maintaining a constant evaporation rate but increasing the amount of bleeding of the concrete, the drying time is delayed to a later point in time, reducing the risk of PS cracking.

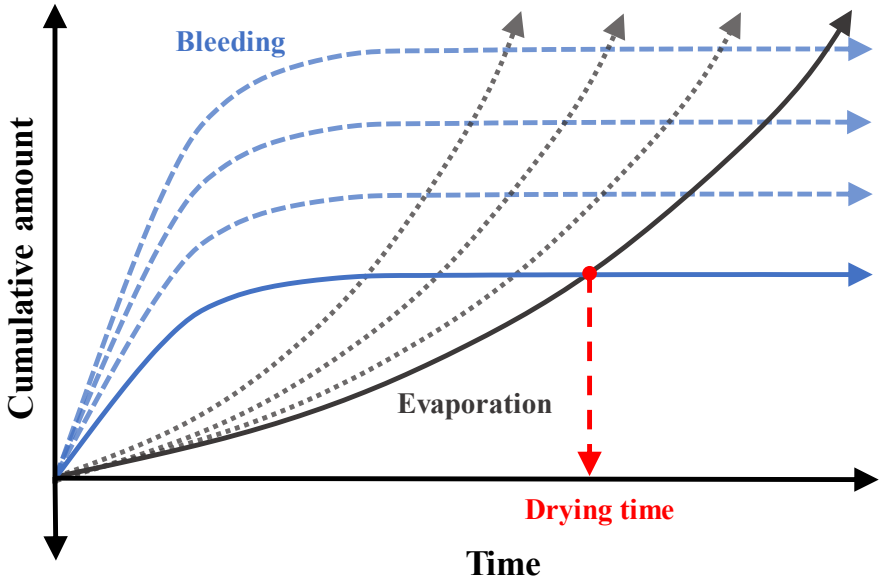

Figure 2-6: Drying time diagram adapted from Kwak and Ha (2006)

2.3.4 Plastic Settlement

Plastic settlement in concrete can be summarised as vertical settlement of the concrete due to gravity. Sayahi *et al.* (2020) stated that plastic settlement and bleeding are qualitatively related to the reduction of concrete volume because bleeding is compensated by settlement in concrete. Figure 2-7 illustrates the occurrence of plastic settlement after placing fresh concrete; the fine and coarse aggregate particles in the concrete start to settle downward with gravity and, after several hours, resulting in settlement. If the concrete is restrained by horizontal reinforcement (such as steel reinforcement, crack inducers, or non-uniform slab depths) from settling downwards, plastic settlement cracks will form. These cracks will form perpendicular to the horizontal reinforcement towards the concrete surface (Soutsos and Domone, 2017).

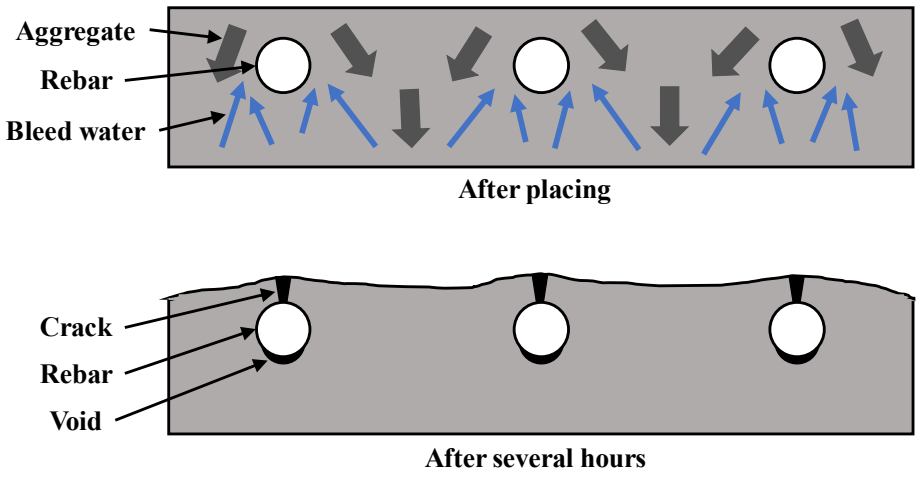

Figure 2-7: The formation of plastic settlement cracks adapted from Soutsos and Domone (2017)

Combrinck *et al.* (2018) identified two distinct types of plastic settlement cracks that can form in concrete, namely tensile cracks that form on the surface of the concrete and shear cracks that form near the restraint in the concrete. Plastic settlement cracks form independently of evaporation and superficial drying in concrete. These cracks are amplified when the concrete is restrained, and the bleeding and settlement of the concrete are high (Mehta and Monteiro, 2001).

According to Sayahi *et al.* (2020), the drying process in fresh concrete can be identified in the plastic settlement curve of the concrete, which is shown in Figure 2-8. The figure shows the concrete settlement over time. The phases and the critical point identified by Sayahi *et al.* (2020) are also shown in the figure.

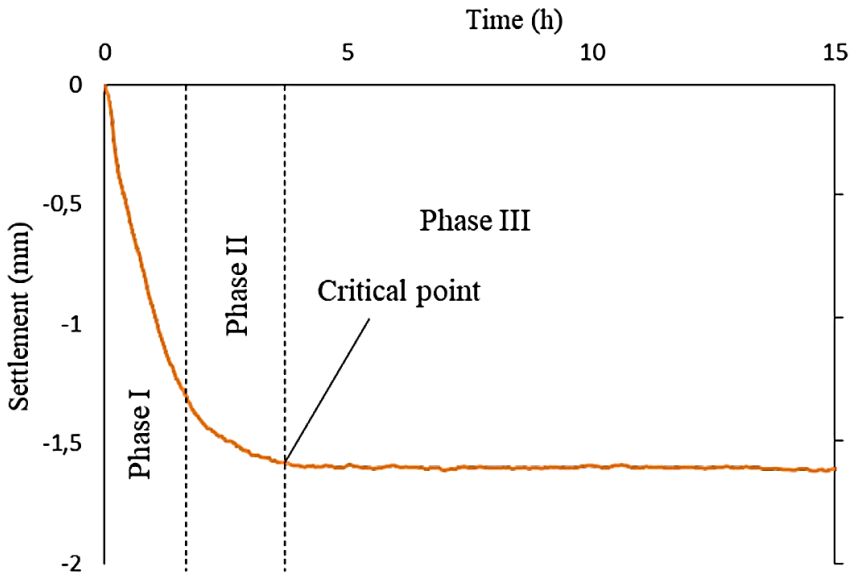

Figure 2-8: Three phases in plastic settlement (Sayahi *et al.*, 2020)

This process is divided into the following three phases:

- **Phase I** in the drying process is the initial drying period, which is the period where the bleed water accumulates at the surface of the concrete. In this phase, the settlement is due to gravity acting on the plastic concrete (Sayahi *et al.*, 2020).
- The first dotted line is the location of the drying time of the concrete. Which is the point in time when the cumulative amount of evaporation and bleeding is equal, indicating the change from the initial to the constant period (Sayahi *et al.*, 2020).
- **Phase II** is the constant rate period in which the cumulative rate of evaporation has exceeded the cumulative bleeding of the concrete, and menisci is formed on the surface of the concrete. Due to the curvature of the menisci, negative CP develops between the pores and commencing the negative CP build-up in the concrete. The negative CP forms in the

pore system of the fresh concrete and induces tensile stresses in the concrete. The particles are pulled closer to each other, resulting in further plastic settlement (Sayahi *et al.*, 2020).

- The **critical point** (second dotted line) indicates the onset of the falling rate period where the menisci move from the surface to the interior of the concrete. The menisci gradually decrease with continued hydration and evaporation (Sayahi *et al.*, 2020).
- **Phase III** is the falling rate period in the drying process of the concrete. In this phase, the menisci recede further into the concrete from the ongoing evaporation and hydration, causing a higher negative pressure (Sayahi *et al.*, 2020). In this phase, bleeding still occurs in the concrete but evaporates at a slower rate, resulting in a more constant settlement rate (Sayahi *et al.*, 2020).

2.4 HARDENING OF FRESH CONCRETE

When water and cement are combined, hydration occurs. As hydration progresses, the cement paste mixture changes from a plastic state to a solid state. The setting time of cement and concrete has two distinct points in time, known as the initial and final set. Figure 2-9 demonstrates the three stages of the hydration process in concrete over time. It shows how the initial and final set divides the hydration process into three stages. The three stages in hydration are known as the stiffening, solidification, and hardening stages. The hydration of the cement between the particles is also shown in each stage. Lastly, Figure 2-9 shows how the relative amount of permeability, porosity and strength changes as the concrete starts to set over time.

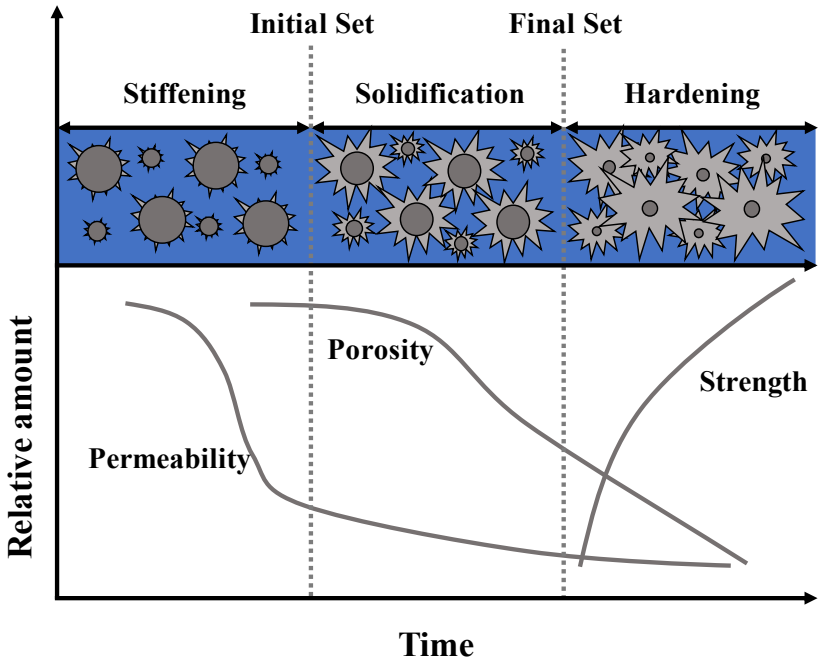

Figure 2-9: Three stages of fresh concrete after cast adapted from Mehta and Monteiro (2006) and Combrinck (2011)

2.4.1 Initial and Final Set

The initial set (also known as the initial setting time) is when the concrete transitions from the stiffening stage to the solidification stage. The initial set of conventional concrete generally occurs between 2 and 4 hours after casting at normal temperatures (Soutsos and Domone, 2017). The final set (also known as the final setting time) is when the concrete transitions from solidification to the hardening stage, which occurs several hours after the initial set. (Mehta and Monteiro, 2001 and Soutsos and Domone, 2017).

Combrinck and Boshoff (2013) found that when fresh concrete is exposed to an evaporation rate, the onset of PS cracks occurs just before or at the initial set of the concrete. Onset refers to when the concrete has begun to crack. As the PS crack continues to widen, the crack will stabilise at the final set of the concrete. Stabilise, or stabilisation, refers to when the crack growth ceases. However, the crack still widens after the final set but at a much lower rate. The widening of the crack that occurs after the final set is due to drying shrinkage, a phenomenon that occurs in concrete after the final setting time is reached.

2.4.2 Stiffening, Solidification, and Hardening

Stiffening is the loss of consistency of the cement paste in the hydration process in concrete and is generally associated with a decrease in the slump reading. The plasticity is due to the free water within the cement paste. The early hydration reaction and evaporation are the leading cause of the gradual loss of free water in the concrete system, resulting in the stiffening of the cement paste and then finally hardening (Mehta and Monteiro, 2001).

The solidification stage is when the cement paste starts to solidify. Solidification starts at the point in time when the cement paste has become unworkable, called the initial set, and ends when the cement paste solidifies completely and becomes fully rigid, which is known as the final set (Mehta and Monteiro, 2001). This stage is a critical period for when concrete is exposed to evaporation because most PS cracking starts and ends in this stage (Combrinck and Boshoff, 2013)

The hardening stage occurs after the final set of the cement paste and is when the porosity and permeability of the cement paste start to decrease, and the strength of the cement paste starts to increase. As the hydration of the tricalcium silicate (C_3S) continues in the cement paste, the progressive filling of the voids in the paste results in decreasing the porosity and permeability of the cement paste and increasing in strength illustrated in Figure 2-9 (Mehta and Monteiro, 2001).

2.5 FACTORS INFLUENCING PLASTIC SHRINKAGE CRACKING

Bleeding, evaporation, drying time, plastic settlement, and setting time are factors that influence PS and PS cracking in concrete (Kwak and Ha, 2006; Combrinck and Boshoff, 2013; Kayondo *et al.*, 2019). The interaction between these influencing factors in concrete can be illustrated in Figure 2-10. The figure shows the cumulative amount of bleeding and evaporation over time. The plastic settlement of the concrete, drying time and setting times are also shown in the figure.

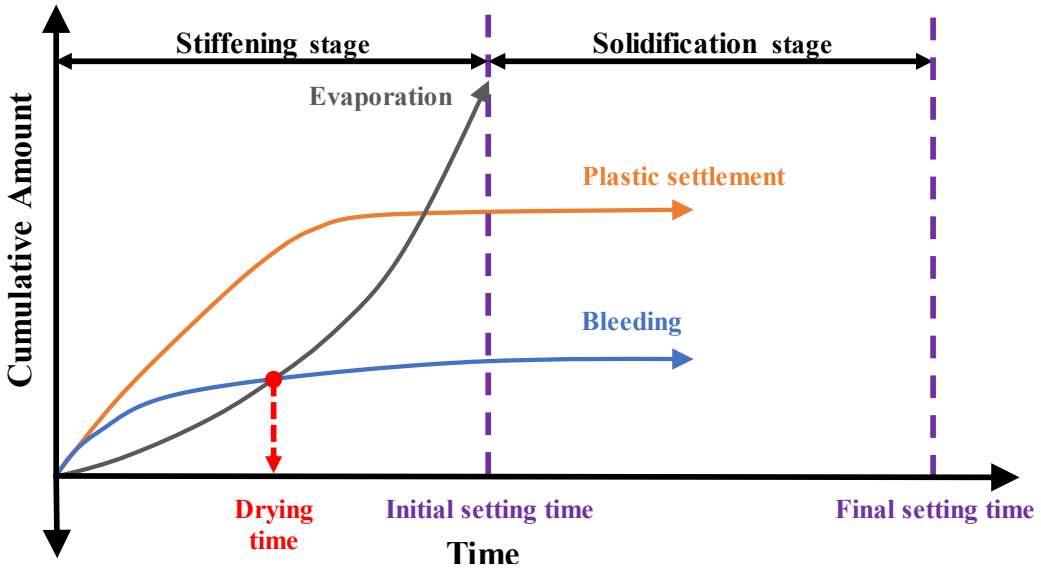

Figure 2-10: The influencing factors of PS cracking adapted from Kwak and Ha (2006), Combrinck (2011) and Sayahi *et al.* (2020)

It can be seen that by affecting one of the factors, the other factors will also be affected and consequently influence the PS and PS cracking of concrete. Bleeding, evaporation, drying time, concrete setting time and plastic settlement in concrete can be affected by several aspects. Some of the aspects are the type of cement, additions, w/c ratio, admixtures, climatic condition, concrete temperature, aggregate grading and concrete depth.

2.5.1 Type of Cement and Additions

Cement with high fineness decreases the amount of bleeding and the bleed rate of the concrete. The concrete bleeding can effectively be reduced when cement having high tricalcium aluminate (C_3A) is used (Lamond and Pielert, 2006; Neville, 2012; Matalkah *et al.*, 2019).

In addition, cement with high fineness will reduce the amount of water evaporation from the concrete and reduce the concrete setting time (Sayahi *et al.*, 2019; Mehta and Monteiro, 2001). According to Soutsos and Domone (2017), the setting time of the concrete can be reduced when cement with high quantities of C_3S and C_3A is used.

In concrete, additions refer to finely divided materials used to improve properties or obtain unique properties in concrete. Some of the most common additions used in concrete are limestone powder, fly ash, silica fume, and ground granulated furnace slag. Additions can be supplied as separate materials which can be added to the concrete or as a pre-blended mixture with Portland cement (Soutsos and Domone, 2017).

The findings of Matalkah *et al*. (2019) showed that the bleeding of the concrete with alkali-activated cement was almost negligible compared to the bleeding found in the Portland cement concrete. When adding additions, such as condensed silica fume to concrete can significantly reduce the bleeding of concrete. This is because condensed micro silica has a very high surface area, making this material an effective bleeding control agent (Soutsos and Domone, 2017).

2.5.2 Water/Cement Ratio and Unit Water Content

When the w/c ratio of the concrete is increased the amount of bleeding and evaporation will increase (Topçu and Elgün, 2004; Lamond and Pielert, 2006; Sayahi *et al.*, 2019). The concrete setting time is also delayed when the w/c ratio increases (Mehta and Monteiro, 2001).

The water content in the concrete affects bleeding and evaporation. Increasing the water content in the concrete mixture results in an increased amount of bleeding in the concrete and evaporation (Topçu and Elgün, 2004; Kwak and Ha, 2006).

2.5.3 Admixtures

Admixtures are chemical materials that are added to fresh concrete to modify the properties of the concrete in the plastic or hardened state. Some examples of admixtures are plasticisers, retarders, accelerators and air-entraining agents (Soutsos and Domone, 2017). The addition of admixtures to concrete has been shown to significantly affect the bleeding, evaporation, plastic settlement and setting times due to the chemical reaction occurring in the concrete mixture.

Plasticisers are a chemical admixture that increases the workability of concrete by reacting with the cement particles on a molecular level. The plasticiser alters the cement particles to have a negative charge, thus repelling each other and becoming more dispersed (Soutsos and Domone, 2017). Superplasticiser (SP), also known as high-range water reducers, are more potent than plasticisers and achieve a higher magnitude of workability in concrete than plasticisers (Domone and Illston, 2010). Sayahi *et al*. (2019) showed that by reducing the percentage of SP in the concrete from 0.8 % (the percentage used in the reference concrete) to 0.6 %, the amount of evaporation decreased and vice versa when the percentage of SP was increased from 0.8 % to 1 %.

Concrete setting time is affected when admixtures are added because the chemical in the admixtures interferes with the hydration reaction in the concrete (Soutsos and Domone, 2017). Combrinck and Boshoff (2013) found that by adding admixtures such as plasticisers or SP to the concrete mix design, the setting time of the concrete was delayed. Increasing the dosages of the admixtures added to the concrete mixture will amplify the delay or increase the setting time.

2.5.4 Climatic Conditions

Increased wind velocity increases the evaporation rate and results in more bleeding (Lamond and Pielert, 2006). Increasing the evaporation rate will increase the capillary force on the concrete surface, drawing the water out of the concrete (Lamond and Pielert, 2006). Low air temperature decreases the rate of hydration in concrete and increases the amount of concrete bleeding (Soutsos and Domone, 2017).

2.5.5 Concrete Temperature

The hydration reaction between the cement and water, like most other chemical reactions, will accelerate when the concrete temperature is increased. Therefore, by reducing the temperature of concrete, the hydration process will slow down (Mehta and Monteiro, 2001; Domone and Illston, 2010).

2.5.6 Grading and ratios of fine and coarse aggregate

Poorly graded aggregate can significantly influence the bleeding in concrete. Increasing the fine aggregate content below a particle size of 300 μm in the concrete mixture will reduce bleeding (Soutsos and Domone, 2017).

2.5.7 Concrete Depth

The amount of bleed water is proportional to the depth of the concrete slab (Kwak and Ha, 2006). Meaning that as the depth of the concrete increases, the amount of bleeding will increase.

2.6 MECHANISMS CAUSING PLASTIC SHRINKAGE CRACKING

PS is caused by the build-up of negative CP in a concrete mass which occurs when the cumulative evaporation exceeds the cumulative amount of bleeding in the concrete. As the negative CP builds up in the concrete, tensile strains occur. If the concrete mass is restrained, the rate of the negative CP build-up increases significantly, and tensile stresses are induced. When a critical pressure is reached, air entry may occur, which leads to the initiation of PS cracks (Slowik *et al.*, 2014). Negative CP build-up and air entry interact. When there is air

entry, there is a redistribution of negative CP. The mechanisms are discussed chronologically, starting with restraint, followed by the CP and air entry.

2.6.1 Restraint

PS cracking describes that PS cracks will form when the concrete is restrained from shrinking (Holt and Leivo, 2004). The reason for this phenomenon is by restraining the concrete, the physical build-up of negative CP in the pores of the concrete increases. Causing tensile strains to form, inducing tensile stresses. When the induced tensile stresses exceed the fresh concrete's tensile strength, cracks initiate and propagate inwards (Sayahi *et al.*, 2020). The strength does not refer to the hydration of the cement particles in the fresh concrete but due to the CP and internal cohesion forces between the particles. Concrete can be restrained in two ways, namely, internal or external:

- **Internal restraints** are restraints caused by internal factors affecting the concrete, such as a strain gradient over the cross-section of the concrete, steel reinforcement or coarse aggregate (Combrinck *et al.*, 2018; Sayahi *et al.*, 2020; Zhu *et al.*, 2016).
- An **external restraint** is induced by external factors restraining the fresh concrete from shrinkage. These external factors are created by the variation in the depth of the concrete, steel reinforcement, or friction between the concrete and the surface on which the concrete is cast (Sayahi *et al.*, 2020).

However, when the concrete is free to shrink without restraint, the concrete will shrink uniformly without cracking.

2.6.2 Capillary Pressure

Capillary pores are small pockets filled with liquid (generally water) that form between particles in plastic concrete (Wittmann, 1976). Figure 2-11 demonstrates how the capillary pores form between the solid particles in fresh concrete. CP is the pressure that builds up from the liquid between the solid particles in the plastic concrete (Knappett and Craig, 2012). The figure also shows how the adhesive forces and surface tension act on the particles when the concrete is exposed to evaporation.

As the evaporation on the concrete surface continues, the mix-water in the concrete reduces, causing water menisci to form between the solid particles. Because of the menisci forming between the particles, a pressure difference occurs between the water and surrounding air pressure within the concrete. This pressure difference is due to the equilibrium of these adhesive forces (Slowik *et al*., 2014). The ongoing evaporation reduces the radius of the menisci between the particles (which causes the adhesive forces acting on the particles to increase) and results

in the build-up of negative CP. As the negative CP acts on the solid particles of the drying suspension in the concrete, resulting in contraction (Schmidt and Slowik, 2009). Slowik *et al.* (2014) state that the negative CP that builds up in the pore system of the concrete is the leading cause of PS in fresh concrete. If a critical CP is reached, PS cracks may occur.

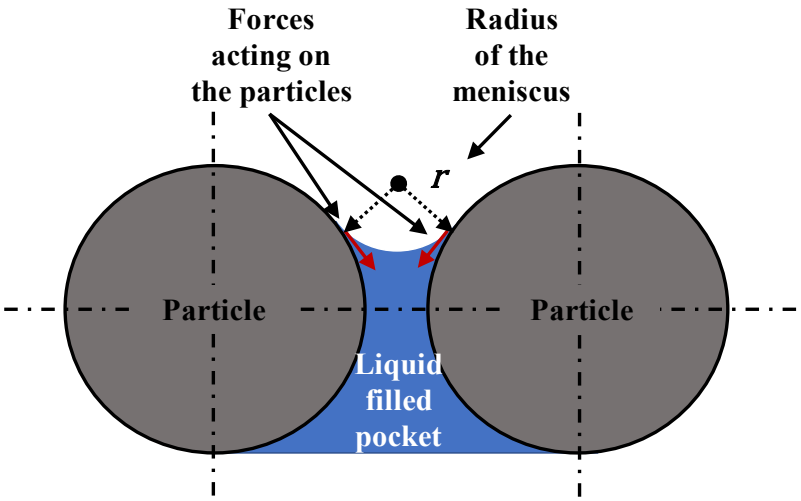

Figure 2-11: Menisci forming in the capillary pores of the concrete adapted from Wittmann (1976) and Combrinck (2016)

The negative CP that forms between the concrete particles, is directly related to the ratio between the surface tension of the mix-water and the radius of the meniscus between two particles (Wittmann, 1976). The higher the surface tension of the mix-water in the concrete, the higher the negative CP build-up rate and vice versa (Wittmann, 1976; Slowik *et al.*, 2008). This expression for the negative CP is called the Gauss-Laplace equation:

$$P = -\frac{2\sigma_t}{r} \tag{2.2}$$

where P is the negative CP [Pa], σ_t is the surface tension [N/m] and r is the radius of the meniscus [m].

The negative CP in the concrete pore walls is the primary mechanism of PS (Wittmann, 1976; Slowik *et al.*, 2008; Slowik *et al.*, 2014; Ghourchian *et al.*, 2021). Given that the CP captures the influence of the climatic conditions (evaporation), specimen geometry, and material composition on the cracking risk of the concrete (Slowik *et al.*, 2014).

2.6.3 Air Entry

Air entry is the point in time when the radius of the meniscus between the particles become too small to bridge the distance between the particles, and air enters the cement paste, resulting in

PS cracking. The air entry location will typically occur at the weak spots (a typical example of where these weak spots are located is where the concrete mass is restrained, as discussed in Section 2.6.1) in the fresh concrete, where cracks are most likely to form (Slowik *et al.*, 2008).

2.7 NEGATIVE CAPILLARY PRESSURE BUILD-UP

As the bleed water evaporates along the surface of the concrete, the internal pore water quantity decreases, and the negative CP in the concrete increases. The increase of the negative CP is referred to as negative CP build-up. This negative pressure within the concrete draws the concrete particles closer, resulting in PS.

Figure 2-12 schematically illustrates negative CP build-up with time. The successive stages are also pointed out. What happens from Stage A to E is described in the following section. The effect of evaporation rate and water-cement ratio, as well as curing, replacing evaporated water and curing compounds on negative CP build-up, are also discussed.

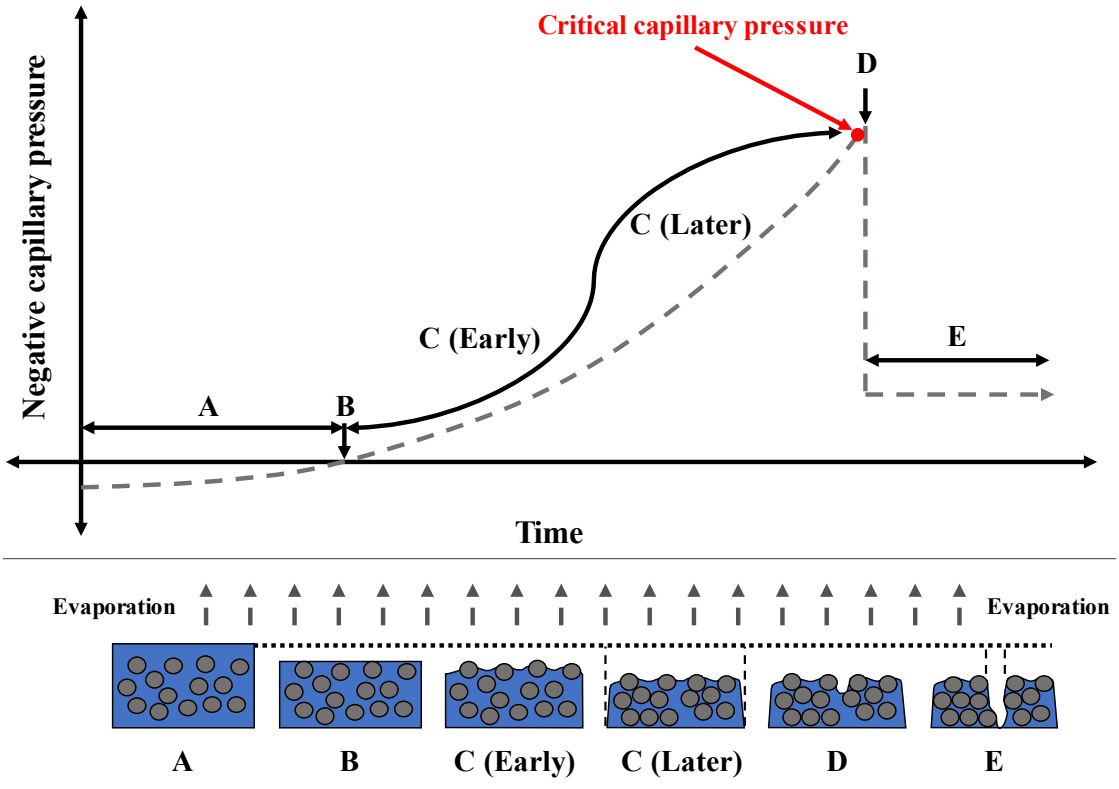

Figure 2-12: Stages during the negative CP build-up and PS cracking in concrete adapted from Combrinck (2016), which were adapted from Slowik *et al.* (2008)

- **Stage A** is the period immediately after the casting and consolidation of fresh concrete. At this stage, the concrete begins to bleed, and the bleed water accumulates on the surface, forming a thin layer known as surface laitance. The spaces between the concrete particles are almost filled with water, forming a system of interconnected pores. At this point, the

cumulative bleeding exceeds the cumulative evaporation rate, and all the particles are covered by the surface laitance (Slowik *et al.*, 2008; Combrinck, 2016).

- **Stage B** is when the surface laitance is reduced to approximately the same height as the top of the particles because of continuous evaporation (or, in some materials, because of self-desiccation). This point is known as the drying time of concrete (as discussed in Section 2.3.3). As the evaporation continues, the negative CP will build up from this point (Slowik *et al*., 2008; Combrinck, 2016)
- **Stage C (Early) and Stage C (Later)** show that the negative CP starts to build up with the continuing rate of evaporation. At **Stage C**, the evaporation exceeds the amount of bleeding, and the particles are no longer covered by surface laitance. The evaporation of the pore water between the particles causes adhesive forces and surface tension to act on the particles, leading to water menisci forming between these particles. At **Stage C (Later),** the negative CP build-up increases significantly with the ongoing evaporation. Because of the effect of the negative CP build-up on the particles, the pores between particles are reduced as more pore water is brought to the surface. This reduction in the pores within the concrete results in shrinkage strain; if this shrinkage is prevented and the cohesive forces are overcome, the cracks form. (Slowik *et al*., 2008; Combrinck, 2016).
- **Critical CP** is a pressure point between **Stage C (Later)** and **Stage D**. At this point, the menisci between the particles have reached the limiting radius where the menisci are still able to bridge the particles; reducing the radius further will result in air entry (Slowik *et al*., 2008; Combrinck, 2016).
- **Stage D** is where the CP "breakthrough" point occurs. Air has penetrated the pore system, starting at the largest pores (the radii of the menisci have been reduced to a point where the bridges between particles are too small, and air can enter the concrete). The point of air entry is localised and does not occur uniformly and simultaneously over the surface of the concrete paste (Slowik *et al*., 2008). As the build-up continues, the locations where the air is most likely to enter the concrete occur at the weakest points on the surface of the concrete and will result in PS cracks.
- **Stage E** illustrates that as more air enters the pores of the concrete, the CP reduces. This is caused by the cement paste, which starts to shrink and relieves the pressure build-up. The location where air gaps are formed and air penetrates the concrete is called PS cracks (Slowik *et al*., 2008; Combrinck, 2016).

2.7.1 Factors Influencing Negative Capillary Pressure Build-Up

According to the CP literature, the following factors affect the negative CP build-up and the air entry value in concrete: the particle size distribution, admixture, additions, the evaporation rate, and the movement of the particles. Especially the amount of small-sized particles in the concrete mixture design such as the cement, silica fume, or fly ash. These small particles form narrow pore systems in concrete, producing smaller menisci between the particles and even higher negative CP values (Schmidt and Slowik, 2009; Leonovich, 2018). In this subsection, some of the main factors influencing the negative CP build-up, such as the evaporation rate, w/c ratios, curing, rewetting and lastly, the effect of admixtures and additions, are discussed.

Figure 2-13 shows the influence of the evaporation rate on the negative CP build-up in fresh concrete. The figure shows that as the evaporation rate (wind speed) on the concrete increases, the earlier the negative CP starts to build up in the concrete (Holt and Leivo, 2004). The earlier the negative CP builds up, the higher the induced tensile stresses in the concrete. When the concrete does not develop enough strength to withstand these tensile stresses, PS cracking will occur (Sayahi *et al*., 2019). The severity of PS cracking in concrete was found to be directly proportional to the product of the volume of evaporated water from the pore network inside the concrete between the drying time and the initial set (Boshoff and Combrinck, 2013; Sayahi *et al.*, 2021).

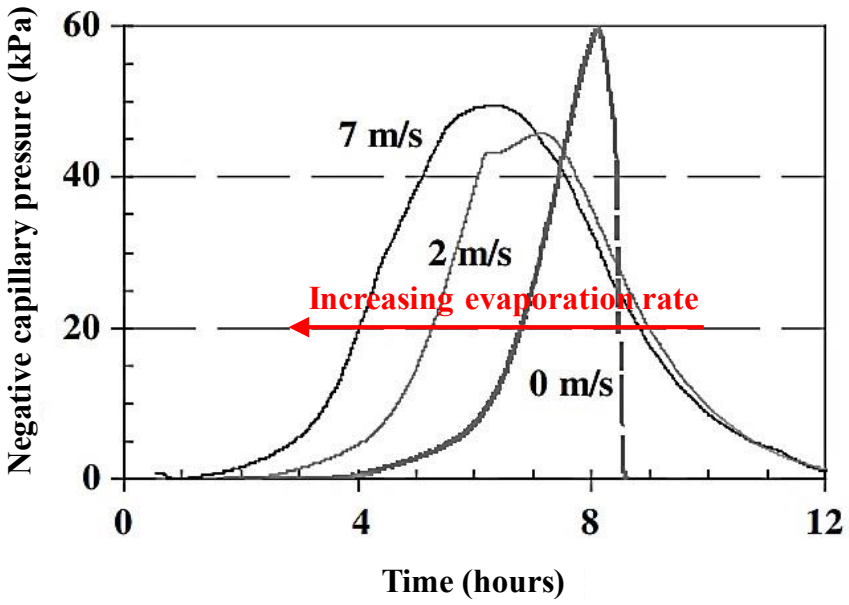

Figure 2-13: Negative CP build-up at different evaporation rates (Holt and Leivo, 2004)

Figure 2-14 demonstrates the effect of different w/c ratios on the negative CP build-up over time (Holt and Leivo, 2004). The figure also shows how these w/c ratios affect the negative CP build-up rate. Schmidt and Slowik (2009) found similar results to that of Figure 2-14, as the

w/c ratio in the concrete increased, the concrete's negative CP build-up rate reduced. The increase in the w/c ratio of the concrete causes an increase in the number of unfilled spaces between the particles resulting in larger capillary pores and a reduced negative CP build-up (Domone and Illston, 2010). High performance concretes, consisting of low w/c ratios, will cause self-desiccation in the concrete and influence the negative CP build-up at an early age (Schmidt and Slowik, 2009).

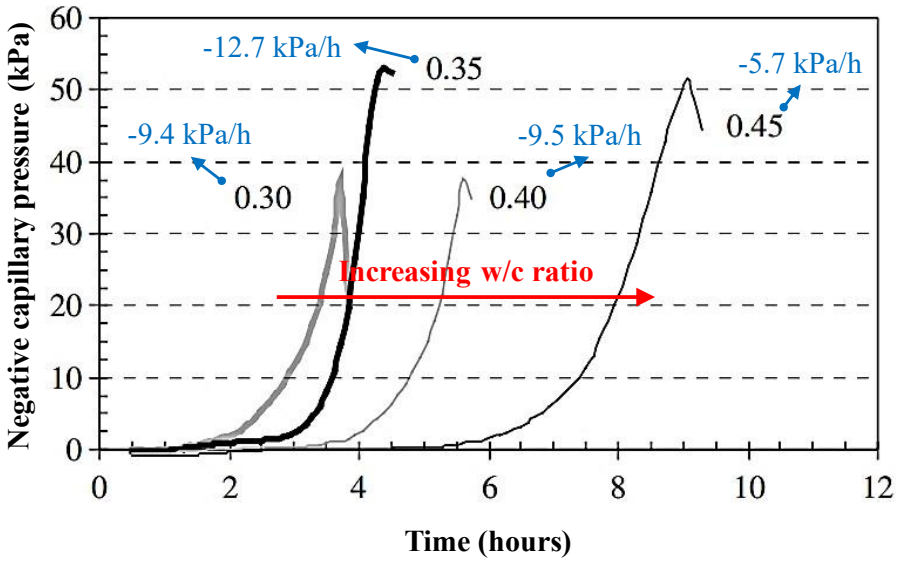

Figure 2-14: Negative CP build-up and the negative CP build-up rates for concrete with different w/c ratios adapted from Holt and Leivo (2004)

The effect of curing and replacing the evaporated water of the concrete on the negative CP build-up over time is demonstrated in Figure 2-15. The uncured sample was exposed to climatic conditions with a temperature of 20 °C and relative humidity of 30 %, while the cured sample was covered with plastic foil to prevent evaporation. The results found by Schmidt and Slowik (2013) show that by curing fresh concrete, the negative CP build-up for the uncured sample started at about 2 hours while the cured sample started at about 8 hours after casting. The figure shows the negative CP build-up rate for the cured sample is higher than that of the uncured sample, which might be due to the start of the cement hydration, which consumes the internal water in the concrete—resulting in narrowing the pore system within the concrete as the concrete moves from plastic to the hardened state.

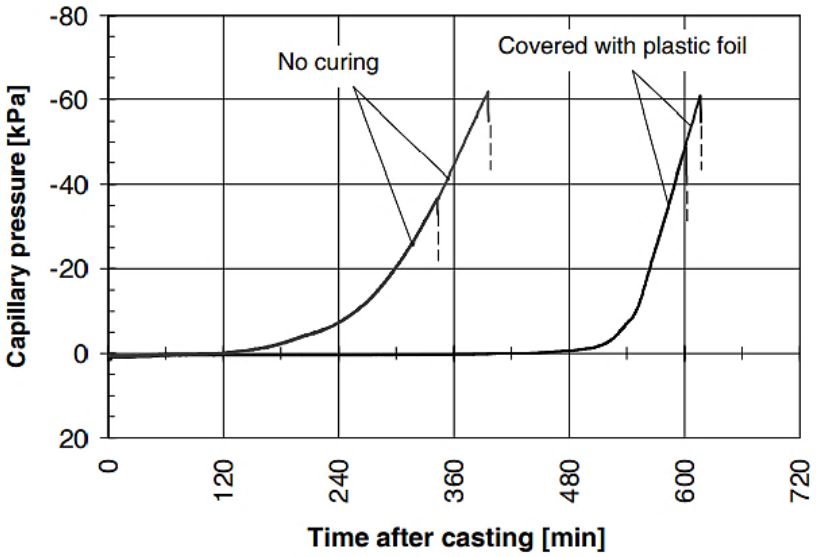

Figure 2-15: Negative CP build-up of cured and uncured concrete specimens (Schmidt and Slowik, 2013)

Figure 2-16 illustrates the negative CP build-up of a cured and uncured sample over time. A curing agent was applied to the cured sample when the evaporation rate reached 0.2 kg/m^2/h. The uncured sample was left exposed to the initial evaporation rate of 0.7 kg/m^2/h (Slowik *et al.*, 2014). No PS cracking measurements were presented in Slowik *et al.*'s paper.

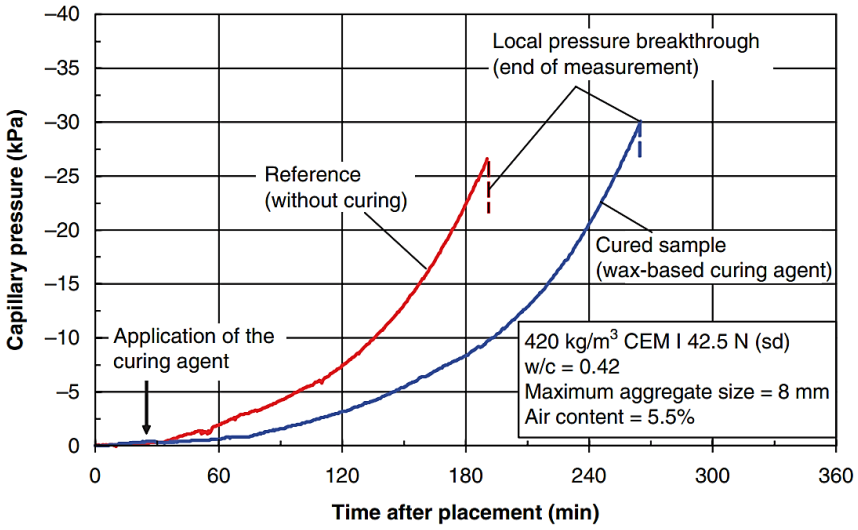

Figure 2-16: Negative CP build-up of cured and uncured concrete (Slowik *et al.*, 2014)

Figure 2-17 demonstrates how adding a small amount of water (at a certain CP) to the surface of the concrete alters the behaviour of the negative CP build-up. The negative CP is reduced by adding water to the surface, which increases the menisci radii. However, as the added water evaporates, the negative CP builds up again (Schmidt and Slowik, 2009).

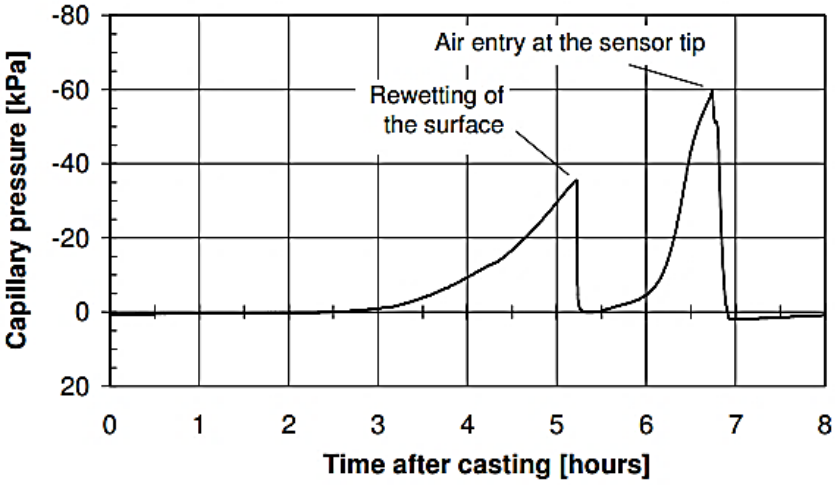

Figure 2-17: Negative CP build-up after rewetting the surface ones after casting (Schmidt and Slowik, 2009)

Slowik *et al.* (2014) state that when a critical CP is reached, the concrete may crack. On the contrary, by preventing negative CP build-up in concrete, the cracking risk of the concrete can be reduced. The delay in the negative CP build-up increases the radii of the menisci between the particles and prevents high tensile stresses from forming on the surface of the concrete. In addition, providing the concrete more time to develop enough strength to resist PS cracking.

Combrinck *et al.* (2019) found that adding the minimum or maximum amount of lignosulphonate-based plasticiser to concrete helped reduce the severity of PS cracking. As the lignosulphonate-based plasticiser dosages increased, a progressive reduction in the negative CP build-up rate was observed. Combrinck *et al*. (2019) believed that the plasticiser altered the surface tension and, therefore, relieved the negative CP build-up that developed in the pores of the concrete.

Combrinck *et al.* (2019) noticed an overall reduction in the severity of the PS cracking and negative CP build-up rate when minimum to maximum dosages of polycarboxylate ethers based or sulphonated melamine formaldehyde-based plasticisers were added to the concrete. Combrinck *et al.* (2019) concluded that PS cracking could significantly be reduced by adding different dosages of liquid admixtures.

Figure 2-18 illustrates the effect of different liquid admixtures on the negative CP build-up in the fresh concrete at the same evaporation rate. The figure shows that the Accelerator (ACC) had the highest negative CP build-up rate compared to the Reference (REF) concrete. While the negative CP build-up rates were reduced for concrete with Stabilisers (STB), Air-Entraining Agents (AEA), Shrinkage Reducing Admixtures (SRA), and Retarders (RET) compared to the

REF (Sayahi *et al*., 2020). It is clear that admixtures have a significant effect on the negative CP behaviour.

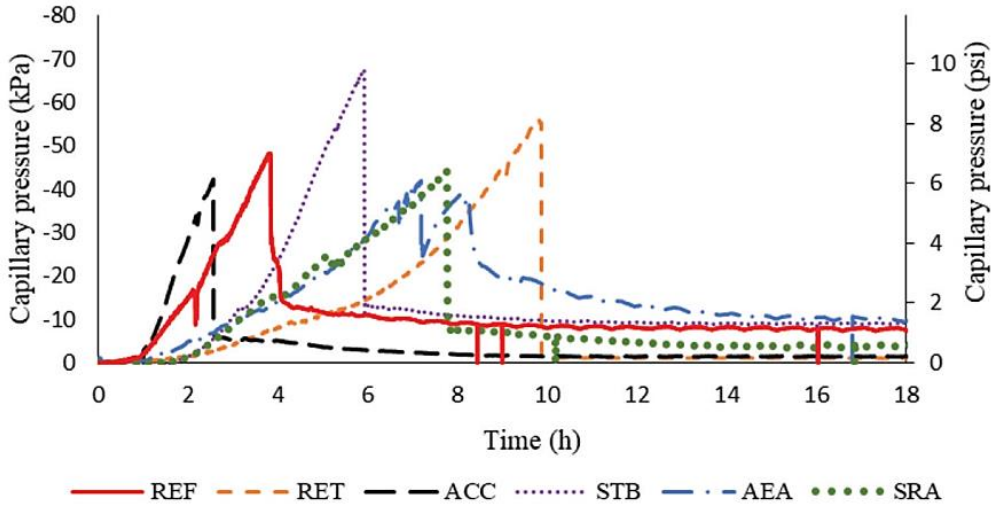

Figure 2-18: The negative CP build-up of concrete mixtures with various types of admixtures (Sayahi *et al*., 2020)

Figure 2-19 shows the effect of different blended cements on the negative CP build-up under the same climatic conditions over time. The figure shows the negative CP build-up for CEM I 52.5 R, CEM II/A-LL 42.5 R and CEM 1 42.5 N having the following specific surface areas of 550, 430 and 310 m^2/kg (Sayahi *et al*., 2019). Sayahi *et al*. (2019) noticed that the type of cement (the specific surface area of the cement) had no significant difference in the development of the negative CP of the concrete, as demonstrated in the figure.

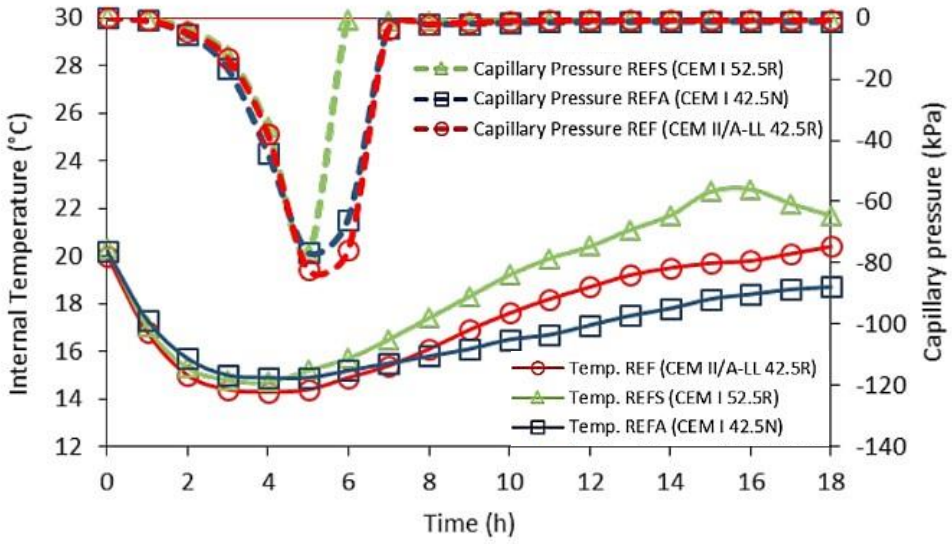

Figure 2-19: Negative CP build-up and internal temperature of different cement types adapted from Sayahi *et al.* (2019)

It is clear that a range of factors influence the negative CP build-up in concrete, which emphasises the importance of the CP mechanism in concrete.

2.8 PLASTIC SHRINKAGE CRACKING PREVENTION

Although various parameters affect PS cracking in fresh concrete, multiple actions exist to prevent these cracks. The following actions are recommended to reduce or prevent the formation of PS cracks in concrete. These actions fall into two categories: internal and external preventative actions. Internal preventative actions involve improving the design of the concrete mix, whereas external preventative actions involve applying the action to the concrete surface.

2.8.1 Internal Preventative Actions

- Adding accelerators to the concrete mixture helps to decrease the concrete setting time. Additionally, avoid adding a retarder to the concrete, which increases the setting time (Uno, 1998; Combrinck *et al*., 2019).
- Using fibres such as polypropylene fibres in concrete showed some improvement in reducing PS cracking according to Uno (1998), Qi *et al*. (2003) and Boshoff and Combrinck (2013).
- The addition of plasticiser, SP, or plastic shrinkage-reducing admixtures to concrete reduced PS cracks by delaying the negative CP build-up in the fresh concrete (Combrinck *et al*., 2019; Mora-Ruacho *et al*., 2009).
- Using alkali-activated cement in concrete showed increased PS cracking resistance compared to Portland cement concrete (Matalkah *et al*., 2019).
- Sayahi *et al.* (2020) state that by adding STB, the cracking tendency of the concrete is reduced, and the addition of AEA and SRA reduces the risk of PS cracking.
- Combrinck *et al*. (2018) stated that providing adequate cover at the top reinforcement steel in concrete will reduce the risk of PS cracking in the concrete.

2.8.2 External Preventative Actions

- Curing concrete to reduce moisture loss by ponding or spraying the surface of the concrete, formwork, or subgrade with water. (Uno, 1998; Mehta and Monteiro, 2001; Soutsos and Domone, 2017).
- Applying windbreaks, sunshades, polythene, hessian or curing membrane to protect the surface of the concrete (Lamond and Pielert, 2006; Soutsos and Domone, 2017).
- Avoid delays in placing ready-mixed concrete (Mehta and Monteiro, 2001).

- Using methods or models to help minimise or prevent PS cracking in concrete is discussed in the next section (Slowik *et al.*, 2008; Boshoff and Combrinck, 2013, Sayahi *et al.*, 2021, Ghoddousi *et al.*, 2019).

2.9 MODELS AND METHODS TO HELP PREVENT PLASTIC SHRINKAGE CRACKING

The preceding discussions clearly show that PS cracking depends on several influencing factors and mechanisms, making this phenomenon challenging to predict. This section focuses on some recent methods and empirical models that help predict and prevent PS cracking.

2.9.1 Method for Concrete Curing by Closed-Loop Controlled Rewetting

Slowik *et al.* (2008) proposed a concrete curing method based on CP measurements and closed-loop controlled rewetting of the surface of the concrete. This method helps to reduce the risk of PS cracking in fresh concrete.

The method is used by determining the CP value of air entry of the concrete using an electrical conductivity sensor. After establishing the air entry CP value, a predefined pressure threshold can be applied to the negative CP build-up, as shown in Figure 2-20. The figure shows that the negative CP build-up can be manipulated and delayed by constantly rewetting the surface of the concrete before the threshold is reached.

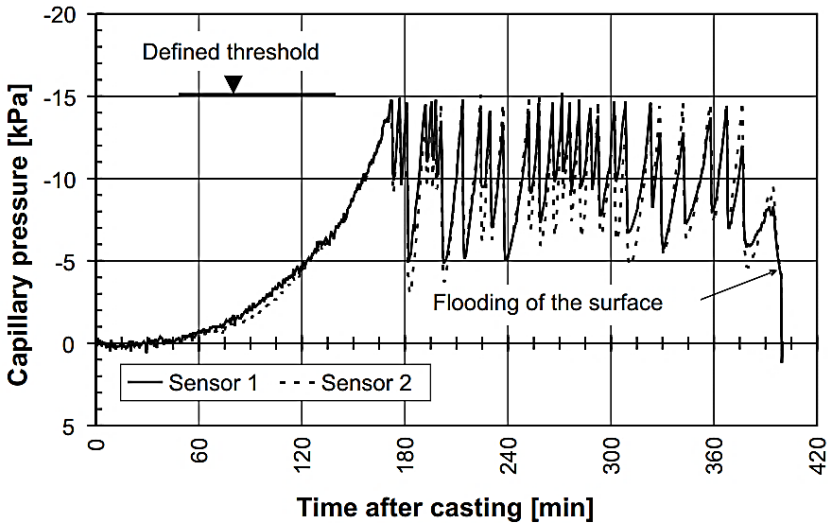

Figure 2-20: Negative CP build-up after rewetting multiple times (Slowik *et al.*, 2008)

2.9.2 Boshoff and Combrinck (2013) Plastic Shrinkage Cracking Severity Model

Boshoff and Combrinck (2013) proposed a model suggesting that the severity of the concrete was dependent on the PS strain. Furthermore, the PS strain in the concrete is directly related to

the rate of evaporation of water, the bleeding properties, and the time until hardening of the concrete. The proposed PS cracking severity model is expressed as:

$$PS\ cracking\ severity\ = ER \cdot t_{iset} - W_{bl} \quad (2.3)$$

Where ER is the evaporation rate [kg/m^2/h], t_{iset} the initial set [h] and W_{bl} the total bleed water [kg/m^2]. The unit for the PS cracking severity is kg/m^2.

Boshoff and Combrinck (2013) state that the PS cracking severity is measured in terms of the amount of water evaporated from the concrete. The model provides a good indication of the degree of PS cracking severity, as illustrated in Figure 2-21. The figure shows the PS cracking severity values plotted against the PS cracking area of the concrete.

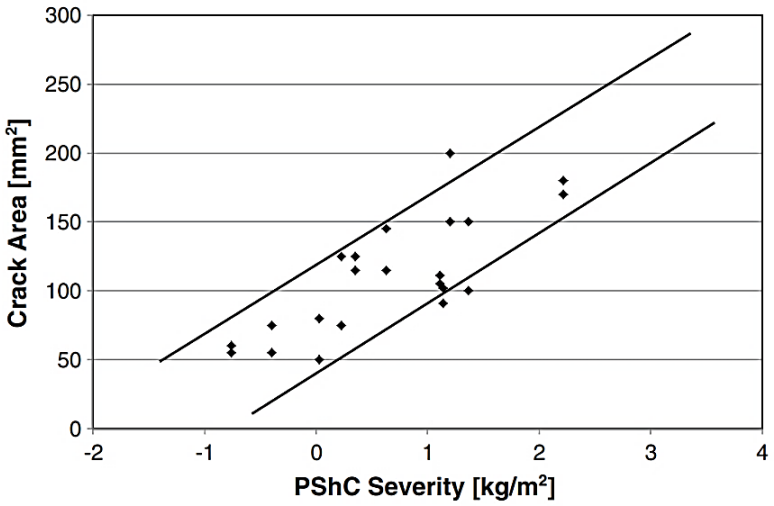

Figure 2-21: The graph shows the PS cracking severity against the measured PS crack area (Boshoff and Combrinck, 2013)

The model also showed that the severity of PS cracking is reduced by adding fibres at low volumes (Boshoff and Combrinck, 2013). The proposed model had a few shortcomings. It has been noticed that cracking has occurred in concrete at a PS cracking severity of 0 kg/m^2 (Boshoff and Combrinck, 2013). This is believed to be due to some interaction between PS cracking and plastic settlement cracking. Another shortcoming noted by Boshoff and Combrinck (2013) was that the severity of PS cracking was inconsistent with the varying volumes of fibres. It should be noted that the suggested model has not been tested with concretes with different admixtures.

2.9.3 Sayahi *et al*. (2021) Plastic Shrinkage Cracking Severity Model

Sayahi *et al*. (2021) suggested a model for estimating the severity of the PS cracking by using a similar approach to that of Boshoff and Combrinck (2013). The initial setting time was used

in the proposed model of Boshoff and Combrinck (2013); however, it was only used to determine the amount of evaporated water within the bulk of the concrete. The additional initial setting time term in Sayahi *et al.*'s model explains the PS cracking in concrete with equal PS cracking severity values, $(ER \cdot t_{iset} - W_{bl})$, but various initial setting times (Sayahi *et al.*,2021). The model is expressed as:

$$C_s = (ER \cdot t_{iset} - W_{bl}) \cdot t_{iset} \quad (2.4)$$

Where ER is the evaporation rate [kg/m^2/h], t_{iset} the initial set [h] and W_{bl} the total bleed water [kg/m^2]. The unit for the severity of PS cracking, C_s, is kg.h/m^2.

Figure 2-22 shows the predicted severity of PS cracking values against the crack area. A direct proportion was noticed in the figure between the severity of PS cracking and the crack area, with only one mixture not following the trend. The model was confirmed with a Self-Compacting Concrete (SCC) and vibrated concrete (Sayahi *et al.*, 2021). Sayahi *et al.* (2021) concluded that according to the model, the tendency for PS cracks to forming in concrete is related to the rate at which the CP increases between the drying time and initial set. The study showed that the proposed model is a helpful tool for estimating the severity of PS cracking in concrete. However, the model is only applicable for concrete with similar restraints, or the severity of the PS cracking values will be scattered. Sayahi *et al.* (2021) stated that the model is significantly dependent on the measuring techniques. Additionally, the model was validated using limited data from earlier literature, and therefore further investigation is required.

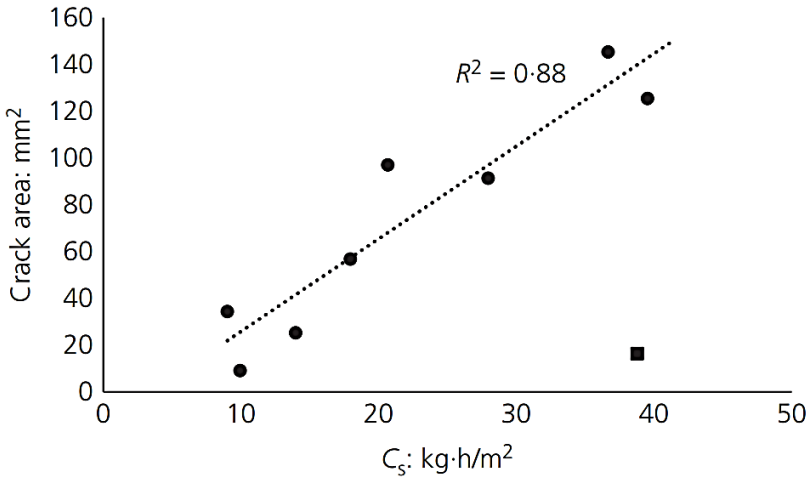

Figure 2-22: The severity of PS cracking values plotted against the measured average crack area from Sayahi *et al.* (2021) using reported data from Sayahi *et al.* (2016)

In both the PS cracking severity model proposed by Boshoff and Combrinck (2013) and Sayahi *et al.* (2021) it was noticed that the PS cracking severity was determined between the drying time and initial setting time of the concrete.

2.9.4 Ghoddousi *et al.* (2019) Plastic Shrinkage Cracking Area Model

A model was proposed by Ghoddousi *et al.* (2019) for predicting the PS cracking area of SCC. The proposed model was developed by testing thirteen SCC mixtures and investigating the influence of different w/c ratios, cement paste volumes, additives and proportion of coarse aggregate to total aggregate on PS. The model for predicting PS cracking area is:

$$PC = \frac{33.73R \cdot (E - B)}{(100(4094D_{av} - 8730V_p + 5320w_c + 1318))} \quad (2.5)$$

Where R is the restraining factor (%), E the total evaporation from the unit concrete surface [g] and B the total bleeding from the unit concrete surface [g]. Furthermore, where D_{av} is the average diameter of the aggregate [cm], V_p the paste volume [m^3/m^3] and lastly w_c the w/c ratio. The PS cracking area, PC, determined from the model, has the units cm^2/m^2.

The model can be used for an initial estimate of the PS cracking area in SCC mixtures. Figure 2-23 shows the predicted PS cracking versus the actual PS cracking area and a 45 ° line. As shown in the figure, the model predicted lower cracking areas than the actual values. The shortcoming of this model is that the model can only be used on SCC concrete and only to provide an estimate of the PS cracking area (Ghoddousi *et al.*, 2019).

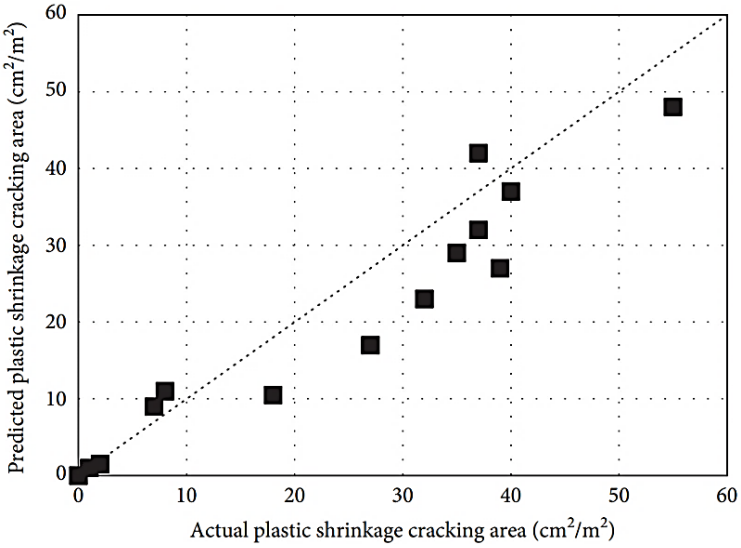

Figure 2-23: The actual PS cracking area against the predicted PS cracking area (Ghoddousi *et al.*, 2019)

When comparing the discussed models, the models could not provide an estimate of a threshold or critical point when PS cracks occur. In addition, the performance of the models in preventing PS cracking in real-time has not been evaluated.

2.10 CAPILLARY PRESSURE SENSORS AND TENSIOMETERS

In previous literature, the CP in concrete was measured using an electrical pressure sensor or a wireless CP sensor (Slowik *et al.*, 2008; Combrinck, 2011; Slowik *et al.*, 2014; Combrinck, 2016). Although these sensors were useful in measuring the CP, the sensors had some shortcomings.

A tensiometer is a device that can directly measure negative pore water pressure (le Roux, 2020; Jacobsz, 2021). Even though tensiometers are mainly used to measure negative pore pressure in soil, these sensors can be beneficial for use in concrete. In this section, the electrical pressure sensor, wireless CP sensors and tensiometers are briefly discussed.

2.10.1 Electrical Pressure Sensor and Wireless Capillary Pressure Sensor

Figure 2-24 a) and b) show both sensors used for measuring CP in concrete. The electrical pressure sensor shown in Figure 2-24 a) consists of a pressure transducer connected to a metal tube filled with water (Slowik *et al.*, 2008; Combrinck, 2011; Combrinck, 2016). Based on the results from Slowik *et al.* (2008), this sensor could measure a maximum CP of about -80 kPa before air entry. When air bubbles reached the pressure transducer in the system, the pressure transducer can no longer measure the CP. The point of air entry can also be referred to as the cavitation. The disadvantages of the electrical pressure sensor are that the concrete has to be placed in a mould (shown in the figure) for the sensor to measure the CP and also the low negative CP readings before cavitating.

The wireless CP sensors shown in Figure 2-24 b) consist mainly of a pressure transducer connected to a water filled measurement tip and power supply. The figure also shows that CP sensors had sensors for measuring the climatic conditions. However, based on the findings of Slowik *et al.* (2014), the sensor was only capable of measuring CP of about -34 kPa before air entered the sensor. The advantage of the wireless CP sensors is the wireless functionality of the sensor and the ability to measure the climatic conditions. The disadvantage of this sensor is not being able to measure high negative CP readings before cavitating.

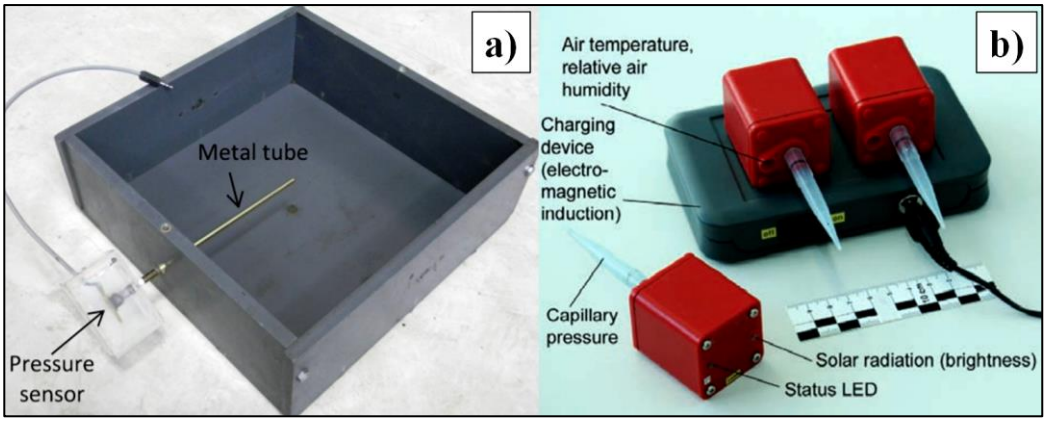

Figure 2-24: Example of a) electrical pressure sensors and b) a wireless CP sensor (Combrinck, 2016; Slowik *et al.*, 2014)

2.10.2 Tensiometers

Tensiometers typically consist of a porous ceramic, water reservoir, spacer, ceramic transducer and a tensiometer body, as illustrated in Figure 2-25. It also shows the dimensions of a tensiometer in millimetres.

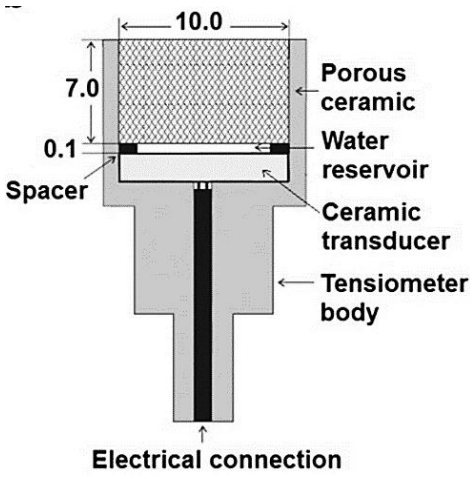

Figure 2-25: Tensiometer design from Toll *et al.* (2013), which was adapted from Lourenço *et al.* (2006)

For tensiometers to measure negative pore water pressure, a continuous link between the transducer and pore water is needed, which means that the porous ceramic and water reservoir needs to completely be filled with water with no air bubbles (le Roux, 2020). Air bubbles in this system can cause early cavitation. Therefore, to completely fill the tensiometer with water, the tensiometer must be saturated to a high degree (le Roux, 2020). The saturation procedure consists of applying high water pressure to the tensiometers to remove any air in the porous ceramic and the water reservoir effectively. The calibration procedure calibrates the

tensiometers with positive water pressure and uses linear extrapolation to determine the negative pore pressure readings (Toll *et al.*, 2013).

After placing the saturated tensiometer in the soil and the water content reduces in the soil, the tensiometer starts to measure the direct suction or negative pressure in the soil (Raviv and Lieth, 2008; Toll *et al.*, 2013).

The advantage of tensiometers is that tensiometers allow for direct measurements of suctions in the soil of up to 2500 kPa, even though most soil measurements have been limited to suctions of 1000 kPa (Toll *et al.*, 2013). Tensiometers are useful for laboratory testing and long-term on-site measurements (Toll *et al.*, 2013; le Roux, 2020). Lastly, a tensiometer is a low-cost device and can be built for the required negative pore pressure reading (le Roux, 2020). The disadvantages of tensiometers are the saturation and calibration procedure, which could be improved. (Toll *et al.*, 2013).

For the full details on tensiometers as well as the saturation and calibration procedure refer to Toll *et al.* (2013) or le Roux (2020).

When comparing the sensors, the previous sensors could only measure low negative CP values before cavitating. In comparison, tensiometers were able to measure high suction values, which can prove to be beneficial for measuring the negative CP in concrete.

2.11 GUIDANCE FROM THE LITERATURE REVIEW

The literature review aimed to provide a brief overview of current knowledge regarding PS cracking, relevant empirical models and methods aiding in the prevention of PS cracking. In addition, the literature review supplied knowledge on tensiometers required for this study.

Influencing factors and mechanisms that cause PS cracking in concrete were investigated. Numerous researchers emphasised that the CP mechanism is the primary driving force for PS and PS cracking in fresh concrete. The CP mechanism captures all the influencing factors such as bleeding, evaporation, setting time and plastic settlement, and the material composition and specimen geometry that affect the cracking risk (Slowik *et al.*, 2014).

The following recurring terms were noticed in the PS cracking literature: drying time, negative CP build-up, and the initial set. Figure 2-26 shows how the terms relate to the PS cracking phenomenon. The cumulative evaporation and bleeding over time are illustrated in the figure. The figure also shows the drying time, negative CP build-up, crack growth and setting times. It was found that the earlier the concrete reached the drying time, the earlier the negative CP started to build up. As the negative CP build-up starts, various influencing factors can affect

the build-up rate. Slowik *et al.* (2014) showed that when a critical pressure is reached in the negative CP build-up, PS cracking will occur. In addition, the literature showed that the onset of PS cracking occurs close to the initial setting time of the concrete (Combrinck and Boshoff, 2013). It is clear that the negative CP build-up over the elapsed time between the drying time and initial set are crucial parameters in the PS cracking phenomenon.

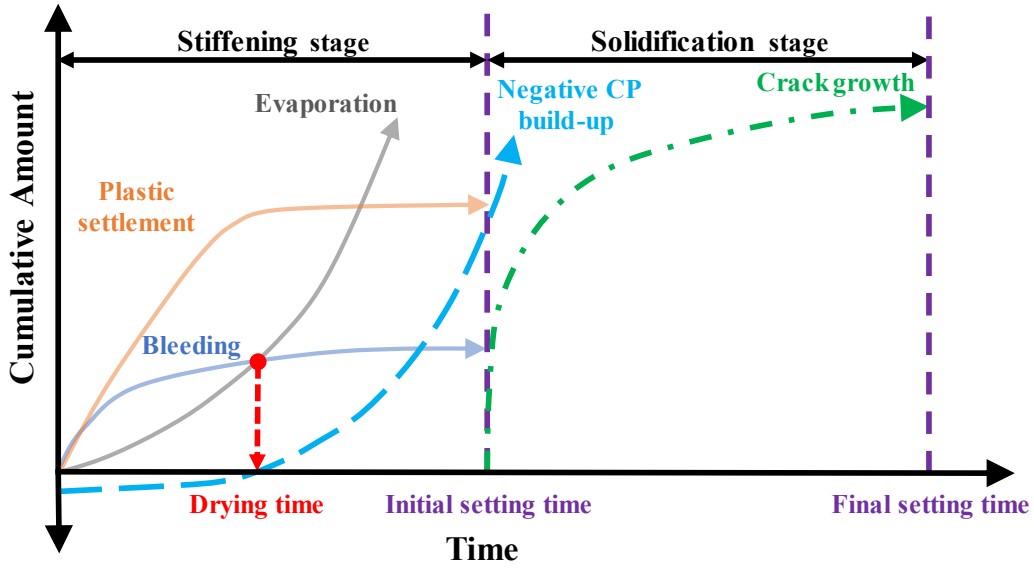

Figure 2-26: Summary of the phenomenological events required for PS cracks to form adapted from Combrinck (2011), Steyl (2016) and Sayahi *et al.* (2020)

Some of the current methods and models used for preventing PS cracking in fresh concrete were reviewed. It was found that the method for curing concrete by closed-looped controlled rewetting proved to be effective in controlling the negative CP build-up and preventing PS cracking. Conversely, this method requires unique instrumentation to determine the defined pressure threshold for when the concrete surface needs to be rewetted. The PS cracking severity models proposed by Boshoff and Combrinck (2013) and Sayahi *et al.* (2021) proved to be effective in indicating the severity of the PS cracks depending on the severity of the evaporation rate between the drying time and initial set. However, the models were limited to a certain restraint used in the moulds. The models also could not indicate when cracking would not occur. Lastly, the model proposed by Ghoddousi *et al.* (2019) for predicting the PS cracking area could only provide a rough estimate of what the PS cracking area in SCC would be.

Reviewed literature on previous CP sensors and tensiometers showed that the previous sensors lacked the ability to measure high negative CP values. In comparison, tensiometers could measure significantly higher negative pore water pressure directly. It was also found that tensiometers are low-cost devices and can be built for the required pressure readings. In

addition, the device could also be used in a laboratory or on-site and can be helpful in measuring negative CP in fresh concrete.

Based on the literature reviewed, the negative CP is the primary driving force of PS, which takes into account all the factors such as the evaporation rate, bleeding, setting time and plastic settlement that affect PS cracking in the fresh concrete (Wittmann, 1976; Slowik *et al.*, 2008; Slowik *et al.*, 2014; Ghourchian *et al.*, 2021). It was also found that the mechanism could be manipulated and controlled to reduce the risk of PS cracking. However, no research has been found that uses the CP mechanism in an empirical model to assist in preventing PS cracking. Investigating the mechanisms and crucial time points in PS to develop a model that aids in preventing PS cracking in concrete will contribute to a better understanding of the CP mechanism and PS cracking phenomenon.

3 MODEL CHARACTERISATION

3.1 INTRODUCTION

The literature showed that numerous factors and mechanisms influence Plastic Shrinkage (PS) and PS cracking in concrete. In this chapter, the No Cracking Capillary Pressure (CP) Boundary Model is developed based on the primary mechanisms and factors influencing PS cracking in fresh concrete.

The proposed No Cracking CP Boundary Model is a Conceptual Model that utilises the pressure-time area under a no crack negative CP build-up curve between the drying time and initial setting time of the concrete. The pressure-time area is used to determine the no cracking CP boundary to prevent PS cracking in the same concrete at higher negative CP build-up rates. The mechanisms and factors influencing PS cracking utilised in the development of the model are discussed. After which, the derivation of the No Cracking CP Boundary Model and the required model parameters are discussed. Furthermore, the determination of the critical pressure limit and the time at which this limit is reached, and significance of the model are covered.

3.2 CHARACTERISTICS OF PLASTIC SHRINKAGE CRACKING AND NEGATIVE CAPILLARY PRESSURE

PS cracking in fresh concrete is caused by a complex combination of parameters that can change at any moment, making this phenomenon challenging to predict. However, some trends have been notices from the literature and previous models and the CP, drying time and initial setting time were identified as the properties of fresh concrete that can be used to develop an empirical model to control PS cracking.

In terms of the CP, Wittmann (1976) and Slowik *et al.* (2008) showed that the negative CP is the primary mechanism for PS in fresh concrete. Slowik *et al.* (2014) concluded that the CP mechanism captures all the influences of the climatic conditions, specimen geometry and material composition on the cracking risk of the concrete. The findings from Slowik *et al.* (2008) and Schmidt and Slowik (2009) showed that by rewetting the concrete when a predefined CP threshold was reached, the negative CP build-up could be controlled and delayed, preventing PS cracking.

The drying time is the point in time at which the cumulative amount of evaporation is equal to the cumulative amount of bleeding of the concrete (Kwak and Ha, 2006). It is the point in time at which the CP changes from positive to negative. After the drying time, the evaporation of

moisture from the concrete surface is faster than the moisture can bleed from the concrete mass to the surface. This results in negative CP build-up and PS.

The initial setting time is the point in time when the fresh concrete changes from the stiffening stage to the solidification stage. According to Combrinck and Boshoff (2013), the PS cracking onset typically occurs close to the initial setting time of the concrete.

Boshoff and Combrinck (2013) and Sayahi *et al.* (2021) found that the severity of PS cracking in concrete was directly proportional to the product of the volume of evaporated water from the pore network inside the concrete between the drying time and initial setting time.

The trends noticed in the literature for the CP, drying time and initial setting time can also be demonstrated in Figure 3-1 and Figure 3-2. Figure 3-1 is a schematic illustration of the negative CP build-up curve at three different build-up rates. Figure 3-2 shows the pressure-time area under the curves in Figure 3-1. Figure 3-1 shows that the elapsed time to drying time decreases when the negative CP build-up rate increases. When the negative CP build-up rate decrease, the elapsed time to drying time increases. Conversely, the negative CP at initial set increases when the negative CP build-up rate increases and decreases when the negative CP build-up rate decreases.

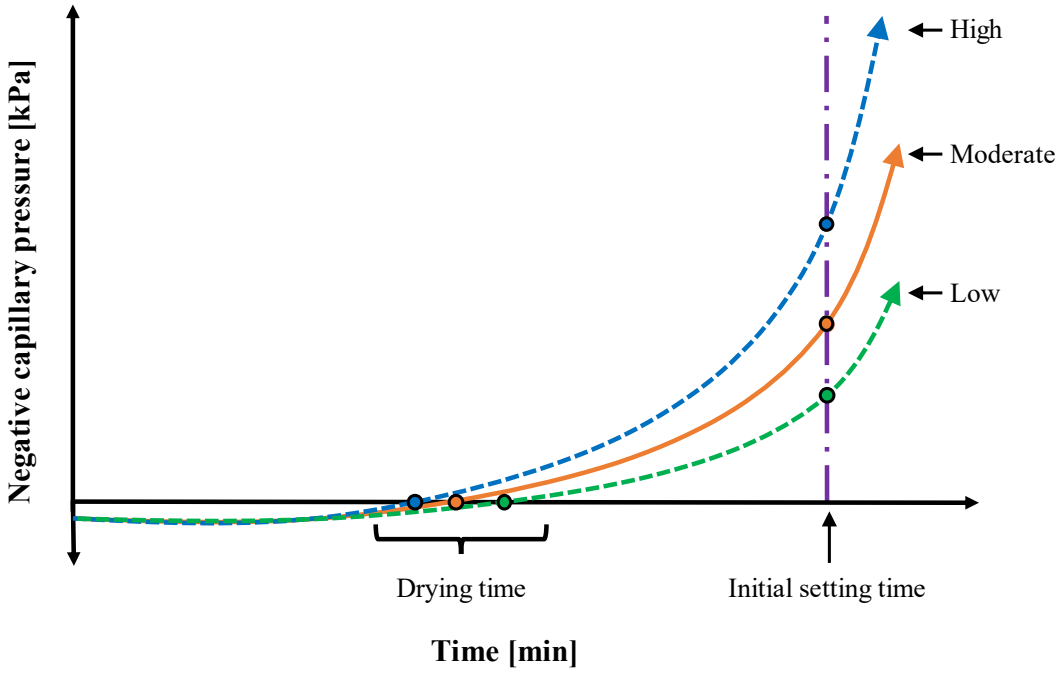

Figure 3-1: A schematic of the negative CP build-up at three different build-up rates

Figure 3-2 shows the pressure-time areas found for the three build-up rates when the area under the negative CP build-up between the drying time and initial setting time is considered. Using the pressure-time area under the negative CP build-up adds a time aspect to the negative CP

build-up in concrete. The figure shows that a high negative CP build-up rate will result in a larger area, while a low negative CP build-up rate will result in a smaller area. This pressure-time area represents the part of PS induced by the negative CP build-up between the drying time and initial set of the concrete. The higher the negative CP build-up rate, the greater the part of PS induced by the negative CP build-up between the drying time and the initial setting on the concrete.

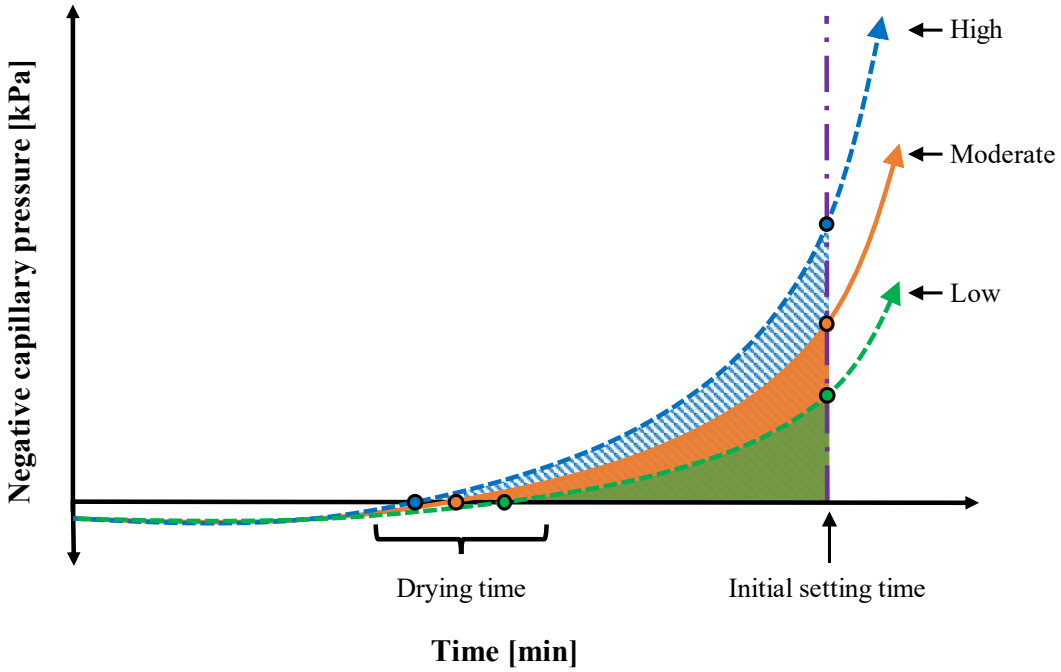

Figure 3-2: A schematic of the pressure -time area under the three different build-up rates

Considering, the effect of negative CP build-up rate between the drying time and initial set, it can be argued that the negative CP build-up rate between these two points is a primary driver of PS and PS cracking (Slowik *et al.*, 2014; Kwak and Ha, 2006; Combrinck and Boshoff, 2013). Negative CP build-up rate, drying time and initial set are thus the characteristics of negative CP curve of fresh concrete that are used as parameters to develop an empirical model that provides guidance on preventing PS cracking.

3.3 THE NO CRACKING CAPILLARY PRESSURE BOUNDARY MODEL

The proposed No Cracking CP Boundary Model is developed from the negative CP build-up rate, the drying time and the initial setting time. The parameters are used to determine the pressure-time area under the negative CP build-up from the drying time to the initial setting time of the concrete. This pressure-time area is a measure of the PS induced by the negative CP build-up in the mentioned timeframe.

It is assumed that for no PS cracks to form, the pressure-time area for a curve with a high negative CP build-up rate, must be equal to the pressure-time area of the no crack CP build-up curve. For the pressure-time areas to be equal, a no cracking CP boundary must be applied. The negative CP of the high negative CP build-up rate concrete must be maintained under this boundary. This boundary can be applied by determining a critical pressure limit on the high negative CP build-up. The higher the negative CP build-up rate, the lower the no cracking CP boundary will be to ensure that the pressure-time area remains equal to the no crack negative CP build-up curve.

The model concept can be explained with the schematic illustrations in Figure 3-3 and Figure 3-4. Figure 3-3 shows two negative CP build-up curves at different build-up rates that passes the initial setting time of the concrete at t_{iset}. The negative CP build-up rate of $g(t)$ is greater than that of $f(t)$. The upper curve, $g(t)$, is the negative CP build-up curve of fresh concrete that will form PS cracks. The second curve, $f(t)$, is the negative CP build-up of the same fresh concrete that will not form PS cracks. If the negative CP build-up rate of $f(t)$ were any higher, PS cracking would occur.

Figure 3-3 also shows the pressure-time area under the negative CP build-up between the drying time and the initial set for $g(t)$ and $f(t)$. The area under $g(t)$ is greater than the area under the no crack curve $f(t)$.

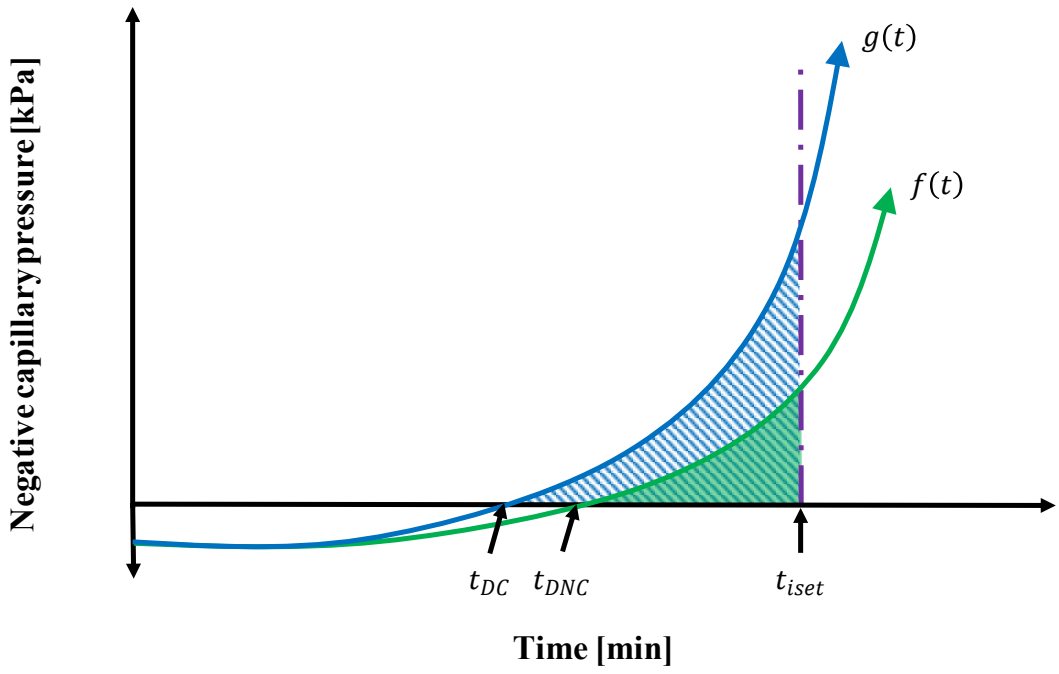

Figure 3-3: The schematic of the negative CP build-up and pressure -time areas of, $g(t)$ that will have PS cracking and $f(t)$ that will have no PS cracking

By applying the No Cracking CP Boundary Model, it is proposed that for no PS cracks to occur on the concrete of $g(t)$, the pressure-time area under $g(t)$ must be equal to the pressure-time area under the no crack curve $f(t)$. For the area under $g(t)$ to be equal to the area under $f(t)$, a no cracking CP boundary must be applied at a specific time to the negative CP build-up curve $g(t)$. The CP of the concrete needs to be maintained under the boundary. Figure 3-4 shows the two negative CP build-up curves, $g(t)$ and $f(t)$, where no cracking CP boundary is applied to curve $g(t)$. The figure illustrates that for the area, A_C, to be equal to the area, A_{NC}, a no cracking CP boundary must be applied to curve $g(t)$ at a specific time, t_B. The no cracking CP boundary marks the critical pressure limit, P_B, for area A_C, for curve $g(t)$ to be maintain under.

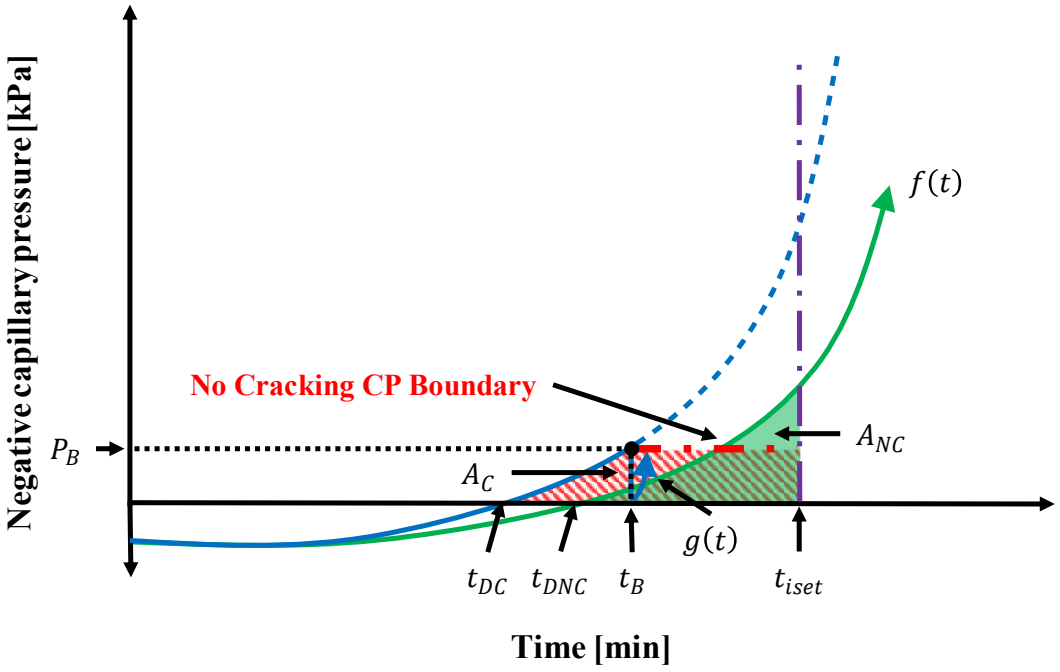

Figure 3-4: The schematic of the negative CP build-ups of $g(t)$ and $f(t)$ with equal pressure-time areas after applying the model concept

Therefore, the critical pressure limit, P_B and corresponding time, t_B needs to be determined to apply the no cracking CP boundary to a negative CP build-up. The critical pressure limit and corresponding time can be derived from Figure 3-4 by considering:

$$A_{NC} = A_C \tag{3.1}$$

Where A_{NC} is the maximum area of the negative CP build-up curve of concrete that will not form PS cracks [kPa.min] and A_C is the area of the negative CP build-up curve of concrete that will form PS cracks [kPa.min].

The pressure-time area of A_{NC} and A_C can be found by integrating the required regions:

$$\int_{t_{DNC}}^{t_{iset}} f(t)\,dt = \int_{t_{DC}}^{t_B} g(t)\,dt + P_B \cdot (t_{iset} - t_B) \tag{3.2}$$

Where t_{iset} is the initial setting time [min], t_{DNC} the drying time of the no crack negative CP build-up curve [min] and t_{DC} drying time of the negative CP build-up curve of the concrete that will form PS cracks [min]. Furthermore, t_B is the time correlating to the critical pressure limit [min] and P_B the critical pressure limit [kPa].

The expression for the negative CP build-up of $f(t)$ and $g(t)$ is unknown, making it challenging to calculate the area under the negative CP build-up with equation (3.2). Therefore, the Trapezoidal rule is used to calculate the areas under the negative CP build-up curves. By substituting the Trapezoidal rule into the previous expression, the no cracking CP boundary equation is found.

$$\frac{h}{2}\left[f(t_{DNC}) + 2\sum_{a=1}^{n-1} f\left(t_{1_a}\right) + f(t_{iset})\right] = \frac{h}{2}\left[g(t_{DC}) + 2\sum_{b=1}^{m-1} g\left(t_{2_b}\right) + g(t_B)\right] + P_B \cdot (t_{iset} - t_B),$$

$$a = 1, 2, \dots, n-2, n-1 \tag{3.3}$$

$$(where\ t_{1_0} = t_{DNC}\ and\ t_{1_n} = t_{iset})$$

$$and$$

$$b = 1, 2, \dots, m-2, m-1$$

$$(where\ t_{2_0} = t_{DC}\ and\ t_{2_m} = t_B)$$

Where h is the time intervals [min] used to determine the pressure-time areas.

By simplifying equation (3.3), the no cracking CP boundary equation can be expressed as:

$$T_{RNC} = T_{RC} + P_B \cdot (t_{iset} - t_B) \tag{3.4}$$

Where T_{RNC} is the Trapezoidal rule estimate for the area under $f(t)$ [kPa.min] and T_{RC} the Trapezoidal rule estimate for the area under $g(t)$ between the drying time and the time when the no cracking CP boundary is applied [kPa.min].

Hence, the No Cracking CP Boundary Model is found. By maintaining the negative CP build-up of $g(t)$ below the no cracking CP boundary which marks P_B, to obtain the same pressure-time area as that of the no crack CP build-up $f(t)$, PS cracking could be prevented.

3.4 THE NO CRACKING CAPILLARY PRESSURE BOUNDARY MODEL DETERMINATION

To apply the proposed model in real-time or with previous CP measurements, equation (3.3) is used to calculate the critical pressure limit and the time at which this limit is reached. Equation (3.3) sets the pressure-time area of the no crack curve equal to the pressure-time area of the curve where PS needs to be prevented. Only three model parameters are required for this equation:

- the area under the no crack negative CP build-up for the relevant concrete
- the drying time of the current negative CP build-up
- the initial setting time of the relevant concrete

The critical pressure limit can then be determined by adding the negative CP measurements and the corresponding time after the current drying time into P_B and t_B into equation (3.3). The CP measurements and corresponding time is added at 60-second intervals until the pressure-time area is equal to the area T_{RNC}. The 60-second intervals were decided on to provide sufficient accuracy to determine the pressure-time area and notice any sudden changes in the negative CP build-up rate. When the critical pressure limit is reached, the negative CP build-up will need to be reduced by rewetting the concrete. The no cracking CP boundary marks the critical pressure limit and is applied when the pressure limit is reached. The negative CP build-up is reduced by rewetting the concrete surface each time the no cracking CP boundary is reached.

The benefit of the proposed empirical model is that the model only requires three parameters and can be applied in real-time and with previous CP measurements in fresh concrete to help prevent PS cracking.

3.5 CONCLUSION

The No Cracking CP Boundary Model was proposed and discussed in this chapter. Based on discussing the mechanisms and factors influencing PS cracking used to develop the model, the

derivation, and limit parameters determination, the proposed model can be utilised to prevent PS cracking.

The discussed model is a conceptual model that will have limitations. Therefore, it is required to verify the No Cracking CP Boundary Model and identify the limitations. To do this, the following properties of a concrete mix are needed:

- The drying time and initial set time of the relevant concrete mix.
- The no crack CP build-up curve of the relevant concrete mix.
- The negative CP build-up curve of the relevant concrete mix at a higher negative CP build-up rate.
- The parameters for the no cracking CP boundary: the critical pressure limit and estimated time when this value will be reached.

4 EXPERIMENTAL FRAMEWORK

4.1 INTRODUCTION

The purpose of the experimental work was to test and verify the proposed No Cracking Capillary Pressure (CP) Model. The experimental work therefore consisted of two testing phases. The two testing phases were conducted on two concrete mixtures. In the first phase, the Plastic Shrinkage (PS) properties of the concrete mixtures at different evaporation rates were tested to find the model parameters. The second phase consisted of using the model parameters to test and verify the model with the relevant concrete.

The experimental outline for the testing phases and the test objectives is presented in this chapter. The setup used for the experimental tests, tensiometer and No Cracking CP Boundary Model, are discussed. Materials and material properties used and the mix design for the two concrete mixtures are covered. The procedures followed for mixing, casting and testing the different PS properties of the concrete mixtures are also covered.

4.2 EXPERIMENTAL OUTLINE

Throughout the study, a quantitative approach was followed to verify the proposed No Cracking CP Boundary Model. Two distinctive testing phases were conducted, namely:

- the PS cracking characterisation phase
- the model verification phase

4.2.1 Plastic Shrinkage Cracking Characterisation Phase

In the PS cracking characterisation phase, the properties of two concrete mixtures were tested at various evaporation rates. A low bleed concrete mixture was tested at six evaporation rates ranging between 0.1 and 0.9 kg/m^2/h. Furthermore, a Self-Compacting Concrete (SCC) mixture (for verification) was tested at two evaporation rates ranging between 0.1 and 0.4 kg/m^2/h. The concrete was evaluated to obtain the required model parameters for the No Cracking CP Model, such as the initial setting time, drying time and a no crack negative CP build-up curve.

The required model parameters were found by conducting non-environmental and evaporation tests to obtain the properties summarised in Table 4-1. The table shows the number of measurements taken during each evaporation test and the number of evaporation rates at which the two concrete mixtures were exposed.

The table shows that only the low bleed concrete setting times were determined by the Penetration Resistant Test Method and the Vicat Test Method. The two test methods were conducted to decide how the concrete setting time would be determined throughout the study. The initial setting time measurements found for the low bleed concrete and SCC mixture was used to determine the testing duration for the respective concrete mixtures throughout the study.

Three concrete PS cracking specimens, three evaporation specimens and one plastic settlement specimen were tested during the evaporation test to obtain the summarised properties. The properties determined in the evaporation tests were measured over the test duration.

Table 4-1: Summary of the test measurements conducted in the initial phase

Tests	Properties	Measurements	Total evaporation rates	
			Low bleed concrete	Self-compacting concrete
Non-environmental	Setting times (Penetration Resistance test)	2	-	-
	Setting times (Vicat test)	2 (Only done for the low bleed concrete)		
	Bleeding	2		
Evaporation	Climatic conditions	3/evaporation rate	6	2
	Evaporation rate	3/evaporation rate		
	Capillary pressure	6/evaporation rate		
	Plastic shrinkage cracking	3/evaporation rate		
	Volumetric moisture content	3/evaporation rate		
	Concrete surface temperature	3/evaporation rate		
	Concrete internal temperature	3/evaporation rate		
	Plastic settlement	1/evaporation rate		

4.2.2 Model Verification Phase

In the model verification phase, the model parameters obtained from the low bleed concrete and SCC were used to test and verify the No Cracking CP Boundary Model. The model was verified by evaluating the model's performance with previous and live CP measurements.

The previous phase's low bleed concrete CP measurements were used to test the model's performance. The results in this section were then used to establish if the model could be simplified for on-site use.

Model Tests A and B were conducted in real-time. In Model Test A, the model was tested with the low bleed concrete at three evaporation rates ranging between 0.3 and 0.9 kg/m^2/h. This was done to determine whether the model could aid in reducing or preventing PS cracking. In Model Test B, the model was tested with the SCC at two evaporation rates ranging between 0.3 and 0.8 kg/m^2/h. This test was used to verify whether the model could prevent or reduce PS crack in a special type of concrete. The findings for the two tests were then used to identify possible limitations that the model might have and to calibrate the model.

The measurements conducted during the two model tests are summarised in Table 4-2. The number of evaporation rates and the number of measurements conducted is shown in the table. Three concrete PS cracking specimens, three evaporation specimens and one plastic settlement specimen were tested during one model test to obtain the measurements summarised in the table. All the properties were measured throughout Model Tests A and B.

Table 4-2: Summary of the test measurements conducted in the second phase

Tests	Properties	Measurements per evaporation rate	Total evaporation rates	
			Low bleed concrete	Self-compacting concrete
Model	Climatic conditions	3	3	2
	Evaporation rate	3		
	Capillary pressure	6		
	Plastic shrinkage cracking	3		
	Volumetric moisture content	3		
	Concrete surface temperature	3		
	Concrete internal temperature	3		
	Water added (Rewetting)	3		

4.3 TEST OBJECTIVES

The following test objectives were set during the study to achieve the primary objective of the study:

- Determining whether there is a difference in setting times between the Penetration Resistance Test Method (ASTM C403/C403M – 16) and Vicat Test Method (SANS 50196-3:2006/EN 196-3:2005) for the same concrete mixture.
- Determine whether the amount of bleeding is influenced by the depth of the concrete.
- Determining the model parameters: the no crack negative CP build-up curve, drying time and initial set for the low bleed concrete and SCC.
- Determining whether PS cracking can be prevented by controlling the negative CP build-up.
- Establishing if the proposed No Cracking CP Boundary Model can help prevent PS cracking by maintaining the negative CP build-up below the no cracking CP boundary.

4.4 EXPERIMENTAL SETUP

The experimental test setup done for the evaporation rates and sensors for the evaporation tests and model tests are covered. The non-environmental tests are also discussed in this section.

4.4.1 Evaporation Rates

The temperature-controlled room, humidity-controlled room and the Mobile Climate Chamber (MCC) were used to obtain the various evaporation rates needed. The required climatic conditions for the climatic rooms and chamber to be set at were obtained by estimating and initial evaporation rate using equation (2.1). The setups used in each climatic room and chamber are described.

i Temperature-controlled and Humidity-controlled Room

The temperature-controlled room is an enclosed room designed to maintain a constant temperature and prevent any external climatic conditions from penetrating the room and influencing the experiments inside the room. The room was set at a constant air temperature of 24 °C (±1 °C) for the evaporation tests.

The humidity-controlled room is similar to the temperature-controlled room, but this room has the feature of increasing the relative humidity to 95 % (±5 %). The humidity-controlled room

was set at an air temperature of 24 °C (±1 °C) and relative humidity of 65 % (±5 %) for the required evaporation tests.

The test setup used for the evaporation tests in the temperature, as well as the humidity-controlled room, are shown in Figure 4-1. The figure shows where the PS cracking specimens, evaporation specimens, plastic settlement specimen (the arrow pointing to the left side), fans and data acquisition system were placed during the tests conducted in these climatic rooms. The PS cracking specimens (the rectangular specimens) were placed 50 mm from the fans and parallel with the wind direction, the evaporation specimens (the cylindrical specimens) were placed next to the PS cracking specimens and parallel to the wind direction of each PS cracking specimen. The plastic settlement setup is discussed in Section 4.4.2.

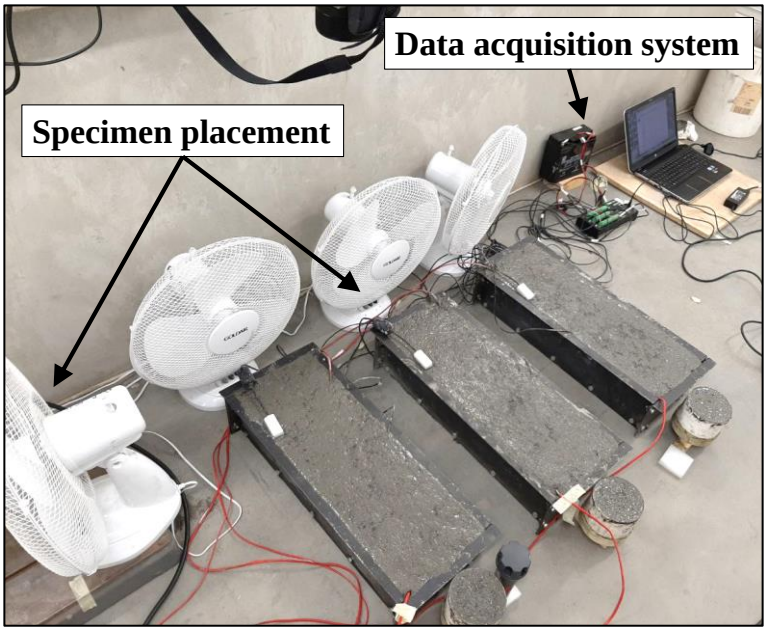

Figure 4-1: The temperature-controlled room test setup

ii Mobile Climate Chamber

The MCC illustrated in Figure 4-2 is a portable chamber designed to simulate moderate to harsh weather conditions on concrete or building materials. The MCC consists of a dehumidifier that removes the moisture from the air, two fans for the wind speed, a heating element and a heat extractor to control the air temperature. Chapter 5 provides a detailed discussion on the design and construction of the MCC and the reachable climatic conditions in this chamber.

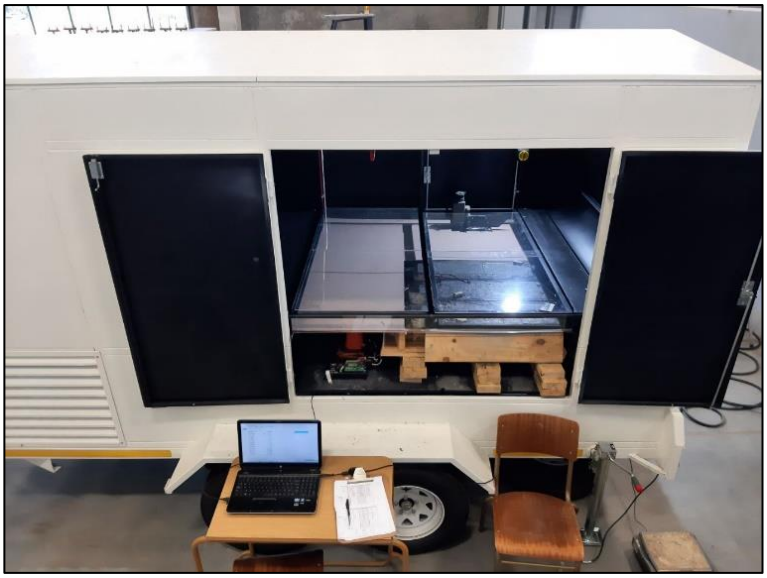

Figure 4-2: The MCC setup

The setup used in the MCC for the three PS cracking specimens, three evaporation specimens and the plastic settlement specimen (the black arrow pointing to the upper right section) is shown in Figure 4-3. This setup was used for the evaporation tests and the model tests. The figure illustrates where all the specimens and the data acquisition system were placed during testing. All the specimens were placed parallel with the wind direction, as shown in the figure, to have a similar setup as in the climate-controlled rooms and ensure comparable test results.

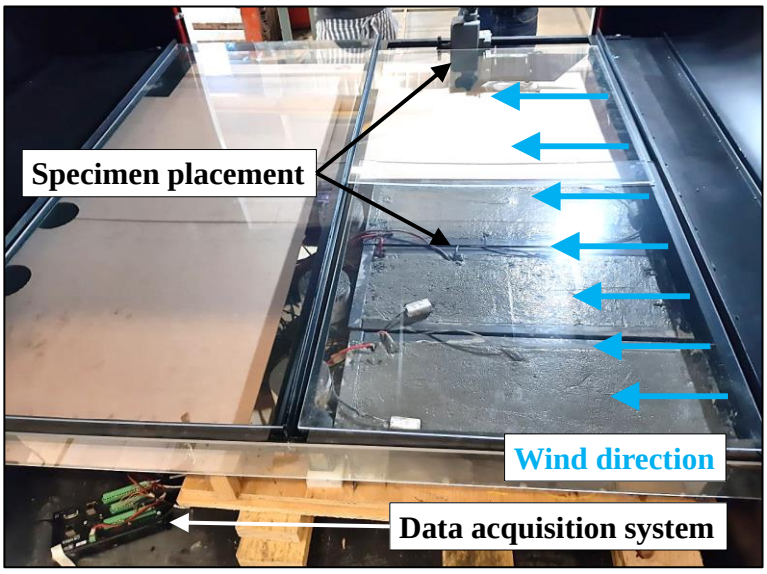

Figure 4-3: Specimen setup in the MCC

4.4.2 Sensor Setup

The sensor setup for the PS cracking specimens and the plastic settlement used throughout both testing phases are discussed.

i PS cracking specimen

Figure 4-4 demonstrates the sensor layout used in each of the three PS cracking specimens to measure the CP, temperature and Volumetric Moisture Content (VMC) of the concrete. These properties were measured using two tensiometers, two thermocouples and one VMC sensor, as shown in the figure. The two tensiometers (1 and 2) were spaced at 200 mm from the end of the mould and embedded at a depth of 32 mm into the concrete to measure the CP behaviour in the surface layer of the concrete. One thermocouple (2) was attached to a tensiometer (1) to measure the internal temperature at the same depth. While the second thermocouple (1) was inserted into the concrete at a depth of 10 mm to measure the temperature at the surface of the concrete. Lastly, the one VMC sensor was inserted 50 mm from the end of the mould into the surface of the concrete at a depth of 54 mm to measure the water content of the concrete. The figure also shows where the crack measurements were taken during the test.

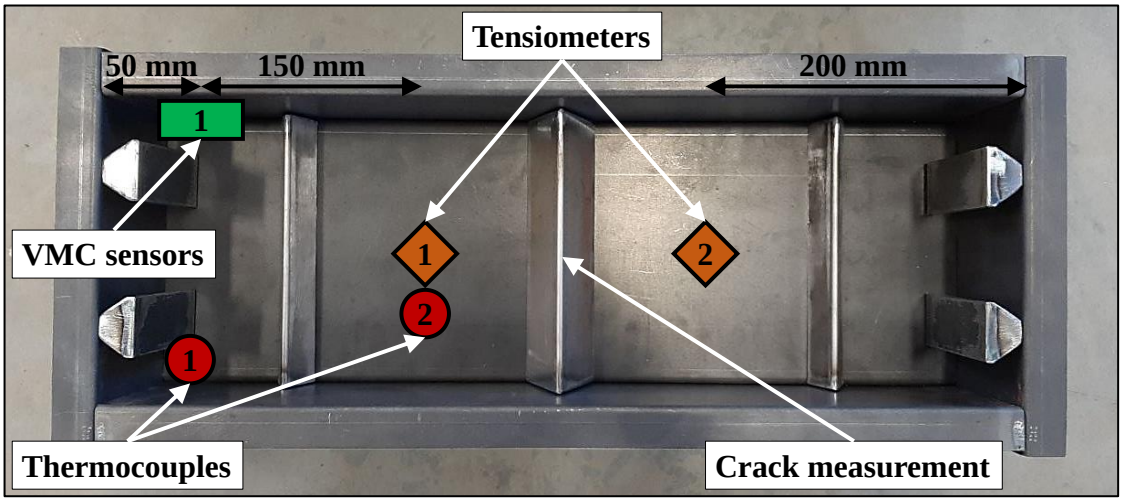

Figure 4-4: Sensor layout used for the PS cracking specimens during the two testing phases

The two tensiometers embedded in the concrete were kept at the desired 32 mm depth using a tenstal illustrated in Figure 4-5 a). The tenstal, is a three-dimensional printed pedestal that kept a tensiometer at the desire position in the concrete. The tenstal positions the ceramic tip of the tensiometer to face upwards to directly measure the CP behaviour close to the concrete surface. Figure 4-5 b) shows how the thermocouple (2) was attached to the tensiometer setup to measure the internal concrete at a 32 mm depth. The tips of the thermocouples were covered with nail polish to protect the thermocouples in the fresh concrete.

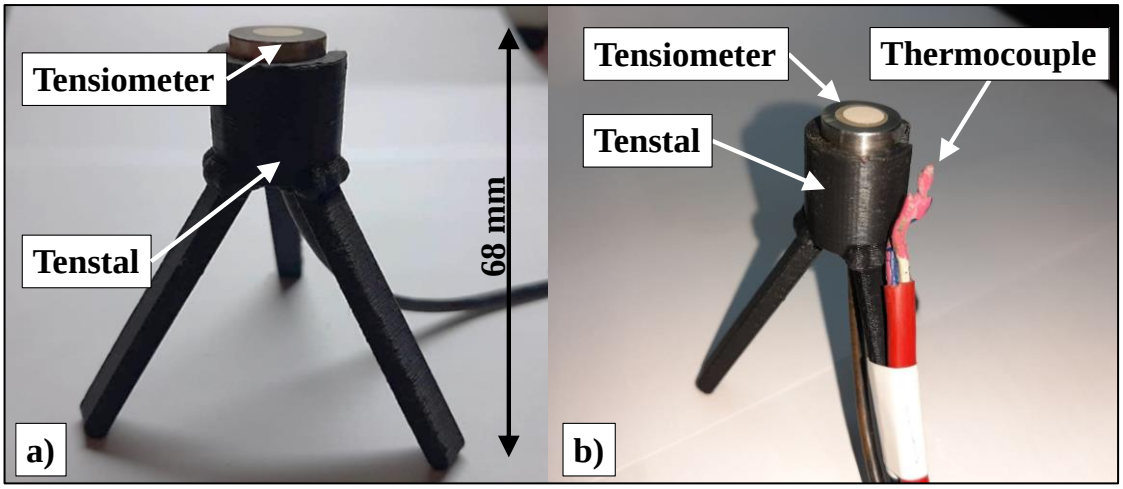

Figure 4-5: Setup for a) tensiometer (2) in the tenstal and b) tensiometer (1) in the tenstal with the attached thermocouple (2)

ii Plastic settlement

The plastic settlement setup during each test is shown in Figure 4-6. Before each evaporation test, the deflector was placed on the plastic settlement specimen, and the high accuracy optoNCDT laser connected to the stand was configured to zero. The range of the optoNCDT laser and the dimensions of the aluminium cone mould is discussed in Section 4.10.7. The bubble wrap seen in the figure was removed during the evaporation tests.

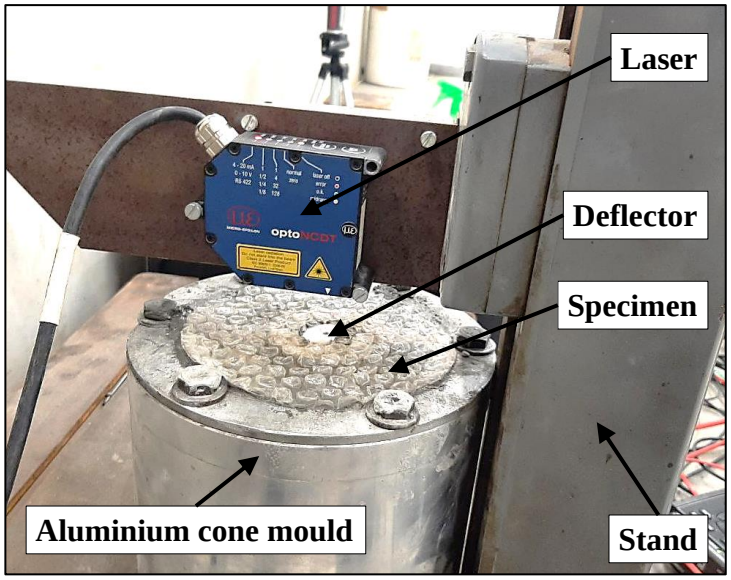

Figure 4-6: Laser and plastic settlement setup

4.4.3 Non-Environmental Test (Standard Test) Setup

The setup for the bleeding tests and the setting times tests conducted in the PS cracking characterisation phase are discussed.

i Bleeding

After filling the bleeding moulds with concrete, the bleeding samples were placed on a flat surface in the humidity-controlled room for the duration of the bleeding test. The room was set at a temperature of 24 °C (±1 °C) and relative humidity of 65 % (±5%). Each of the bleeding moulds had a syringe and a container for measuring the bleed water.

ii Setting times

Figure 4-7 shows the setup used for determining the setting times of the concrete with the Penetration Resistance Test Method (ASTM C403/C403M–16). The Penetration Resistance Test Method was done with the LRX Plus Series Material Testing Machine with a force range of 5 kN. The specimen was placed such that the needle penetrates an undisturbed mortar section. The mortar was tested with penetration needles having the following diameters of 645, 323, 161, 65, 32, and 16 mm. The penetration needle was changed when the load on the apparatus reached 2 kN.

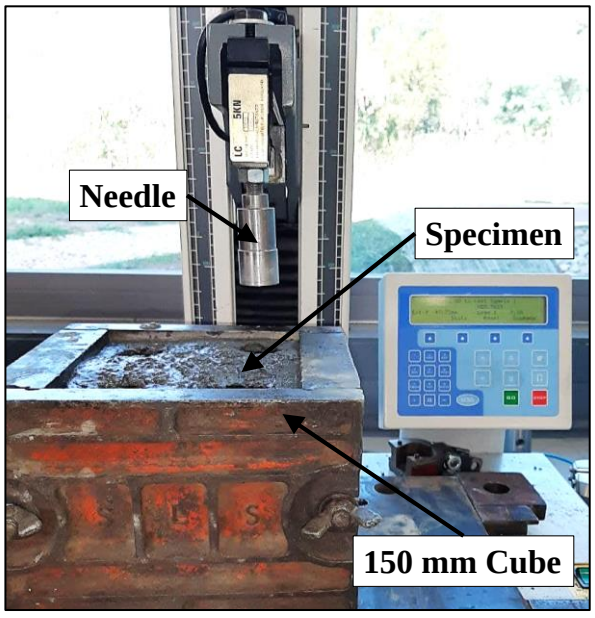

Figure 4-7: Loading apparatus setup for the Penetration Resistance Test Method

The setup used for determining the setting time of the concrete with the Vicat Test Method (SANS 50196-3:2006/EN 196-3:2005) is shown in Figure 4-8. The figure shows that the 300 g

mass penetrates the specimen with the needle. The specimens were cast into the 40 mm deep cone mould with a bottom plate. The initial setting time was determined by using a needle with a length of 45 mm and a diameter of 1.13 mm, and for the final setting time, a ring attachment having a diameter of 5 mm was attached to the needle.

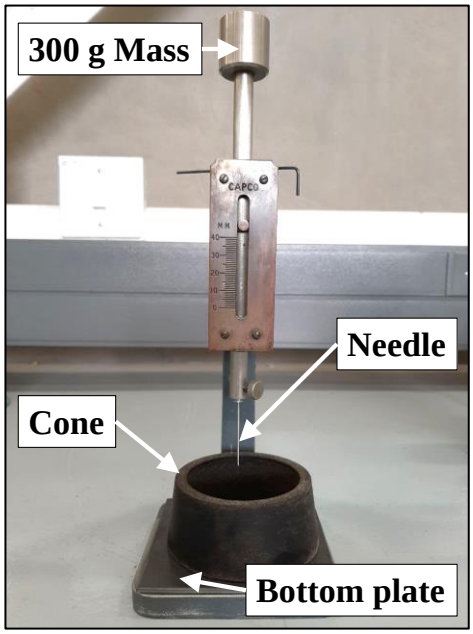

Figure 4-8: The setup used for the Vicat Test Method setup

4.5 TENSIOMETERS

In this study, the University of Pretoria tensiometers were used to measure the negative CP build-up in the concrete mixtures. The design of these tensiometers and the preparation and testing procedures are discussed in this section.

4.5.1 Tensiometer Design

As illustrated in Figure 4-9, the tensiometers consisted of a porous ceramic tip and a pressure sensor glued to the end of the ceramic tip and covered with a stainless-steel cap to protect the sensor and increase sensor's durability. The figure provides the dimensions of the steel cap used in a tensiometer in distinctive colours. Figure 4-10 shows two completed tensiometers. The ceramics tips of the completed tensiometers were capped to have an even surface for the pore water to enter.

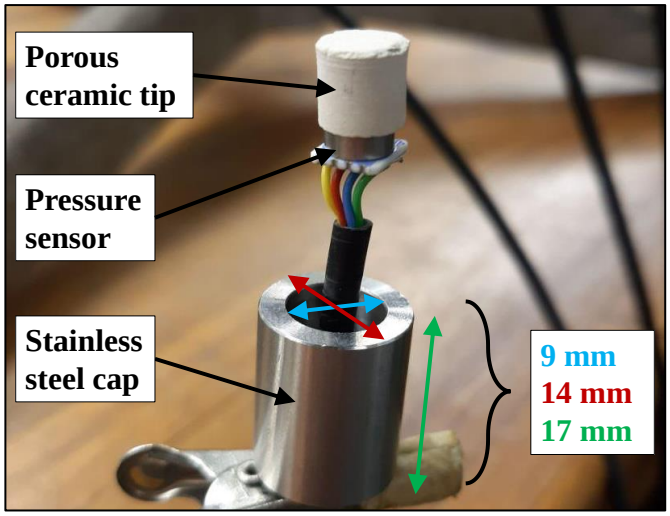

Figure 4-9: Tensiometer before adding epoxy resin

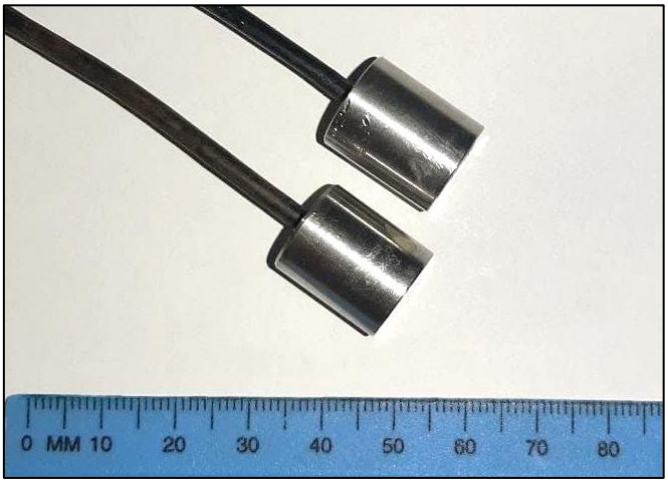

Figure 4-10: Tensiometers after epoxy and caping the ceramic tip

4.5.2 Preparation Procedure

Before starting the saturation procedure, the tensiometers were placed in an oven at 65 °C for 24 hours to ensure that all the water evaporated from the tensiometers. Figure 4-11 illustrates the procedure followed to saturate the tensiometers before each test. The procedure is broken down into the following steps, referring to Figure 4-11. All the valves are assumed to be closed.

a) After opening valves (1.4), (1.2) and (1.1), the deaerator (1) was filled with clean water to the maximum allowable water level. When the deaerator was completely filled, the opened valves were closed (le Roux, 2020).

b) After closing the surrounding valves, valves (2.3) and (2.1) were opened, and the high vacuum pump (2) was turned on to remove the air from the water. The water was deaired under a constant vacuum of -85 kPa for 30 minutes. When the water was completely

deaired, the high vacuum pump (2) was turned off, and valves (2.3) and (2.1) were closed (le Roux, 2020).

c) The water control valves (1.3), (3.4), (3.3) and (3.2) were then opened to allow the deaerated water to flow through the control panel (3) towards the closed valve (5.3) (le Roux, 2020).

d) After the dry tensiometers were placed in the dry saturation cell (5), the cell was closed. Valves (2.3), (2.2) and (5.1) were opened, and the high vacuum pump (2) was turned on. The vacuum within the cell removed the air and created negative pressure on the ceramic tips of the tensiometers, which helped to accelerate the saturation procedure. The vacuum was applied for 10 minutes (le Roux, 2020).

e) While the vacuum was applied, valve (5.3) was slowly opened, allowing the deaerated water to slowly fill the saturation cell (5) with the tensiometers (connected to a data acquisition system). After the saturation cell was filled with deaerated water, valves (5.3) and (5.1) were closed, and the vacuum was turned off. The tensiometers were left for several hours at 25 kPa to equilibrate (allowing the water to penetrate the ceramic tip and saturate the tips) (le Roux, 2020).

f) After the tensiometers have equilibrated, the cell is pressurised using the air-water interface (4) in conjunction with the air compressor (6) or the high-pressure controller (7). The air-water interface and air compressor (6) system (of up to 800 kPa) was used for supplying low pressure, and the high-pressure controller (7) was used for high pressure (of up to 3 MPa). The cell was pressurised for 48 hours to fully saturate the tensiometers and remove any remaining air (le Roux, 2020).

g) Tensiometers were then calibrated while in the cell with a data acquisition system (5.7), the air-water interface (4) (supplying the water pressure) and the pressure gauge (3.1). The calibration process for the tensiometers is provided in Appendix A.

The saturation procedure can range from 6 to 48 hours, depending on the porosity of the ceramic tips of the tensiometers. After saturation and calibration procedures, the tensiometers were stored in a bottle with deaerated water and ready for use. Before using the tensiometers, the sensors were removed from the bottle and embedded in the desired position in the fresh concrete. The tensiometers were placed within a timeframe of 60 seconds; longer than 60 seconds could result in tensiometer cavitating, especially for highly porous ceramic tips.

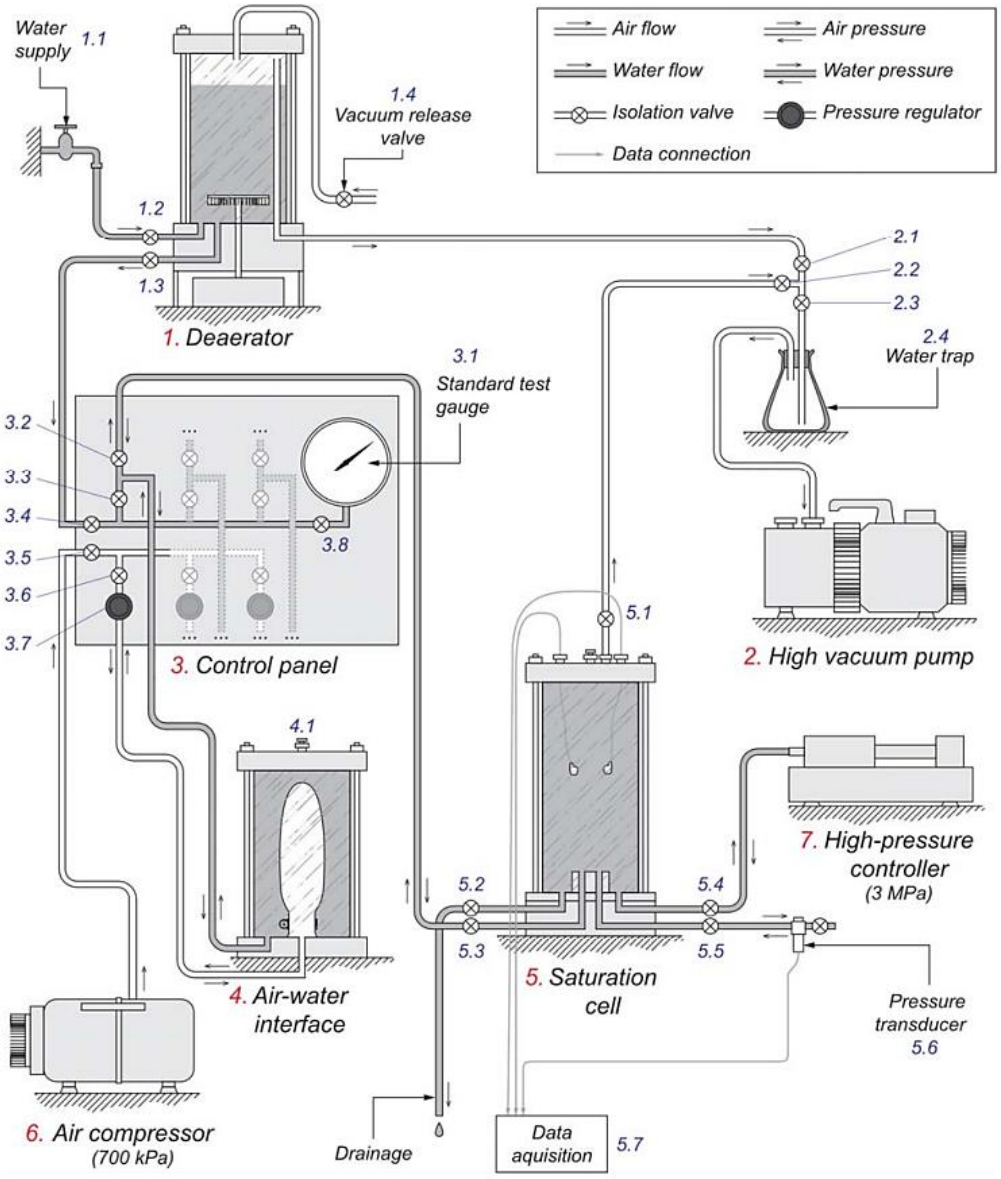

Figure 4-11: Tensiometer saturation and calibration set up (le Roux, 2020)

4.5.3 Testing Procedure

The negative CP build-up in the fresh concrete was measured with the tensiometers. The tensiometers built and used throughout the study consisted of 700 and 1200 kPa sensors with ceramic tips having a porosity of 300 kPa and 1500 kPa. The tensiometers were calibrated as described in Appendix A. The tensiometers were connected to a Campbell Scientific CR 1000X Series data acquisition system. The CP behaviour of the concrete was measured in 1-second intervals for the duration of the testing period. As mentioned, two tensiometers with the tenstal setup were embedded in each PS cracking specimen at third points (spaced at 200 mm).

4.6 NO CRACKING CAPILLARY PRESSURE BOUNDARY MODEL

The following setup and testing procedures were conducted to test and verify the No Cracking CP Boundary Model with the low bleed concrete and SCC. The no cracking CP boundary calculation for the tests conducted in the model verification phase is discussed. The preventative measure used to reduce the negative CP build-up is also covered.

4.6.1 The No Cracking Capillary Pressure Boundary Setup

Figure 4-12 shows the excel spreadsheet used to determine the no cracking CP boundary for the low bleed concrete and SCC in the Model Tests. The figure shows that the no cracking CP boundary spreadsheet only required the three model parameters and the CP value and corresponding time after the drying time. The spreadsheet used equation (3.3) to calculate the total pressure-time area of the current CP build-up until the area was equal to the no cracking area. The figure also shows the two if statements used to indicate when the areas were close and when the boundary would be reached. Once the total area exceeded the no cracking area, the critical pressure limit was calculated by interpolating between the total area, no crack area and the CP below and over the boundary.

INPUT VALUES:	
Drying time [min]	42
Initial Set [min]	233
Time Steps [min]	1
No Crack Pressure-Time Area [kPa.min]	-634.8

Interpolation	
Lower Bound Area [kPa.min]	-601.5
Upper Bound Area [kPa.min]	-714.9
Lower CP [kPa]	-3.30
Upper CP [kPa]	-3.95
Critical Pressure Limit[kPa]	-3.49

Actual Time [min]	Time [min]	mV	CP [kPa]	Trapezoidal Rule	Total of the Trapezoidal Rule	Area of the Rectangle	Total Area	Total Area >= 0.9*No Crack Area	Boundary Below/Over
42	0	0	0	0	0	0	0	-	-
43	1	0.54	-0.99	-0.4952789	-0.50	-188.21	-188.7	-	-
44	2	0.533	-1.26	-1.1251396	-1.62	-238.09	-239.7	FALSE	BELOW BOUNDARY
45	3	0.543	-0.88	-1.0674617	-2.69	-164.54	-167.2	FALSE	BELOW BOUNDARY
46	4	0.535	-1.18	-1.0290097	-3.72	-221.19	-224.9	FALSE	BELOW BOUNDARY
47	5	0.529	-1.41	-1.2981732	-5.02	-262.92	-267.9	FALSE	BELOW BOUNDARY
48	6	0.533	-1.26	-1.3366252	-6.35	-233.05	-239.4	FALSE	BELOW BOUNDARY
49	7	0.537	-1.11	-1.1828175	-7.53	-203.49	-211.0	FALSE	BELOW BOUNDARY
50	8	0.543	-0.88	-0.9905578	-8.53	-160.16	-168.7	FALSE	BELOW BOUNDARY
51	9	0.543	-0.88	-0.875202	-9.40	-159.29	-168.7	FALSE	BELOW BOUNDARY
52	10	0.525	-1.57	-1.2212694	-10.62	-283.69	-294.3	FALSE	BELOW BOUNDARY
53	11	0.503	-2.41	-1.990308	-12.61	-434.39	-447.0	FALSE	BELOW BOUNDARY
54	12	0.502	-2.45	-2.4325052	-15.04	-438.86	-453.9	FALSE	BELOW BOUNDARY
55	13	0.507	-2.26	-2.3556013	-17.40	-402.19	-419.6	FALSE	BELOW BOUNDARY
56	14	0.506	-2.3	-2.2786975	-19.68	-406.73	-426.4	FALSE	BELOW BOUNDARY
57	15	0.503	-2.41	-2.3556013	-22.03	-424.74	-446.8	FALSE	BELOW BOUNDARY
58	16	0.492	-2.84	-2.6247648	-24.66	-496.34	-521.0	FALSE	BELOW BOUNDARY
59	17	0.48	-3.3	-3.066962	-27.73	-573.80	-601.5	TRUE	BELOW BOUNDARY
60	18	0.463	-3.95	-3.624515	-31.35	-683.58	-714.9	TRUE	OVER BOUNDARY

Figure 4-12: Spreadsheet used for finding the critical pressure limit and corresponding time to apply the boundary

Figure 4-13 shows the graph created from the spreadsheet and how the no cracking CP boundary was applied to the current negative CP build-up.

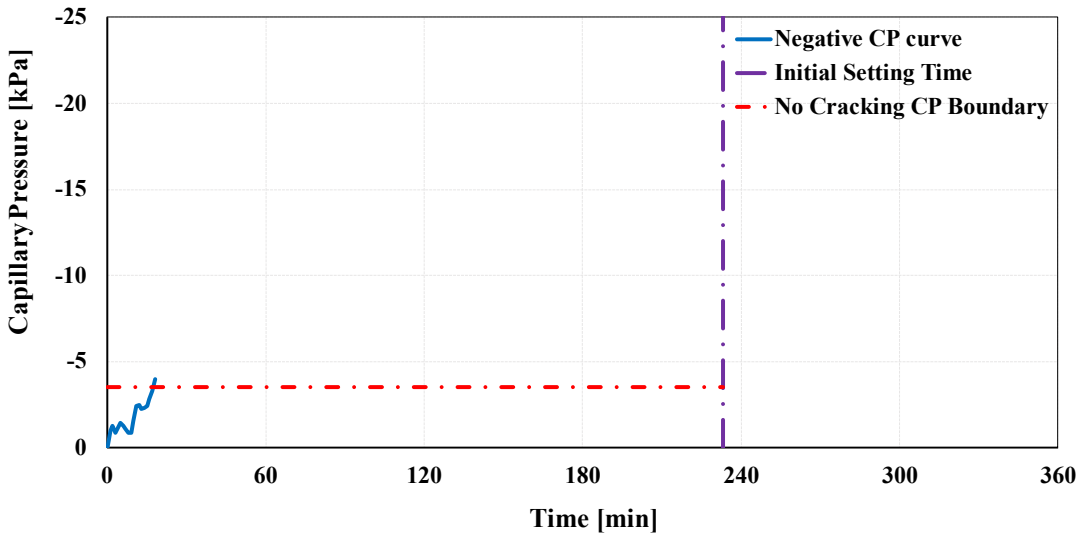

Figure 4-13: The No cracking CP Boundary applied to the CP measurements

Once the critical pressure limit was reached, the no cracking CP boundary was applied to the current negative CP build-up. The concrete needed to be rewetted each time the boundary was reached to reduce the negative CP build-up and maintain the same pressure-time area as the no cracking area.

4.6.2 Testing Procedure

The no cracking CP boundary for each of the three specimens was determined using the spreadsheet. The CP measurements were read into the spreadsheet at 60-second intervals. Whenever the negative CP build-up reached the boundary, the fans of the MCC were turned off, and the surface of the specimen was rewetted with water. After rewetting the concrete surface, the fans of the MCC were switched on again. The surface of the concrete was sprayed until the negative CP build-up of the concrete started reducing. Figure 4-14 shows the spray bottle used for rewetting the surface of the specimen. One spray bottle was used per specimen, and each spray bottle was weighed before and after the Model Tests. The specimens were only sprayed up until ±40 minutes after reaching initial set to observe the negative CP behaviour after the boundary was applied.

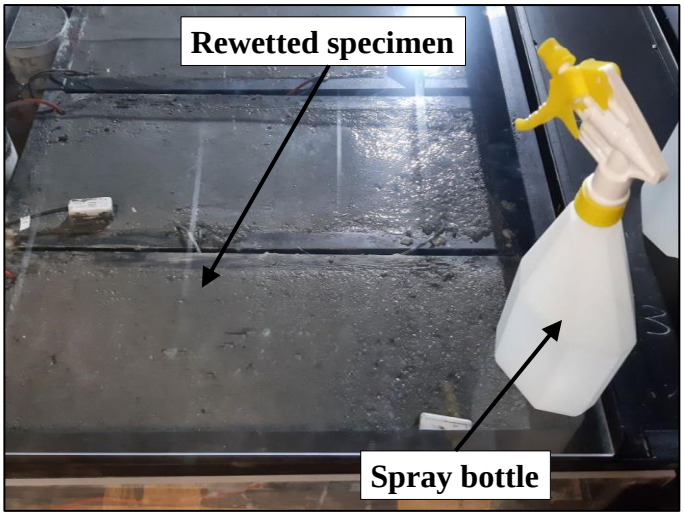

Figure 4-14: Rewetting the concrete setup

Two of the three evaporation moulds were rewetted with a spray bottle to determine how the measured evaporation was affected by rewetting the concrete. The one evaporation specimen that was not rewetted was used as the reference evaporation rate.

4.7 MATERIALS AND PROPERTIES

The properties of the constituents used in the low bleed concrete and SCC are summarised in Table 4-3. Portland cement (CEM I 52.5 R) produced by AfriSam was used in both concrete mix designs throughout the study. According to AfriSam (2021), the cement obtained a 28-day strength of 59 MPa and initial set of 191 minutes. The additional cement properties are available in Appendix B. The Superplasticiser (SP) used in the SCC was Chryso Premia 100. Silicon Smelters supplied the silica fume and Ash Resources the fly ash used in the SCC mix.

Table 4-3: The properties of the material

Materials	Relative density	Dust content [%]	Fineness modulus	Particle shape
CEM I 52.5 R	3.039	-	-	Angular
Silica fume	2.342	-	-	Spherical
Fly ash (unclassified)	2.224	-	-	Spherical
13.2 mm Dolomite crusher stone	2.845	0.4531	-	Angular
Dolomite crusher sand	2.845	6.903	3.037	Angular
SP	1.050	-	-	-

The Particle Size Distribution (PSD) for the CEM I 52.5 R, silica fume and fly ash are illustrated in Figure 4-15. The figure shows the average PSD found between laser and ultrasound.

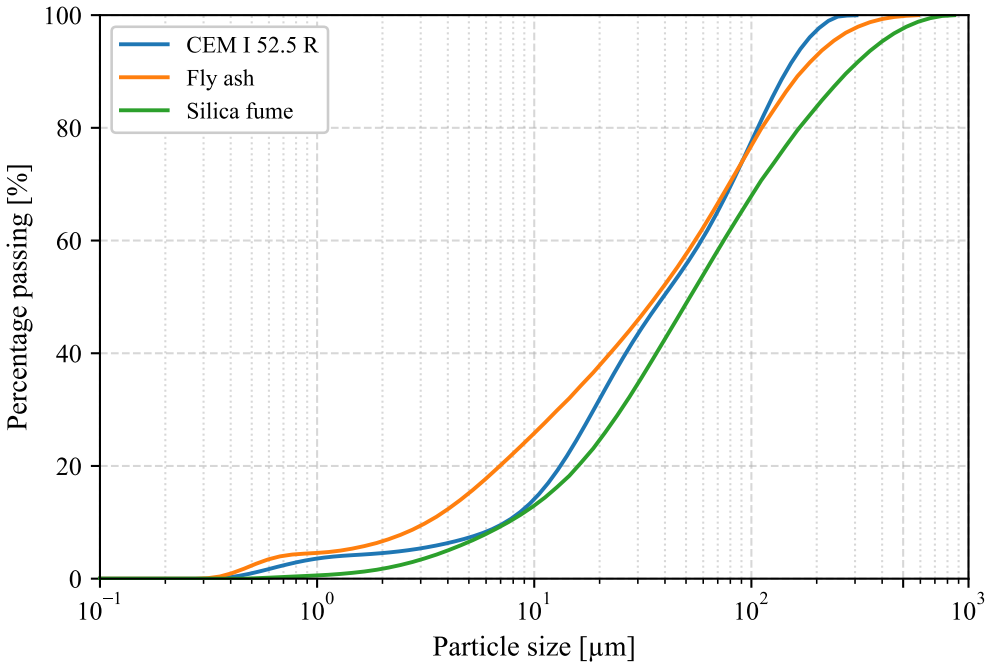

Figure 4-15: Average PSD of the CEM I 52.5 R, Fly ash and Silica fume

The grading of the dolomite crusher sand and the 13.2 mm dolomite crusher stone is shown in Figure 4-16. The aggregate grading was done following the SANS 1083 (2017).

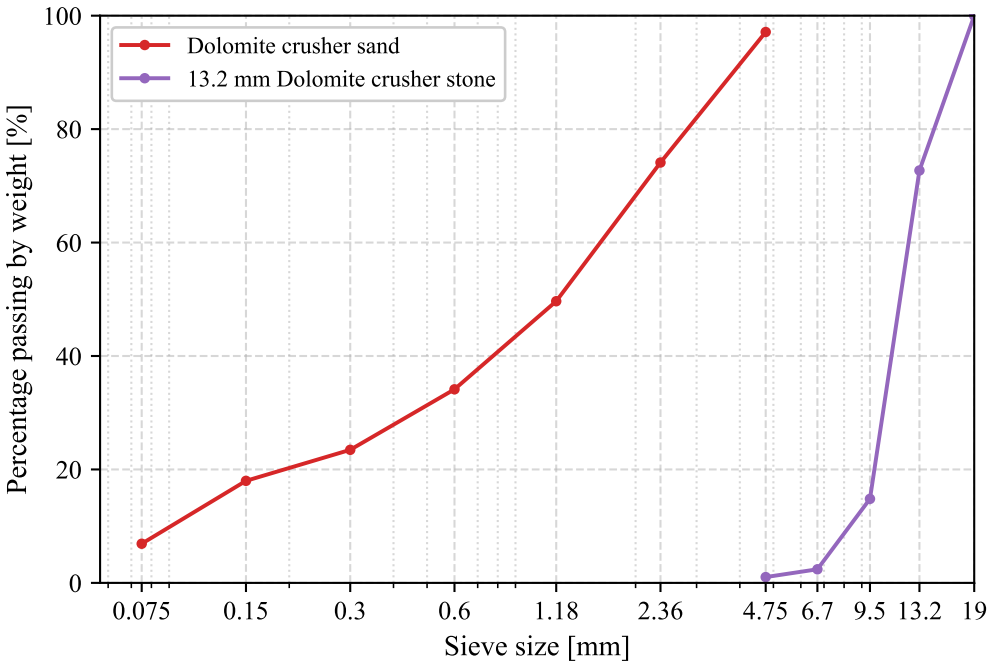

Figure 4-16: Grading of the dolomite crusher sand and 13.2 mm dolomite crusher stone

4.8 MIX DESIGN

This section covers the mix designs for the low bleed concrete and SCC as well as the grading for the two concrete mix designs used throughout the study.

4.8.1 Low Bleed Concrete

The low bleed concrete had a water/cement (w/c) ratio of 0.5 and consisted of the constituents shown in Table 4-4. Soutsos and Domone (2017) stated that by increasing the amount of fine material passing the 300 μm sieve in the concrete mixture, the bleeding of the concrete could be reduced. The reduced bleeding helped in increasing the risk of PS cracks forming on the concrete (Matalkah *et al*., 2019). Therefore, the aggregate ratio was modified to 75 % and 25 % for the fine and coarse aggregate to obtain the low bleed concrete mixture.

Table 4-4: Material constituents for the low bleed concrete mixture

Water [kg/m^3]	CEM I 52.5 R [kg/m^3]	13.2 mm Dolomite crusher stone [kg/m^3]	Dolomite crusher sand [kg/m^3]
220	440	453	1359

Table 4-5 provides the compressive strength, slump and setting times of the low bleed concrete. The additional compressive strength results for the cubes are located in Appendix C.

Table 4-5: Properties of the low bleed concrete

28-day Compressive strength [MPa]	Slump [mm]	Initial setting time [min]	Final setting time [min]
49.5	10	283	430

4.8.2 Self-Compacting Concrete

The SCC constituents presented in Table 4-6 was designed by following some of the guidelines provided by Aggarwal *et al.* (2008). The fly ash used in this mix design was unclassified, and silica fume was added to reduce the segregation in the concrete and provide an adequate SCC. The 9.5 mm dolomite stone was obtained by sieving the 13.2 mm stone used in the low bleed concrete. The SCC had a w/c ratio of 0.4 and a water/binder ratio of 0.28.

Table 4-6: Material constituents for the SCC mixture

Water [kg/m^3]	CEM I 52.5 R [kg/m^3]	Fly ash [kg/m^3]	Silica fume [kg/m^3]	9.5 mm Dolomite crusher stone [kg/m^3]	Dolomite crusher sand [kg/m^3]	SP [kg/m^3]
174	430	163	38.7	504	1174	6.10

Table 4-7 presents the properties for the SCC such as the compressive strength, slump flow and setting times. The additional cube results are located at Appendix D.

Table 4-7: Properties of the SCC mixture

28-day Compressive strength [MPa]	Slump flow [mm]	Initial setting time [min]	Final setting time [min]
101	590	511	601

4.8.3 Concrete Dry Material Grading

The grading analysis for the dry constituents of the low bleed concrete and SCC are shown in Figure 4-17. The grading shows that roughly 80 % of the dry constituents (for both mixtures) passed through the 4.75 mm sieve and about 40 % passed the 300 µm sieve.

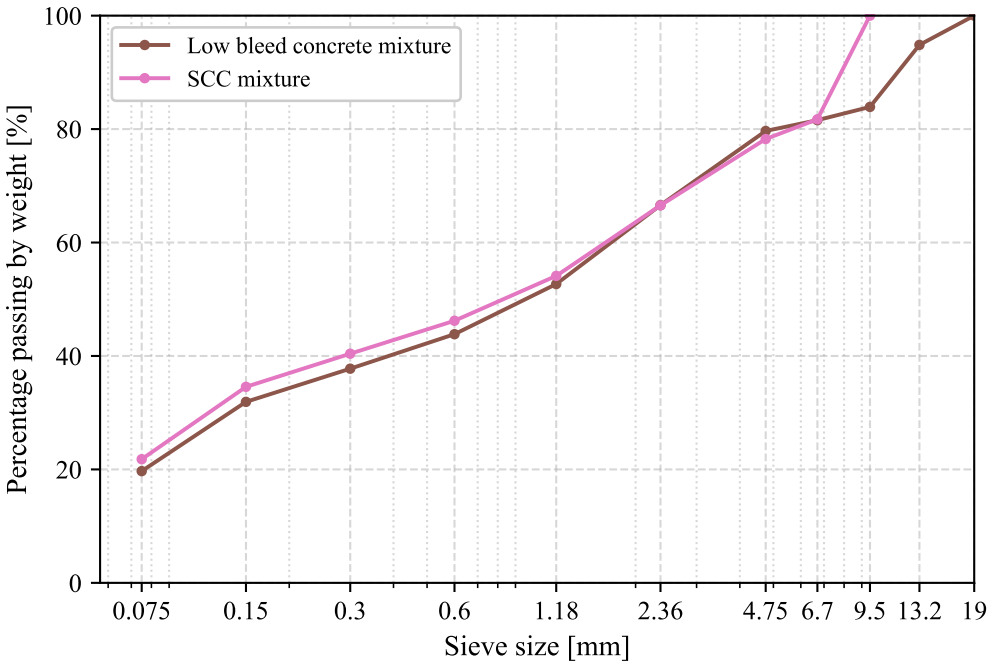

Figure 4-17: The grading for the dry constituents of concrete mixtures

4.9 EXPERIMENTAL PROCEDURES

The testing preparations, mixing and casting procedures and the testing procedures conducted for the experimental work are covered in this section.

4.9.1 Testing Preparations

The preparation procedure conducted for the evaporation and model tests is discussed.

i Temperature-controlled and Humidity-controlled Room

The climatic conditions for the temperature-controlled and humidity-controlled room were set 48 hours before testing.

ii Mobile Climate Chamber

The MCC was switched on for two hours before starting the evaporation tests and model tests to provide enough time for the climate chamber to obtain the desired evaporation rate.

iii Materials And Moulds

The concrete constituents and the moulds were placed in a temperature-controlled room set at an air temperature of 24 °C (±1 °C) for 24 hours before casting. To ensure that all the tests were conducted in the same conditions to provide accurate results.

4.9.2 Mixing and Casting

A 100-litre pan mixer, shown in Figure 4-18, was used for mixing the concrete in all the tests. The mixing procedure for the low bleed concrete started by wetting the pan mixer to prevent absorption of the mixing water of the concrete. After that, the dry constituents were added to the mixer and mixed; the water was then added after 60 seconds of dry mixing. The concrete was then mixed for 2 minutes, adding up to a total mixing time of 3 minutes. The same procedure was followed for the SCC, except for the mixing time. The SCC were mixed for 4 minutes, which adding up to a total mix time of 5 minutes. Time zero for the concrete was when the water made contact with the cement.

Figure 4-18: The 100-litre pan mixer

After the mixing procedure, the moulds were filled halfway with concrete and vibrated for 60 seconds. The sensors measuring the internal properties were then placed in the relevant moulds. The moulds were then filled with concrete to the desired 100 mm height, and the last sensors were placed in the surface of the concrete and vibrated for another 60 seconds. The total duration of the vibration of the concrete added up to 2 minutes, ensuring that the majority of the air bubbles were removed from the concrete. The concrete surface was then finished with a plastic trowel and then with a steel trowel to ensure a smooth surface. The same casting procedure was followed for the SCC, except no vibration was required.

4.9.3 Testing

All the sensors were connected 24 hours before testing to the relevant data acquisition system, namely the Graphtec midi logger GL220 and Campbell Scientific CR 1000X Series. Time zero for the tests began once the two data acquisition systems were recording data and the desired climatic conditions were achieved. All the evaporation tests and model tests were conducted within 24 hours.

4.10 TESTING PROCEDURES

This section consists of the testing procedures conducted in the two testing phases. The PS properties measured during the evaporation tests and model tests were the PS cracks, CP, concrete temperature, VMC, evaporation, climatic conditions and plastic settlement. The PS properties measured during the non-environmental test were the bleeding, setting times and compressive strength. The time increments, sensors, and moulds used for measuring the respective PS properties are also covered in this section.

4.10.1 Plastic Shrinkage Cracks

The mould used for the PS cracking specimens throughout the experimental work is shown in Figure 4-19. This modified PS cracking mould originated from the modified ASTM C1579 mould, which was adapted by Combrinck (2011) from the original ASTM C1579 mould design. The mould was further altered by adding four vertical triangular prisms taken from a design by Steyl (2016), with two at each end point. The dimensions and the placement of the four triangular prisms in the modified ASTM C1579 mould are shown in Figure 4-19.

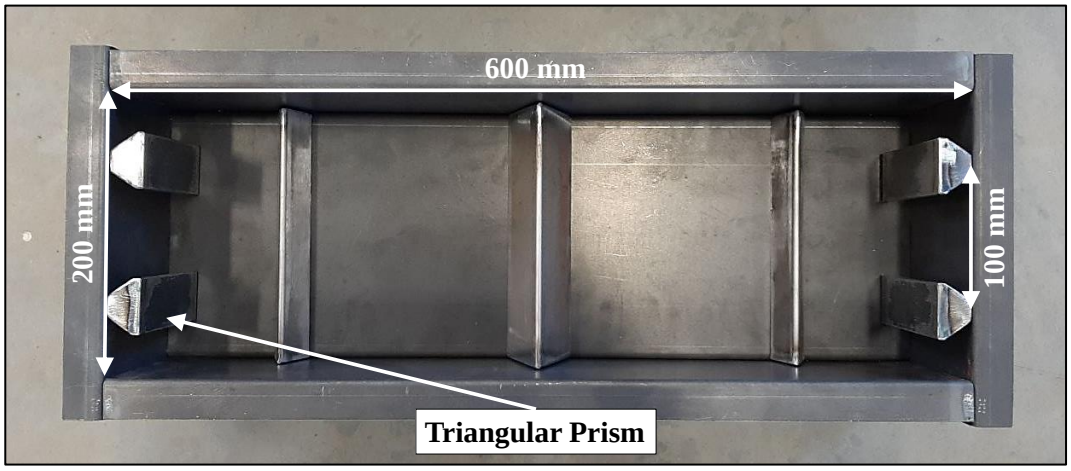

Figure 4-19: Top view of the modified ASTM C1579 mould with dimensions

Figure 4-20 provides the dimensions for one of the vertical triangular prisms used to restrain the concrete at the end points.

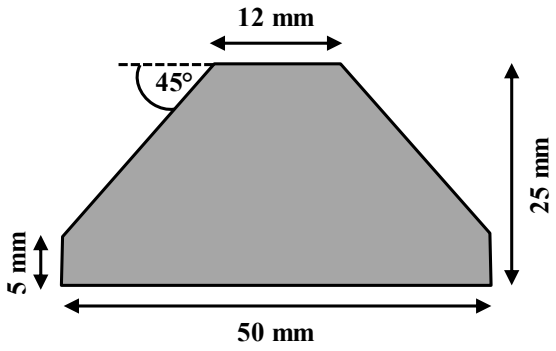

Figure 4-20: The dimensions of the triangular prism restraint (Steyl, 2016)

The side view of the modified ASTM C1579 mould is shown in Figure 4-21. The figure shows the side dimensions of the mould and the three horizontal crack inducing triangles.

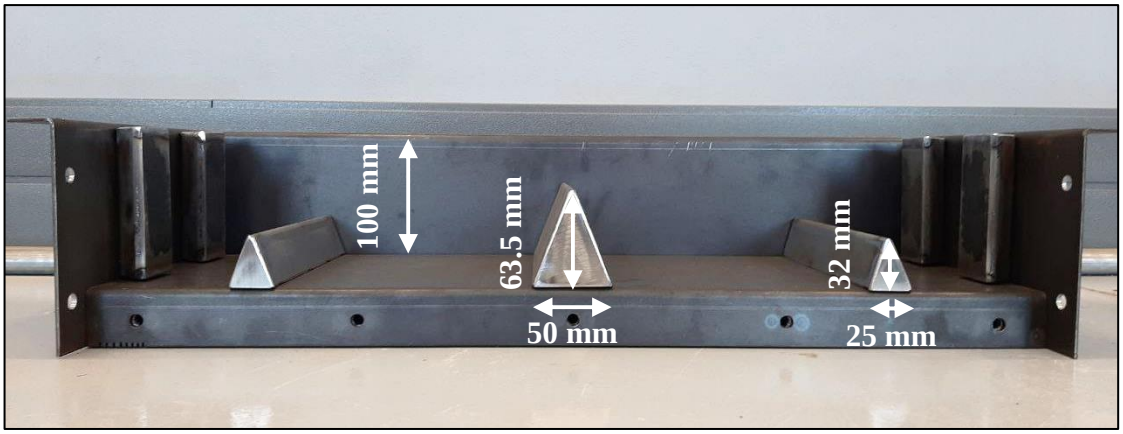

Figure 4-21: Side view of the modified ASTM mould with dimensions

The crack growth on the fresh concrete was measured every 20 minutes from the start of the test with the crack width card shown in Figure 4-22. The crack width card can measure crack widths from 0.05 to 10 mm. Photos were also taken of the PS cracks that formed on one concrete specimen every 20 minutes for the duration of the test.

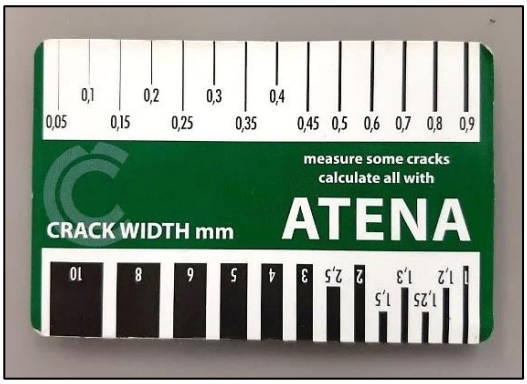

Figure 4-22: The crack width card

4.10.2 Capillary Pressure

As discussed in Section 4.5.3, the CP in the concrete was measured with tensiometers. The tensiometers were connected to a Campbell Scientific CR 1000X Series data acquisition system. The CP of the concrete was measured in 1-second intervals for the duration of the tests.

4.10.3 Concrete Temperature

The internal and surface temperature of the concrete was measured using type T thermocouples. Two thermocouples were used per PS cracking specimen, one for the internal concrete temperature and one for the surface temperature of the concrete. The thermocouples were connected to a Graphtec midi logger GL220, and the temperature was measured at 1-second increments for the duration of the test. The internal temperature of the concrete was measured

at a depth of ±32 mm from the concrete surface (as shown in the sensor setup section). The surface temperature of the concrete was measured by inserting the thermocouples ±10 mm into the surface of the fresh concrete.

4.10.4 Volumetric Moisture Content

The VMC in the concrete was measured using two Teros 10 sensors and one GS1 (the predecessor of the Teros 10). The sensors were connected to the Campbell Scientific CRX1000 Series and measured the VMC every second for the duration of the test. Figure 4-23 shows the VMC sensor as well as the dimensions of the sensor. The calibration procedure utilised throughout this study for the VMC sensors is provided in Appendix A.

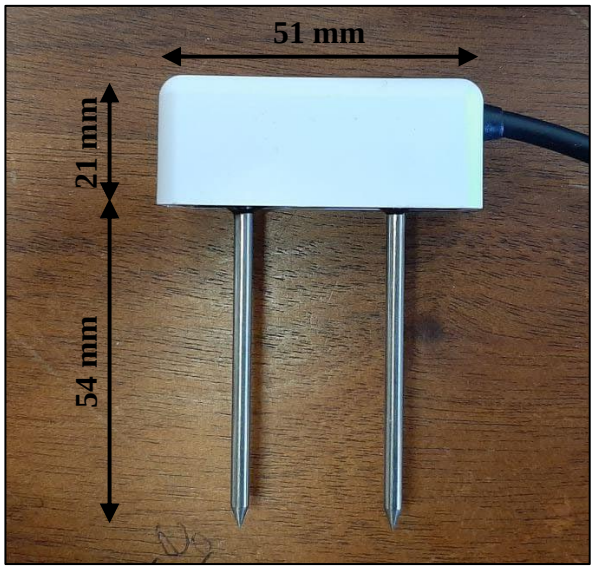

Figure 4-23: Teros 10 VMC sensor (METER, 2021)

4.10.5 Evaporation

The evaporation of the concrete was measured by weighing three specimens filled with fresh concrete. The specimens were measured on a Jadever JWA 30K scale; the scale had a range of 0.02 to 30 kg and an accuracy of 0.001 kg. The specimens were measured before starting the test and after that in intervals of 20 minutes for the test duration.

The three specimens used were cylindrical PVC (polyvinyl chloride) moulds which had a diameter of 110 mm and a height of 100 mm (±1 mm), as shown in Figure 4-24 a) and b). The figure shows the evaporation moulds from all the relevant viewing angles.

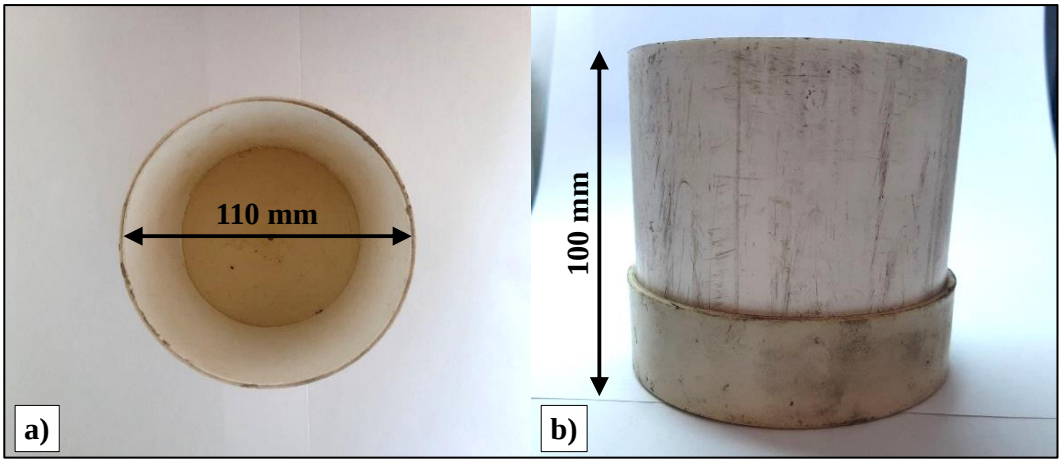

Figure 4-24: a) Top view and b) side view of the evaporation mould

4.10.6 Climatic Conditions

The climatic conditions measured during the tests included the air temperature, wind velocity and relative humidity. The Skywatch Atmos Thermo-Hygro-Anemometer shown in Figure 4-25, was used to measure the climatic conditions. The Skywatch Atmos was accurate to ±3 % for the wind velocity, ±0.4 °C for the temperature measurement and ±3 % for the humidity, which provided sufficient accuracy for the experimental tests (SA, 2021). Each of these conditions was measured every 20 minutes for the duration of the test.

Figure 4-25: Skywatch Atmos Thermo-Hygro-Anemometer

These climatic conditions, along with the concrete surface temperature (Section 4.10.3), were used to estimate the evaporation rate using equation (2.1) and the ACI (1999) nomograph.

4.10.7 Plastic Settlement

The plastic settlement was measured using a high accuracy optoNCDT laser and a deflector placed on the surface of the specimen as discussed in the sensor setup. The optoNCDT laser

had a range of 2 mm. The cone mould was covered with Teflon on the inside to reduce friction between the mould and the fresh concrete as plastic settlement occurred. Figure 4-26 shows the viewing angles of the moulds used to measure plastic settlement. The cone aluminium mould consists of a 140 mm diameter base and a height of 125 mm. The cone mould was covered with a Teflon layer and held in position with a steel top plate. The settlement of the fresh concrete was measured every second with the Graphtec midi logger GL220 data acquisition system.

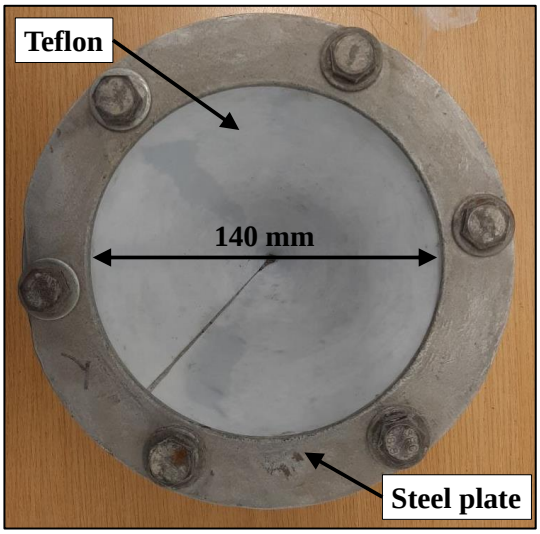

Figure 4-26: The top view of the plastic settlement aluminium cone mould

4.10.8 Bleeding

The bleeding tests for the different concrete mixtures were conducted according to the EN 480-4:2005 standard. The bleeding mould is shown in Figure 4-27. The mould had a diameter of 250 mm and a height of 280 mm. Two bleeding tests were conducted during this study, consisting of the standard test where the mould was filled up to a height of 250 mm (±1 mm). The second (alternative) test consisted of filling the bleeding mould to a height of 100 mm (±1 mm), which was the same height as all the specimens tested in the evaporation and model tests (excluding the plastic settlement specimens). Both the bleeding tests were filled in third layers and each compacted with 25 blows using a tamping rod.

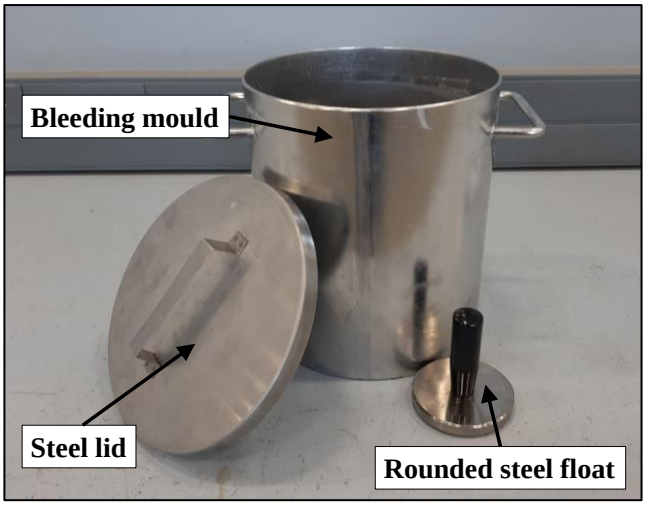

Figure 4-27: Bleeding mould, lid and steel float

The bleed water on the concrete surface was obtained with a 10 ml syringe. The measurement was taken in intervals of 10 minutes during the first 40 minutes of the test and thereafter every 30 minutes until the bleeding ceased. Two minutes before each measurement, 40 mm wooden blocks were placed underneath one side of the bleeding mould. Lifting the moulds helped the bleed water accumulate on the opposite side, making it easier to collect.

4.10.9 Setting Time

The setting times of the concrete were measured using the ASTM C403/C403M – 16 standard test method and the SANS 50196-3:2006/EN 196-3:2005 standard test method. Both tests are user sensitive.

i Penetration Resistance Test Method (ASTM C403/C403M-16)

The ASTM C403/C403-16 is the standard test method used to determine the setting time of concrete. This method required the mortar of the concrete mixture; therefore, the concrete was sieved through a 4.75 mm sieve. After the sieving process, the mortar was cast into two 150 mm cubes. The cubes were covered with bubble wrap and stored in the temperature-controlled room set at an air temperature of 24 °C (±1 °C). The first penetration started 2 to 3 hours after the cement and water made contact and after that, every hour until the initial set (when the penetration resistance of the mortar reaches 3.5 MPa). After the initial set was reached, the measuring intervals changed to 30 min until final set was reached (27.6 MPa).

ii Vicat Test Method (SANS 50196-3:2006/EN 196-3:2005)

The Vicat is the most used apparatus to determine the initial and final setting times of the cement paste. According to the standard, the initial setting time of the cement is the point in time when the needle can no longer penetrate the 40 mm deep cement paste within 5 to 7 mm from the bottom paste. The final setting time is when the ring attachment does not make an impression on the surface of the paste.

In the study, this Vicat method was adapted to determine the setting time of the concrete by using the mortar of the concrete mixture. The concrete was sieved through a 2.36 mm sieve to obtain a fine mortar mixture. The mortar was then used to determine the setting times of the concrete in the same manner as for the cement paste described in the standard. Two mortar specimens were cast in the cone moulds to obtain an average setting time for the concrete. Only the setting time of the low bleed concrete was determined with this test method.

4.10.10Compressive Strength

The compressive strength of the concrete was determined following the SANS 5863:2006 standard. Four 100 mm concrete cubes were cast and tested after 28 days of curing.

4.11 CONCLUSION

In this chapter, the experimental outline for the two testing phases was presented and discussed. The PS properties tested and the number of evaporation rates that the concrete mixtures were exposed to were discussed. Test objectives for the two testing phases were presented. The setup required for the experimental tests, tensiometer and No Cracking CP Boundary Model were covered. The materials and material properties, as well as the mix designs for the two concrete mixtures, were described. Lastly, the procedures for the experimental preparation, mixing, casting, and testing of the PS properties were discussed.

5 MOBILE CLIMATE CHAMBER DETAILS AND DESIGN

5.1 INTRODUCTION

A climate chamber capable of maintaining harsh climatic conditions was required for the study. Therefore, the Mobile Climate Chamber (MCC) was designed and constructed. The author designed the MCC with guidance from the supervisors. This chapter provides details on the design and construction of the MCC. The design concept and all the equipment of the MCC are covered in the following sections.

5.2 DESIGN OF THE MOBILE CLIMATE CHAMBER

Figure 5-1 shows the MCC. The MCC was designed for testing different specimens in harsh drying climatic conditions in a laboratory or on-site. All four corners of the MCC have stands capable of levelling the trailer and the specimen area in any terrain.

Figure 5-1: The Mobile Climate Chamber

Figure 5-2 demonstrates the design of the MCC with the different compartments and placements of the main parts. The design shows where the dehumidifier, air conditioner, air duct, and specimen area is located in the MCC.

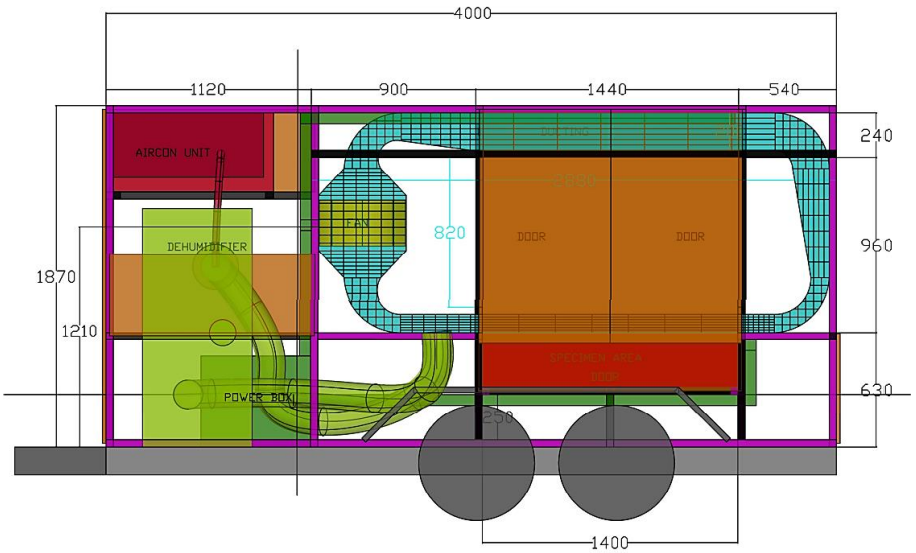

Figure 5-2: MCC concept design

The trailer consists mainly of three compartments: the testing room, instrumentation room, and control room. Each of the important functionalities of the rooms are discussed in the subsections.

5.2.1 Testing Room

The MCC has two doors on both sides of the trailer leading to the testing room, as illustrated in Figure 5-3. This room consists of an air duct and the specimen area.

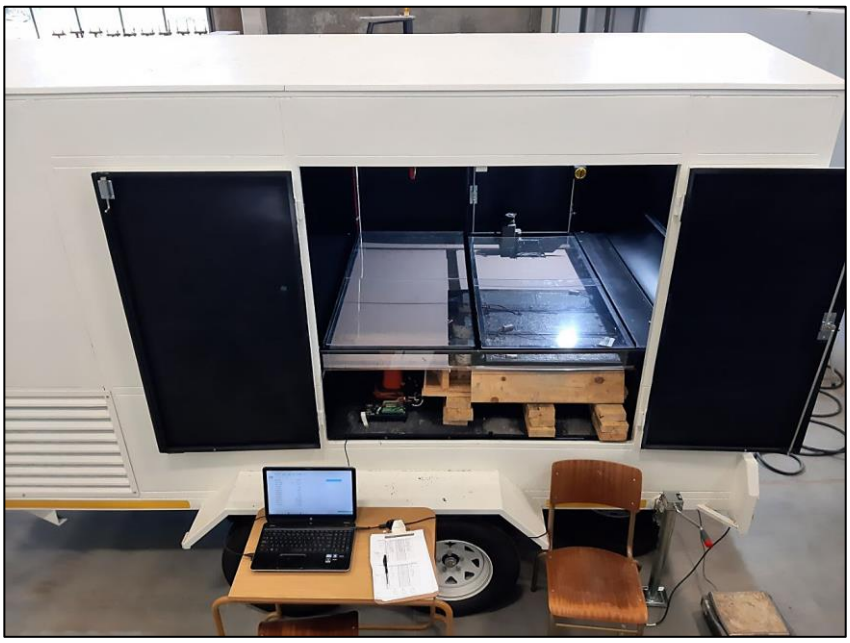

Figure 5-3: Testing room of the MCC

i Air Duct

The air duct was designed to guide a volume of dry air at different velocities towards the exposed surface area at the specimen area, creating the desired environment. The MCC's air duct design is illustrated in Figure 5-4. The design shows the direction of the airflow (in dark blue) and the location of the heater elements, fans, and the inlet and outlet of the dehumidifier.

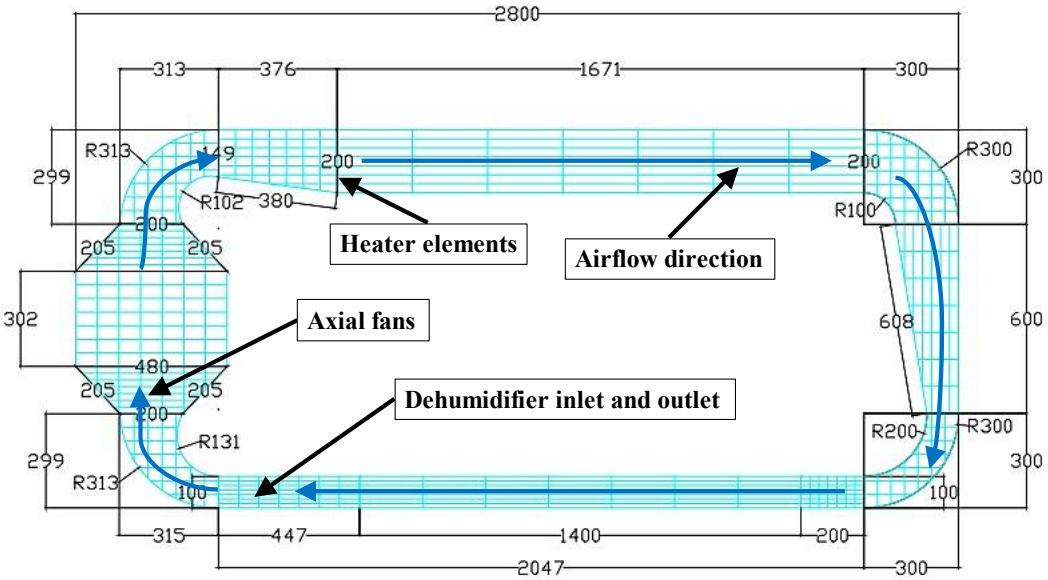

Figure 5-4: Air duct design of the MCC

Most of the air duct was covered with thin sheet metal except for the air duct over the specimen area. This section was covered with Plexiglass Resist 65 (Perspex), which allowed easy access to the specimens, as shown in Figure 5-5.

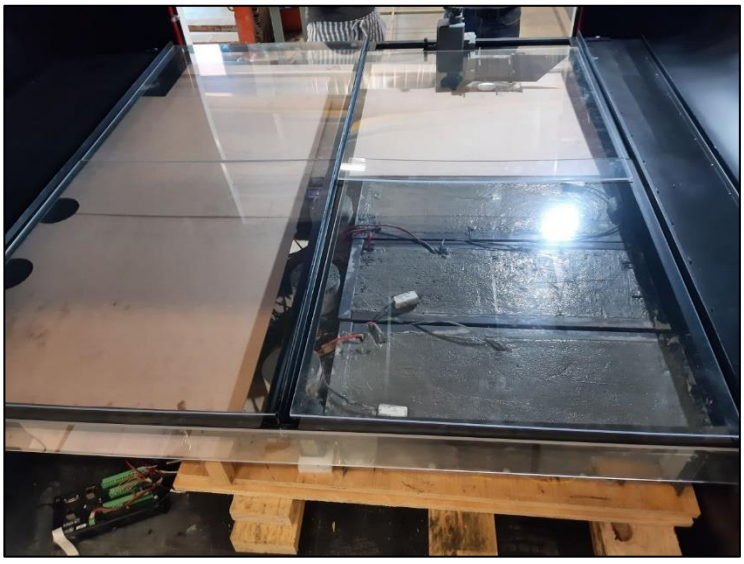

Figure 5-5: Plexiglass Resist 65 air duct with the specimen area below

ii Specimen Area

The specimen area (shown in Figure 5-5 and Figure 5-6) was designed to have a surface area and volume of 2.1 m^2 and 0.63 m^3, capable of testing most types of specimens of all different shapes and sizes. The specimen area is designed to have sufficient space for loadcells to measure the mass of different specimens.

The specimen area consisted of five angle sections and six movable Perspex parts guiding the dry wind across the surface of the specimens and creating an enclosed system. The entire specimen area of the MCC was designed to be taken apart and changed if needed. The Perspex parts are durable and lightweight making it easier to open when modifications are needed.

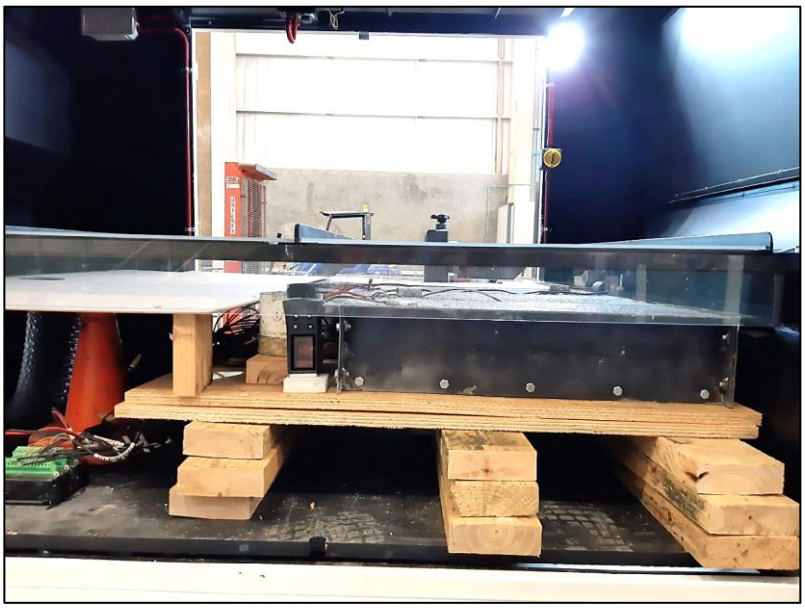

Figure 5-6: Concrete specimens placed in the MCC specimen area

5.2.2 Instrumentation Room

Figure 5-7 shows the instrumentation room. This room was designed to contain all the measuring instrumentation, such as the data acquisitions, computers, monitors and modems uploading the data to the internet, allowing the data to be monitored anywhere.

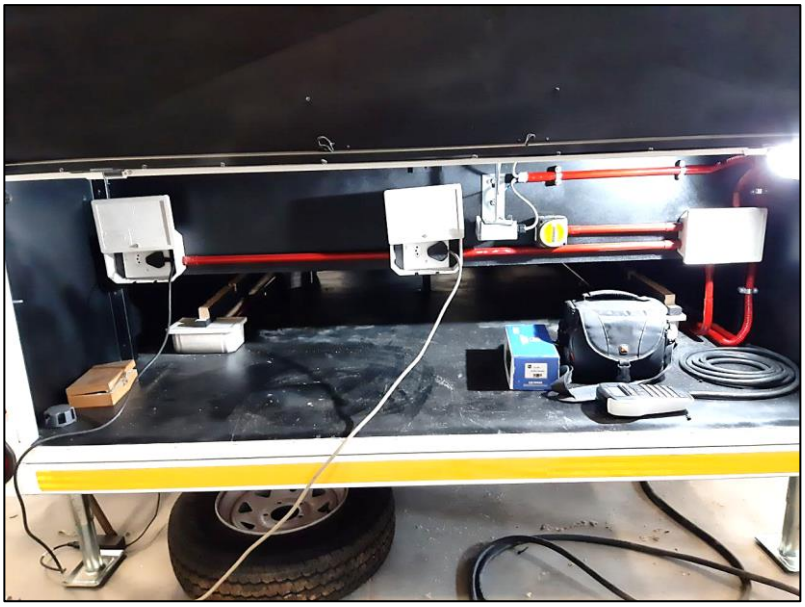

Figure 5-7: Instrumentation and storage room

5.2.3 Control Room

The control room shown in Figure 5-8 contained the controls for the climatic conditions and all the electronic equipment, such as the main three-phase power socket, power boxes, dehumidifier, air conditioner, and temperature controllers (for the air conditioner and heater elements).

Figure 5-8: Control room of the MCC

5.3 CLIMATIC CONDITIONS

The MCC is designed to simulate moderate and harsh drying environments in this chamber by decreasing the relative humidity and increasing the wind velocity and air temperature.

5.3.1 Relative Humidity

The relative humidity in the air duct was controlled and dehumidified by the Munters ML420 dehumidifier shown in Figure 5-9. The ML420 dehumidifies the air at 155 m^3/h (or 0.043 m^3/s) and can reduce the relative humidity to 5 %. The dehumidifier is connected to a sensor that control the humidity. The sensor was placed at the air duct outlet to measure dry wind moving towards the specimen area.

Figure 5-9: Munters ML420 dehumidifier

5.3.2 Wind Velocity

The wind velocity for the MCC was obtained by the DELTA CP2000 variable speed drive, controlling two 400 mm axial flow fans. The DELTA CP2000 variable speed drive is illustrated in Figure 5-10. The MCC was calibrated using the Skywatch Atmos Thermo-Hygro-Anemometer. The MCC can produce a wind velocity of up to 65 km/h exiting the air duct.

Figure 5-10: DELTA CP2000 variable speed drive

5.3.3 Air Temperature

The air temperature in the MCC was controlled by the warm air exiting the dehumidifier and two temperature controllers, the heating and cooling controllers shown in Figure 5-11. The heating controller was connected to a PT100 temperature sensor, and two heater elements were attached to each side of the ducting. In contrast, the cooling controller was connected to a PT100 temperature sensor, and an air conditioner was connected to the outlet pipe of the dehumidifier. The air conditioner used in the MCC is an HCBC-302-2R air conditioner. The air conditioner has two 300 mm inlet fans and produces an airflow of 0.83 m^3/s. The air temperature in the air duct could be cooled down to 20 °C with the air conditioner or heated to 40 °C with the heating elements. This provided an air temperature range of 20 to 40 °C in the specimen area.

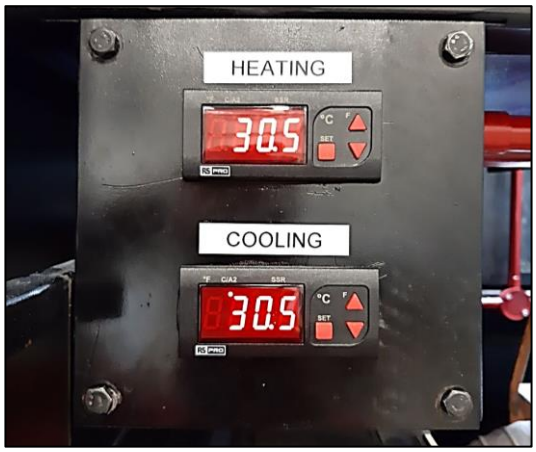

Figure 5-11: Heating and cooling controllers

As the dehumidifier reduces the relative humidity of the air in the air duct, heat is produced, increasing the dry air temperature moving out of the outlet. The setup of these two temperature controllers is used to maintain the desired air temperature in the air duct. The heating controllers switched the heating elements on when the temperature is below the desired temperature and off when the temperature has been reached. The cooling controller works similarly; when the temperature is too high, the air conditioner is turned on and off when the desired temperature is reached.

5.4 CONCLUSION

The MCC was the focus of this chapter consisting of discussions on the different compartments and features. The compartments consisted of the testing room, instrumentation room, and control room, and all the features of the MCC, such as controlling relative humidity, wind velocity, and air temperature in the air duct.

6 PLASTIC SHRINKAGE CRACKING CHARACTERISATION OF THE LOW BLEED CONCRETE MIXTURE

6.1 INTRODUCTION

The chapter consists of the measurements obtained from the non-environmental and evaporation tests conducted on the low bleed concrete. The purpose of this chapter is to determine the model parameters required for testing the developed model. The model required the initial setting time, a means to determine the drying time, and a negative Capillary Pressure (CP) build-up curve where no Plastic Shrinkage (PS) cracking occurs.

The non-environmental tests consist of the concrete setting times and the bleeding. The evaporation tests include testing the low bleed concrete in six diverse evaporation rates; to obtain the PS cracking, CP, Volumetric Moisture Content (VMC), concrete temperature and plastic settlement. Each characteristic is discussed throughout the chapter and summarised in the concluding summary.

6.2 NON-ENVIRONMENTAL TESTS

In this section, the setting times and bleeding of the low bleed concrete are presented and discussed. The setting times measurement was needed for the model and to determine the duration of the evaporation tests.

6.2.1 Setting Time

The average setting times for the Penetration Resistance Test Method (ASTM C403/C403M – 16) and Vicat Test Method (SANS 50196-3:2006/EN 196-3:2005) are presented in Table 6-1. The Standard Deviation (SD) for the setting times is shown in brackets in the table. The test measurements from which the setting time was calculated can be viewed in Appendix C.

The average initial and final setting time for the Vicat Test Method occurred 53 minutes and 77 minutes earlier in time than the Penetration Resistance test method, which was expected for the two tests. The notable difference between the tests might be due to the difference in needles and forces used for determining the setting time. The Vicat Tests Method induced a slightly lower force onto the mortar samples, for instance, 2.93 MPa at the initial set compared to the 3.5 MPa at the initial set for the Penetration Resistance test method. Another possibility is that the smaller sieve (2.36 mm) used in the Vicat Test Method affected the water/cement (w/c) ratio of the mortar by retaining more water and resulting in increased setting times. This is in agreement with the literature from Mehta and Monteiro (2001); by increasing the w/c ratio will reduce the setting time of the concrete.

Table 6-1: Setting times of the two test methods with the SD in brackets

Setting time	Penetration resistance	Vicat
Initial, min	283 (2.83)	230 (7.07)
Final, min	430 (17.7)	353 (10.6)

The Penetration Resistance Test Method (ASTM C403/C403M – 16) is the standard method for determining the concrete setting time, and these measurements were therefore used throughout the study. Hence, a testing duration of 360 minutes is used to ensure that low bleed concrete reaches initial set in the evaporation tests.

6.2.2 Bleeding

Figure 6-1 shows the cumulative bleed water of the 250 mm depth and 100 mm depth specimens over time. The cumulative bleed water of the 250 mm depth specimen was significantly higher than that of the 100 mm specimen.

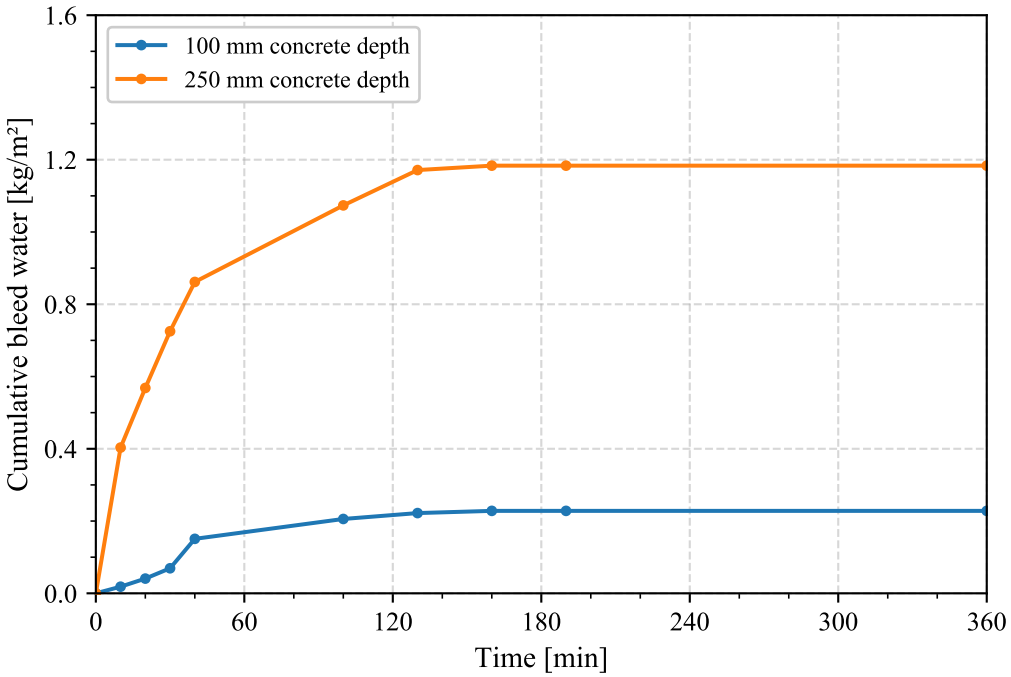

Figure 6-1: Concrete bleeding at different depths

The bleeding results are summarised in Table 6-2. The table presents the bleeding capacity and the bleeding capacity per unit depth. The bleeding capacity refers to the amount of water extracted from a specimen. In contrast, the bleeding capacity per unit depth refers to the water extracted per unit depth from a specimen.

When comparing the 100 mm depth specimen with the 250 mm depth specimen (done according to the EN 480-4:2005 standard). The bleeding capacity and bleeding capacity per unit depth had a difference of 0.956 kg/m^2 and 2.45 kg/m^2/m, respectively. The bleeding findings confirmed that depth affects the bleeding capacity, as Kwak and Ha (2006) found, stating that the amount of bleeding is proportional to the depth of the concrete.

Table 6-2: Bleeding of the two concrete depths

Bleeding	100 mm depth	250 mm depth
Capacity, kg/m^2	0.228	1.18
Capacity per unit depth, kg/m^2/m	2.28	4.74

To ensure that the measured bleed water could be used in conjunction with the evaporation specimens to determine the drying time, the 100 mm specimens were used.

6.3 CLIMATIC CONDITIONS AND EVAPORATION RATES

This section consists of the climatic conditions and evaporation rates obtained from the evaporation tests.

6.3.1 Climatic Conditions

The measured climatic conditions in each of the six evaporation tests are shown in Table 6-3. The table presents the average climatic conditions and the SD in brackets obtained during the evaporation tests. The six evaporation tests are presented throughout this chapter as ERL-1 to ERL-6. The relative humidity greater than 95 % for ERL-1 was obtained by applying a thin water layer to the concrete surface. Water was sprayed each time the water layer evaporated.

Table 6-3: Climate conditions of six evaporation tests with the SD in brackets

Conditions	ERL-1	ERL-2	ERL-3	ERL-4	ERL-5	ERL-6
Relative humidity, %	>95.0	67.1 (3.04)	23.6 (2.02)	37.8 (1.11)	46.1 (1.72)	20.5 (1.20)
Concrete surface temperature, °C	23.0 (1.198)	24.6 (0.461)	22.0 (0.603)	21.8 (0.721)	22.0 (0.382)	23.5 (1.90)
Air temperature, °C	24.2 (0.348)	25.2 (0.409)	24.8 (0.255)	24.9 (0.376)	24.6 (0.307)	29.2 (0.935)
Wind velocity, km/h	0	0	0	8.7 (0.842)	11.4 (0.368)	16.2 (0.638)

6.3.2 Evaporation Rates

Table 6-4 shows the actual evaporation rate as well as the estimated evaporation rates found in the evaporation tests. The estimated evaporation rate was determined from equation (2.1) and the ACI (1999) nomograph using the climatic conditions from Table 6-3.

Table 6-4 shows a noticeable difference between the estimated and actual evaporation rates. The estimated evaporation rates from equation (2.1) compared to the actual evaporation rate had a difference of -125, -51.0, -52.1, -43.7, -44.2 and -10.5 %. A similar difference of -21.8, -35.9, -39.0, -35.0, -36.1 and -3.20 % was seen between the estimated evaporation rates from the ACI nomograph when compared to the actual evaporation rate of the concrete. The following trend was noticed from the findings, which showed that with the increase in the evaporation rate, the smaller the difference between the estimated evaporation rates (of the ACI (1999) nomograph and equation (2.1)) became compared to the actual evaporation rate. A reason for the difference is that equation (2.1), and the ACI (1999) nomograph estimates the evaporation of water on the surface of the concrete (Uno, 1998).

The actual and estimated evaporation rates show that ERL-4 and ERL-5 obtained a similar evaporation rate with different climatic conditions. Table 6-3 showed that the temperature parameters of the evaporation rates were roughly the same while ERL-4 had a lower relative humidity and ERL-5 had a higher wind velocity. Despite ERL-4 and ERL-5 having similar evaporation rates, the variation in the climatic conditions could affect the concrete differently.

Table 6-4: The average evaporation rate of the climatic conditions

Conditions	ERL-1	ERL-2	ERL-3	ERL-4	ERL-5	ERL-6
Equation (2.1) evaporation rate, kg/m^2/h	-0.0145	0.0730	0.146	0.351	0.357	0.756
ACI nomograph evaporation rate, kg/m^2/h	0.0455	0.0955	0.186	0.405	0.409	0.818
Actual evaporation rate, kg/m^2/h	0.0582	0.149	0.305	0.623	0.640	0.845

Due to the inconsistency in estimating the evaporation rate from the ACI (1999) nomograph and equation (2.1), it was decided that the actual evaporation rate would be used throughout the study as reference points for the climatic conditions.

6.4 PLASTIC SHRINKAGE CRACKING

The PS crack growth at the various evaporation rates is illustrated in Figure 6-2. Each line represents the average crack growth in that evaporation rate. The figure also shows when the

concrete reached the initial setting time of 283 minutes in each test. The variability in the setting times was due to the different starting times of each test. The final PS cracks for each evaporation test can be found in Appendix C. Figure 6-2 clearly shows that as the evaporation rate increased, the crack width increased. This corresponds with the literature stating that the PS cracking severity is influenced by higher evaporation rates (Boshoff and Combrinck, 2013; Kayondo *et al*., 2019; Sayahi *et al*., 2021). Higher evaporation rates induce higher tensile stresses on the surface of the concrete, resulting in earlier PS cracking.

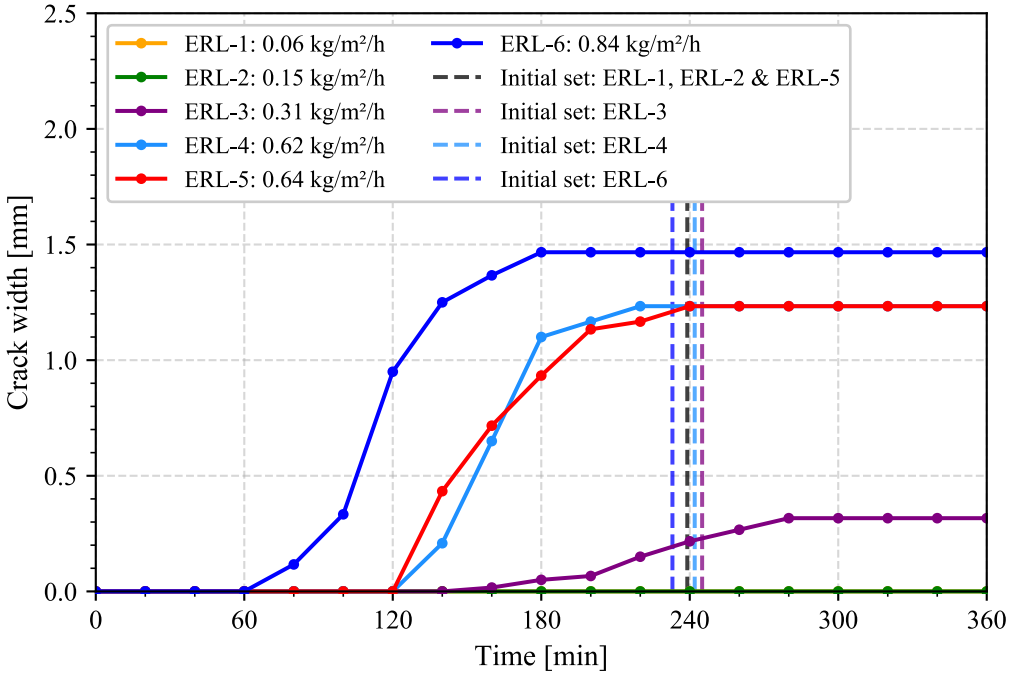

Figure 6-2: The average crack width at different evaporation rates

The PS crack growth during each evaporation rate is summarised in Table 6-5. The time when the cracking onset and stabilisation occur is shown in the table, along with the crack widths at onset and stabilisation.

The PS crack onset time at evaporation rates ERL-4: 0.62 kg/m^2/h and ERL-5: 0.64 kg/m^2/h coincided. It is due to the ERL-4 and ERL-5 having similar evaporation rates, with the evaporation rate of ERL-5 being slightly higher. The graph illustrates that between 120 and 240 minutes, the crack growth of ERL-4 and ERL-5 had different cracking patterns but obtained the same stabilisation crack width. The reason for this might be due to the difference in climatic conditions shown in Table 6-3. The findings suggest that when the concrete is exposed to roughly the same evaporation rate, the PS crack will obtain the same stabilisation crack. Furthermore, the results show that by decreasing the evaporation rate from ERL-4: 0.62 kg/m^2/h to ERL-3: 0.31 kg/m^2/h, the crack onset time and the crack stabilisation time were

delayed by 53.30 and 60 minutes. In all of the evaporation rates, PS cracking occurred before the concrete reached the initial setting time, which corresponds with what Turcry and Loukili (2006) and Combrinck and Boshoff (2013) noticed.

The average onset cracks width and cracks width at stabilisation of the concrete in each evaporation rate increased as the evaporation rate increased. When comparing the width of the crack at stabilisation for the concrete in ERL-3: 0.31 kg/m^2/h with ERL-4: 0.62 kg/m^2/h. The width of the crack at stabilisation from ERL-3 to ERL-4 increased significantly by 284 %. Emphasising how the crack width of the PS cracks increases as the evaporation rate increases.

Table 6-5: Average PS cracking of the low bleed concrete at different evaporation rates

Conditions	ERL-1	ERL-2	ERL-3	ERL-4	ERL-5	ERL-6
Average onset time of PS cracks, min	-	-	193	140	140	93.3
Average PS crack after stabilisation time, min	-	-	280	220	240	180
Initial setting time during the test, min	239	239	245	242	239	233
Average PS crack width at onset, mm	0	0	0.07	0.21	0.43	0.30
Average PS crack width at stabilisation, mm	0	0	0.32	1.23	1.23	1.47

6.5 CAPILLARY PRESSURE

The negative CP build-up envelopes for the low bleed concrete at the various evaporation rates are shown in Figure 6-3. The negative CP build-up envelope represents the region where the negative CP build-up curves are located for a certain evaporation rate. Each envelope was obtained either using the highest and lowest negative CP build-up or the most representable curves for that evaporation rate. The individual CP measurements of each test are shown in Appendix C.

The figure clearly shows that as evaporation rates increased relative to ERL-1: 0.06 kg/m^2/h, the build-up of negative CP increased. This is consistent with the findings from Slowik *et al.* (2014), that the greater the rate of evaporation, the greater the negative CP build-up. A reason for this was that the higher evaporation rates resulted in decreasing the menisci radii between solid particles at a higher rate, causing the negative CP build-up to increase substantially. The

significant increase in the negative CP build-up induced high tensile stresses on the concrete surface, leading to earlier crack growth.

According to the findings from Holt and Leivo (2004) and Slowik *et al.* (2008), a drop in pressure in the negative CP build-up of the concrete occurs either with air entry or by rewetting the concrete surface. Pressure drops were noticed in the individual negative CP build-up curves shown in Appendix C (Figure C.1). The pressure drops were found to occur between the PS cracking onset and stabilisation. Some of the pressure drops could also be seen in the negative CP curve envelopes of ERL-4, ERL-5 and ERL-6. The pressure drops might, therefore, be due to sudden water movement or air entry within the concrete as a crack formed.

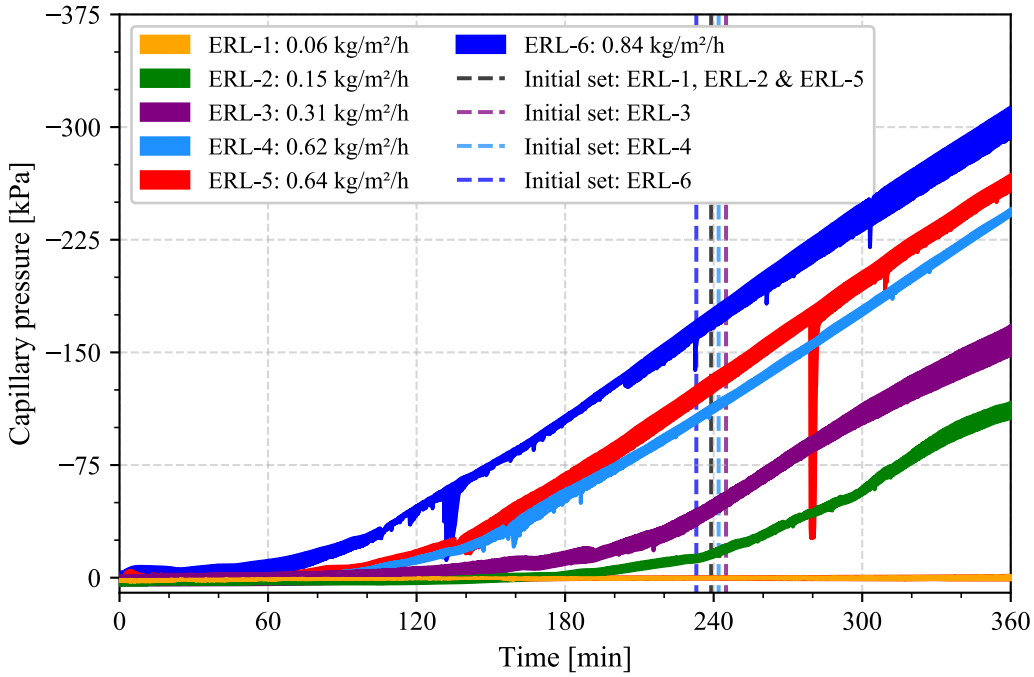

Figure 6-3: The negative CP build-up envelopes at the different evaporation rates

Table 6-6 shows the CP values at the time of specific events of crack formation and initial set for the different evaporation rates. The specific events of crack formation include the CP before PS cracking and at the onset of PS cracking. It should be noted that crack measurements were measured at 20-minute intervals, which means that the critical CP at which PS cracks form could be higher than the recorded CP values.

The findings in Table 6-5, showed that the specimens exposed to ERL-1: 0.05 kg/m^2/h and ERL-2: 0.15 kg/m^2/h had no PS cracking. However, only the concrete exposed to ERL-2 obtained a negative CP build-up during the test, as illustrated in Figure 6-3. Therefore, confirming that a negative CP build-up exists where no PS cracking occurs in the concrete.

An interesting finding shown in the figure is that at the low evaporation rate ERL-2, the negative CP build-up obtained an S-type curvature. A possible cause is that the concrete surface has stiffened to a point where low evaporation does not affect negative CP build-up in the concrete and that the build-up is now due to cement hydration within the concrete.

Another notable aspect presented in the table is that the CP before PS cracking and the CP at the onset of PS cracking at different evaporation rates occurred roughly at the same CP values. The CP values before any PS cracks formed was between -14.3 and -12.5 kPa in evaporation rates between ERL-3: 0.31 kg/m^2/h to ERL-6: 0.84 kg/m^2/h. The CP at the onset of the PS cracking occurred between -24.5 and -20.1 kPa for evaporation rates between 0.31 and 0.84 kg/m^2/h (ERL-3 to ERL-6). It can be argued that by maintaining the negative CP build-up for the low bleed concrete below -12.5 kPa, no PS cracks will form. This confirmed the conclusion made by Slowik *et al.* (2014) that when a critical CP is reached, the concrete may crack.

When comparing the PS crack width results (Table 6-5) with the CP results, the crack width increased as the negative CP build-up rate increased. The reason for this is that the higher the rate of the negative CP build-up in the concrete, the sooner the concrete will reach high negative CPs. The higher negative CP will result in high tensile stresses forming in the concrete and more severe PS cracking. The crack growth started at the point in time when a critical CP was reached, which corresponds to the conclusion Slowik *et al.* (2014) made that the negative CP build-up is the primary driver for PS, and when a critical CP is reached, PS cracks might occur. In addition, the findings showed that the PS cracks continued to grow until the initial setting time, where the cracks started to stabilise towards the final set, which correlates with the findings from Combrinck and Boshoff (2013).

As expected, the negative CP values at the initial setting time increased with the increase in the evaporation rate. The reason for this is that as the evaporation rate increased, the negative CP build-up rate increased significantly.

Table 6-6: Average CPs of the low bleed concrete at the different evaporation rates

Conditions	ERL-1	ERL-2	ERL-3	ERL-4	ERL-5	ERL-6
CP before cracks, kPa	-	-	-14.1	-12.5	-12.9	-14.3
CP at the onset of cracks, kPa	-	-	-22.6	-20.1	-21.8	-24.5
CP at the initial setting time, kPa	0.231	-18.1	-52.2	-114	-106	-158

The findings also showed that as the negative CP build-up rate increased with the increase in the evaporation rate, the pressure-time area under each curve (between the drying time and initial set) increased. This corresponds with the pressure-time area term explained in Chapter 3, which increases with the increase in the negative CP build-up rate.

The negative CP build-up in ERL-2 for the low bleed concrete mix will be used in the empirical model as the no cracking negative CP curve. It is not known whether this ERL-2 is the true no cracking negative CP build-up curve and might be conservative. However, ERL-2 will be sufficient for testing the model.

6.6 DRYING TIME

Figure 6-4 shows the cumulative evaporation for the low bleed concrete at the different evaporation rates and the cumulative bleeding. The drying time was determined from the graph at the point in time when the cumulative evaporation was equal to the cumulative bleeding of the concrete.

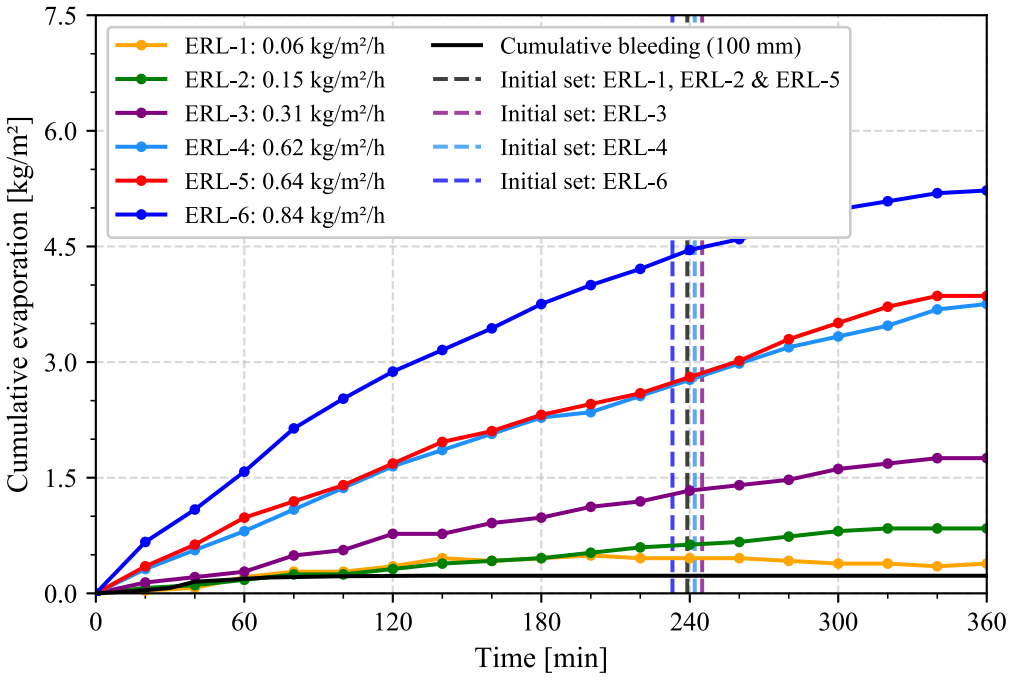

Figure 6-4: Cumulative evaporation at different climatic conditions

Table 6-7 provides the drying time determined from Figure 6-4 and the average CP drying time found from the CP measurements at the six evaporation rates. The CP drying time refers to the time at which the negative CP build-up in the concrete reached 0 kPa.

The table shows that only the drying time at evaporation rate ERL-1: 0.06 kg/m^2/h and ERL-2: 0.15 kg/m^2/h was determined. When the evaporation rate was higher than ERL-2: 0.15 kg/m^2/h, the cumulative bleeding curve could not intersect the cumulative evaporation. The drying time of the concrete with evaporation rates higher than ERL-2 could not be determined. A probable reason for not being able to determine the drying time at higher evaporation rates might be because of the concrete mixture's low bleeding property. However, the results did not correlate with the drying time literature. The literature stated that the drying time is the point at which the cumulative amount of evaporation is equal to the cumulative amount of bleeding (Kwak and Ha, 2006). The findings show that the drying time literature does not apply to all concrete mixtures.

The results showed that as the evaporation rate increased, the CP drying time occurred sooner in time. The CP drying time for ERL-4 occurred 13.06 minutes earlier than that of ERL-5. The reason for this could be that at a certain point in time, the evaporation rate of ERL-4 was slightly higher than that of ERL-5, which could have influenced the CP drying time. However, the CP drying times found at the different evaporation rates confirmed the findings from Kwak and Ha (2006) on the drying time of concrete. Which states that as the evaporation rate increase and the bleeding remains constant, the drying time will occur sooner in time.

Table 6-7: Drying time of the low bleed concrete at different evaporation rates

Conditions	ERL-1	ERL-2	ERL-3	ERL-4	ERL-5	ERL-6
Drying time from Figure 6-4, min	25	30	0	0	0	0
CP drying time, min	234	133	87.9	54.7	67.8	20.5

The drying time could not be found by locating the point in time at which the cumulative evaporation equals the cumulative bleeding. Therefore, the CP measurement (CP drying time) was used to find the drying time of the concrete throughout the study.

6.7 PROPERTIES TO VERIFY PLASTIC SHRINKAGE CRACKING CHARACTERISATION

In this section the verification properties are presented which consists of the VMC, concrete temperatures and plastic settlement.

6.7.1 Volumetric Moisture Content

Figure 6-5 shows the VMC envelopes of the concrete at different evaporation rates over time. It can be seen that as the evaporation rate increased the measured VMC in the concrete decreased.

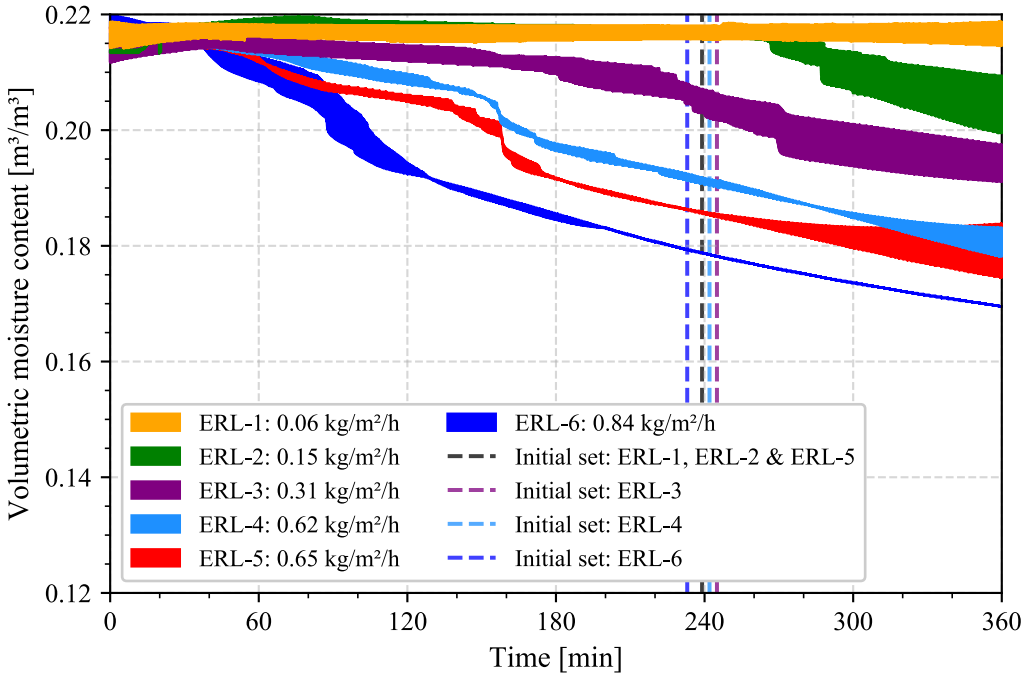

Figure 6-5: VMC envelopes of the concrete at different evaporation rates

Table 6-8 provides a summary of the VMCs for the concrete at the six different evaporation rates. The VMCs at; the start of the test, before cracking, the onset of the crack, initial set and after the 6-hour test are presented in the table.

The results clearly show that as the evaporation rate increased, the VMC in the concrete reduced. When comparing the total amount of moisture loss throughout the test from ERL-1: 0.06 kg/m^2/h to ERL-6:0.84 kg/m^2/h, the moisture loss decreased by -0.461, -3.93, -9.32, -16.3, -16.7 and -22.5 % as the evaporation rate increased. The decrease in moisture loss is due to the ongoing evaporation and cement hydration. The findings indicated that when the amount of moisture loss from the concrete over the 6 hours was lower than -3.93 %, PS cracking might occur.

The tables show that the VMC in the concrete before any cracks occurred at ERL-3: 0.31 kg/m^2/h to ERL-6: 0.84 kg/m^2/h were between 0.2111 and 0.2020 m^3/m^3. It was also seen in the table that the onset of the PS cracks would occur at the VMC range of 0.2105 and 0.1947 m^3/m^3. ERL-6 had a lower VMC before cracks than ERL-4: 0.62 kg/m^2/h, and

ERL-5: 0.65 kg/m^2/h had at the VMC at the onset of the cracks. Therefore, showing that PS cracking was not dependent on the VMC in the concrete. However, as the evaporation rate in each environment increased, the VMC at the time of the onset of the cracks decreased. The VMC results agree with the findings of Holt and Leivo (2004); the higher the evaporation rate, the sooner the negative CP builds up in the concrete. Meaning that the sooner the negative CP starts building up, the more water must be extruded from the concrete at an earlier time.

Table 6-8: The VMC of the low bleed concrete at the different evaporation rates

Conditions	ERL-1	ERL-2	ERL-3	ERL-4	ERL-5	ERL-6
Initial VMC, m^3/m^3	0.2169	0.2136	0.2136	0.2159	0.2151	0.2187
VMC before cracks, m^3/m^3	-	-	0.2111	0.2088	0.2045	0.2020
VMC at the onset of cracks, m^3/m^3	-	-	0.2105	0.2071	0.2020	0.1947
VMC at the initial setting time, m^3/m^3	0.2172	0.2102	0.2047	0.1909	0.1958	0.1867
Average VMC after the test, m^3/m^3	0.2168	0.2052	0.1937	0.1807	0.1792	0.1695

6.7.2 Concrete Temperature

The internal and surface concrete temperature measurements at the six evaporation rates are presented.

i Internal Temperature

The internal concrete temperature measured at the different evaporation rates is shown in Figure 6-6. The temperature curve illustrates that most of the specimens exposed to the six evaporation rates followed more or less the same pattern except for ERL-1: 0.06 kg/m^2/h to ERL-3: 0.31 kg/m^2/h. The figure shows that the concrete temperature initially decreased with the ongoing evaporation and increased as the concrete reached initial set. When considering the internal temperature findings and the air temperature in Table 6-3 in each evaporation test, it was seen that the higher the air temperature of the evaporation rate, the higher the temperature rise of the concrete temperature, as seen with ERL-6: 0.84 kg/m^2/h. As the concrete started to solidify (initial set), the temperature increased more rapidly, increasing toward the air temperature of that environment. The reason for this phenomenon was that a solid material conducts heat better than a liquid. Another reason for the increase in concrete temperature was

the hydration of the cement, which relates to the literature on the heat of hydration. As the hydration of the cement commences, heat is generated from within the concrete.

In addition, the temperature pattern of the concrete in ERL-1: 0.06 kg/m^2/h followed a different pattern than the concrete exposed to the higher evaporation rates. The temperature slightly increased from the start of the tests, and as the concrete began to approach the initial setting time and solidify, the concrete temperature rapidly increased.

The concrete in ERL-2: 0.15 kg/m^2/h and ERL-3: 0.31 kg/m^2/h followed a more constant pattern than the other evaporation rates. ERL-2 showed a linear increase, while ERL-3 showed a slight curve. The similar pattern seen between ERL-2 and ERL-3 could be due to the fact that the concrete in these evaporation rates was not exposed to any wind.

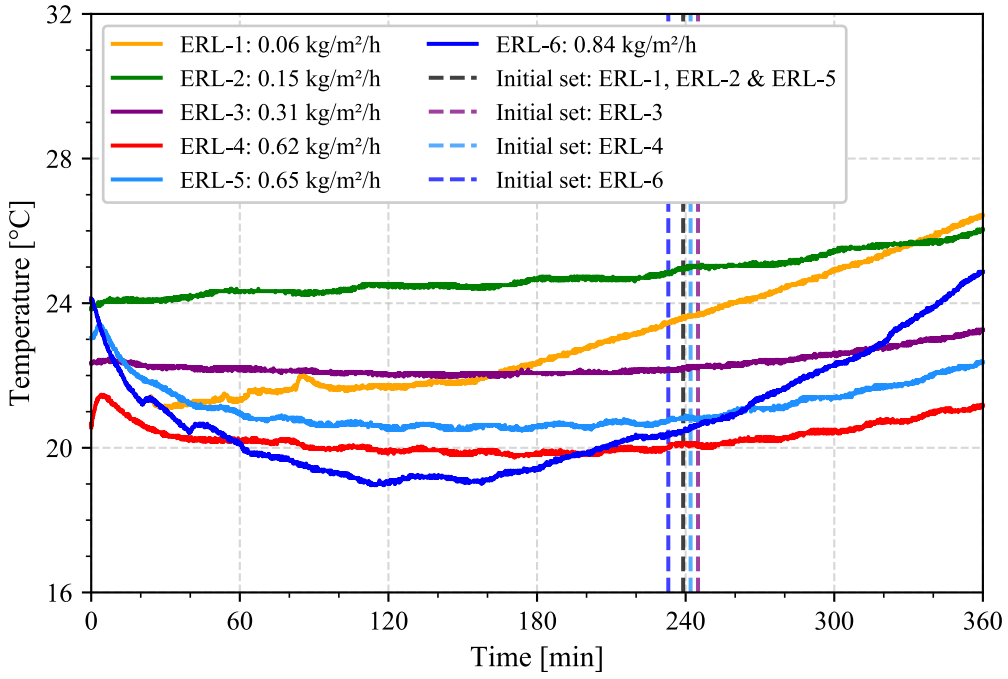

Figure 6-6: The internal temperature at different evaporation rates

The internal temperature at the initial setting time and after the 6-hour at different evaporation rates are shown in Table 6-9. The internal temperature for ERL-1: 0.06 kg/m^2/h and ERL-2: 0.15 kg/m^2/h compared to the ERL-3: 0.31 kg/m^2/h to ERL-6: 0.84 kg/m^2/h had the highest internal temperature after the test. A similar occurrence is observed in the temperature at the initial set of concrete. ERL-1, and ERL-2 had the highest temperature compared to the rest of the evaporation rates, with ERL-2 being significantly higher than ERL-1.

When comparing the concrete temperature after 6 hours with the air temperature (Table 6-3). ERL-1: 0.06 kg/m^2/h obtained a temperature of 26.4 °C while the air temperature of the

evaporation rate was 24.2 °C. At the same time, ERL-2: 0.15 kg/m^2/h obtained an internal temperature of 26.0 °C, while the air temperature was 25.2 °C. A probable reason for this was that more cement hydration took place for the concrete in ERL-1, which resulted in developing more heat from within the concrete.

Table 6-9: Internal temperature of the low bleed mix at different evaporation rates

Conditions	ERL-1	ERL-2	ERL-3	ERL-4	ERL-5	ERL-6
Temperature before crack, °C	-	-	22.1	20.2	20.5	19.8
Temperature at the onset of cracks, °C	-	-	22.2	20.0	20.5	19.4
Temperature at the initial setting time, °C	23.6	25.0	22.3	20.1	20.8	20.4
Temperature after 6 hours (360 minutes), °C	26.4	26.0	23.3	21.2	22.4	24.9

Therefore, the internal temperature of the concrete is dependent on the heat released from the hydration of cement and the air temperature of the environment.

ii Surface Temperature

Figure 6-7 illustrates the measured concrete surface temperature at each evaporation rate over time. The lines represent the average surface temperature for the concrete at each evaporation rate.

The figure shows that the surface temperatures at the different evaporation rates obtained similar patterns to that of the internal temperature (Figure 6-6). Conversely, the surface temperature for ERL-4 to ERL-6 started increasing earlier than the internal temperature. The reason for the increase might be because ERL-4 to ERL-6 were the only tests where the concrete was exposed to a dry and warm wind blowing on the surface of the concrete. After the initial set time was reached, the surface temperature increased significantly. The increase in surface temperature as the concrete reaches the initial set time is because the concrete changes from the stiffening stage to the solidification stage and the solid concrete conducts the heat faster than the concrete in the plastic state.

When comparing the decreasing section of the surface temperature curve with the decreasing section of internal temperature (Figure 6-6), the surface temperature had a slighter decrease. The slight decrease is possibly due to the surface of the concrete being physically exposed to the air temperature, causing the surface temperature to rise earlier.

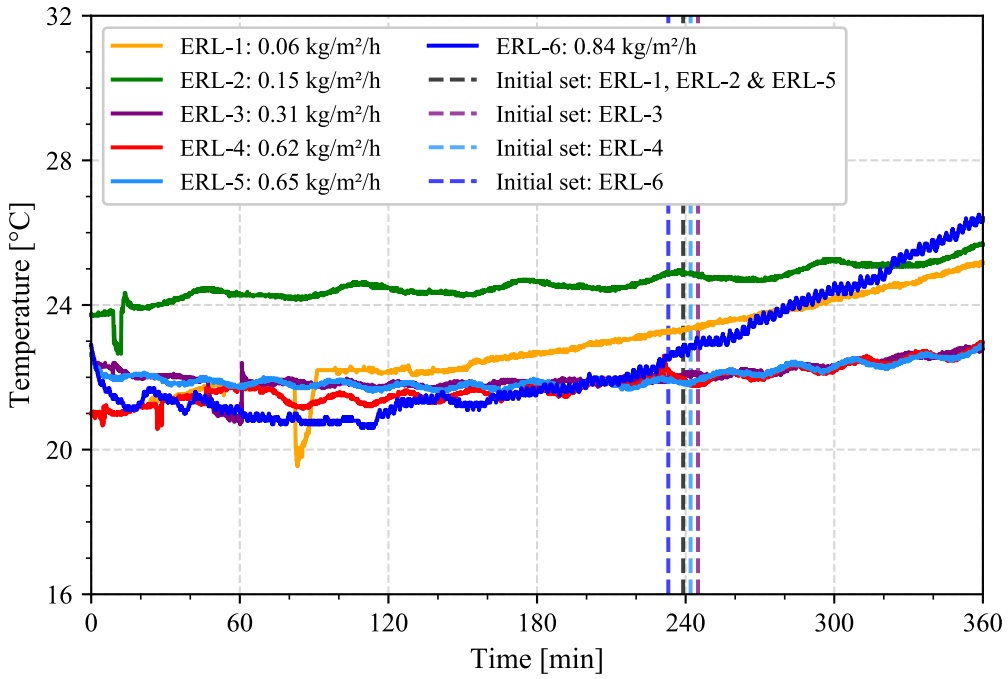

Figure 6-7: The surface temperature at the different evaporation rates

The concrete surface temperature results at the six evaporation rates are shown in Table 6-10. The graph and table show that ERL-1: 0.06 kg/m^2/h and ERL-2: 0.15 kg/m^2/h had the highest surface temperatures in the initial set of concrete, and after 6 hours, ERL-1, ERL-2, and ERL-6: 0.84 kg/m^2/h had the highest surface temperature. When considering the surface temperature measured after 6 hours and air temperature in Table 6-3 for ERL-1 and ERL-2, the surface temperature was 1 °C and 0.5 °C higher than the air temperature. While ERL-6 had the highest air temperature of 29.2 °C compared to all the evaporation rates, which resulted in a notable rise in temperature as the concrete reached the initial set time. The findings, therefore, suggest that the concrete surface temperature is not only influenced by the heat generated from cement hydration but also by the high air temperature.

Another essential fact noticed from the findings is that the internal temperature of the concrete after 6 hours (Table 6-9) at ERL-1: 0.06 kg/m^2/h to ERL-3: 0.31 kg/m^2/h was higher than the surface temperature of the concrete. A plausible cause is the heat extrusion from cement hydration in the concrete or because the concrete was not exposed to wind at these evaporation rates, which might have affected the concrete differently.

The findings showed no significant difference between the temperature before cracks and the temperature at the onset of the cracks. However, PS cracking of ERL-3: 0.31 kg/m^2/h to ERL-6: 0.84 kg/m^2/h occurred at a surface temperature range of 21.3 to 21.8 °C.

Table 6-10: Surface temperature of the low bleed mix at difference evaporation rates

Conditions	ERL-1	ERL-2	ERL-3	ERL-4	ERL-5	ERL-6
Temperature before crack, °C	-	-	21.8	21.3	21.7	21.9
Temperature at the onset of cracks, °C	-	-	21.8	21.3	21.6	21.5
Temperature at the initial setting time, °C	23.3	24.9	22.0	21.4	21.8	22.7
Temperature after 6 hours (360 minutes), °C	25.2	25.7	22.8	23.0	22.9	26.2

The correlation between the internal and surface temperature of the concrete is that the concrete temperature is influenced by the heat generated from hydration and the high air temperatures.

6.7.3 Plastic Settlement

The plastic settlement measurements for the concrete at the six evaporation rates are illustrated in Figure 6-8. The findings demonstrate that the evaporation rate on concrete increased the amount of settlement increased. The noise seen in some of the plastic settlement measurements was possibly due to the wind blowing on the deflector causing some movement. It should be noted that the plastic settlement and PS cracking specimens had different concrete depth. Therefore, the CP, VMC and temperature results was not compared to the settlement results.

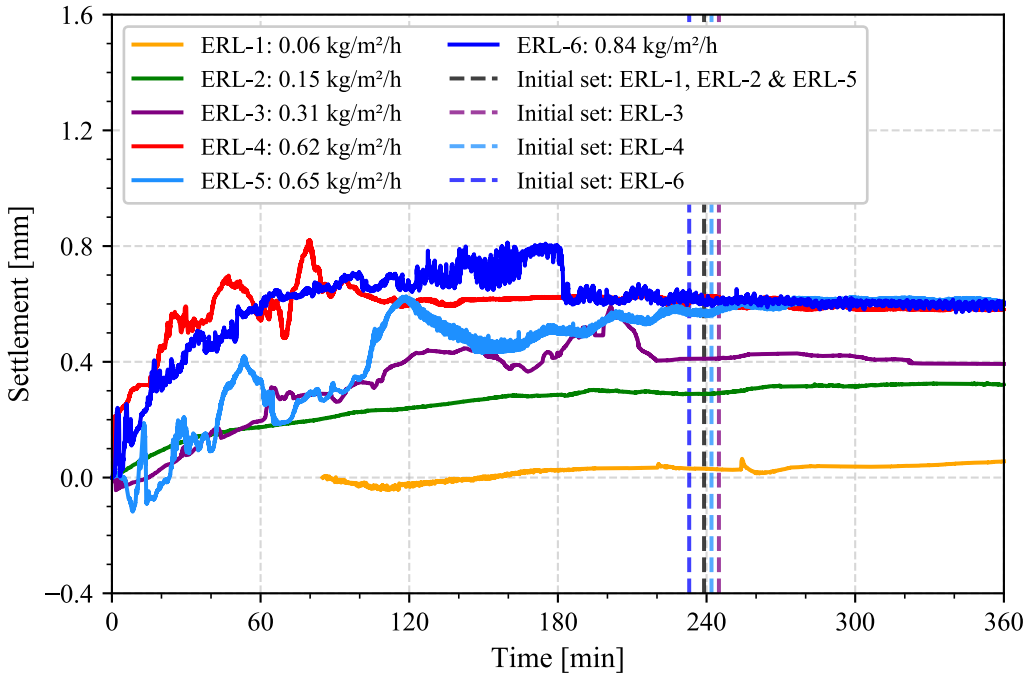

Figure 6-8: Plastic settlement at the different evaporation rates

Table 6-11 shows the settlement at the initial setting time and after the 6 hours. The figure and table show that the settlement for the specimens in ERL-4: 0.62 kg/m^2/h, ERL-5: 0.65 kg/m^2/h and ERL-6: 0.84 kg/m^2/h obtained roughly the same amount of settlement at the end of the test. A plausible reason for this phenomenon is that the concrete has reached a settlement point where the aggregates have interlocked.

The concrete settlement at six evaporation rates showed that as the concrete reached initial set, the concrete started to settle at a more constant rate. This confirm Sayahi *et al.*'s (2020) findings that after the concrete has reached the critical point (initial setting time), the concrete moves from the constant rate period to the falling rate period. After the critical point, bleeding occurs at a lower rate, causing the concrete to settle at more constant rate.

Table 6-11: Plastic settlement of the low bleed concrete at different evaporation rates

Conditions	ERL-1	ERL-2	ERL-3	ERL-4	ERL-5	ERL-6
Settlement at initial setting time, mm	0.0309	0.290	0.412	0.627	0.569	0.641
Settlement after 6 hours, mm	0.0560	0.322	0.393	0.581	0.605	0.601

6.8 CONCLUDING SUMMARY

The PS cracking characteristics of the low bleed concrete were determined to obtain the model parameters required for testing the proposed model. The conclusions drawn are summarised in the following sections: the non-environmental tests, the relationship between PS cracking and the evaporation rate and the model parameters required for the empirical model.

6.8.1 Non-Environmental Tests Conclusions

- The setting time tests showed a significant difference in the initial and final setting time between the Penetration Resistance and the Vicat Test Method. Therefore, the initial and final setting times for the Penetration Resistance Test Method (ASTM C403/C403M – 16) was used as the concrete's setting times.
- The bleeding results showed that the concrete's bleeding depends on the concrete depth. By comparing the two different depths, the bleeding capacity of the 250 mm concrete depth increased by 0.956 kg/m^2 when compared to the 100 mm concrete depth. Therefore, it was decided to use 100 mm for the cumulative bleeding to determine the drying time.

- The findings showed that the drying time could not be determined using the cumulative bleeding of the 100 mm specimen. The cumulative bleeding of the 100 mm specimen was only able to intersect the two lowest cumulative evaporation curves.

6.8.2 Relationship between Plastic Shrinkage and the Evaporation Rate

- The CP results showed that the evaporation rate affected the rate of the negative CP build-up in the concrete, and by increasing the evaporation rate the negative CP build-up rate increased. The results also showed that the negative CP build-curve forms an S-type of curvature at a low evaporation rate.
- It was found that the plastic shrinkage crack width increased, and the cracking onset time decreased with the increase in the evaporation rate.
- The findings showed that as the negative CP build-up rate increased the pressure-time area increased.
- The VMC results showed that the VMC in the concrete reduced as the evaporation rate increased.
- The internal and surface temperature of the concrete showed that the evaporation rate decreased the concrete temperature up until the initial setting time. Heat released by cement hydration and high air temperature notably influenced the concrete temperature. The surface temperature showed that the PS cracking of each environment occurred in a range of 21.3 to 21.8 °C.
- The results showed that as the evaporation rate increased, the plastic settlement of the concrete increased.

6.8.3 Model Parameters Required for the Empirical Model

- The initial setting time of the 283 minutes obtained from the Penetration Resistance Test Method will be used in the No Cracking CP Boundary Model.
- The CP measurements proved to be successful in determining the concrete's drying time (0 kPa) and was used throughout the study to determine the drying time required in the model.
- The findings showed that a negative CP build-up curve for low-bleed concrete (ERL-2: 0.15 kg/m^2/h) exists where no PS cracks will form. Therefore, ERL-2 is used in the model as the no crack negative CP build-up curve for the low bleed concrete.

7 PLASTIC SHRINKAGE CRACKING CHARACTERISATION OF SELF-COMPACTING CONCRETE MIXTURE

7.1 INTRODUCTION

The Plastic Shrinkage (PS) cracking characteristics of a Self-Compacting Concrete (SCC) were obtained by exposing the concrete to two distinct evaporation rates. The purpose of this chapter is to determine the model parameters needed to verify the No Cracking Capillary Pressure (CP) Boundary Model. The model parameters include the no crack CP build-up curve and the initial setting time of the SCC.

This PS cracking characterisation of the SCC mixture is obtained from the non-environmental and evaporation tests. The non-environmental tests include the setting time and bleeding. The evaporation tests include the climatic conditions, evaporation rates, CP, drying time, PS cracking, Volumetric Moisture Content (VMC), concrete temperature and plastic settlement.

7.2 NON-ENVIRONMENTAL TESTS

The setting times and bleeding of the SCC are presented and discussed in this section. The initial set for the SCC will be used to determine the duration of the evaporation tests for the SCC.

7.2.1 Setting Time

The setting times obtained for the SCC from the Penetration Resistance Test Method are shown in Table 7-1. The Standard Deviation (SD) of the setting times is also shown in brackets in the table.

Table 7-1: Setting times for the SCC with the SD in brackets

Setting time	Penetration resistance
Initial, min	511 (6.36)
Final, min	601 (2.12)

The initial setting time of the SSC was at 511 minutes; therefore, a testing duration of 540 minutes was decided upon.

7.2.2 Bleeding

The bleeding of the SCC was tested at a concrete depth of 100 mm and 250 mm. As expected for a SCC mixture, neither the 100 mm depth specimen nor the 250 mm specimen showed any bleeding or mass change. This verifies the conclusion made in Chapter 6 that by determining the drying time at which the cumulative amount of evaporation is equal to the cumulative amount of bleeding does not apply to all concrete mixtures.

7.3 CLIMATIC CONDITIONS AND EVAPORATION RATES

In this section, the climatic conditions and evaporation rates during each evaporation test for the SCC are presented and discussed.

7.3.1 Climatic Conditions

The SCC was exposed to the climatic conditions in the two evaporation tests shown in Table 7-2. The SD of each climatic condition is also shown in brackets in the tables. The evaporation tests are represented throughout this chapter as ERS-1 and ERS-2. An essential fact to remember is that the triangular prism restraints at the end of the PS cracking mould shown in Figure 4-19 were removed for all the tests on the SCC.

Table 7-2: Climate conditions of the two evaporation rates with the SD in brackets

Conditions	ERS-1	ERS-2
Relative humidity, %	66.8 (3.46)	33.2 (7.55)
Concrete surface temperature, °C	24.6 (0.277)	27.1 (1.26)
Air temperature, °C	25.1 (0.455)	31.8 (0.480)
Wind velocity, km/h	0	7.00 (0.171)

7.3.2 Evaporation Rates

The estimated and actual evaporation rates of the two evaporation tests are summarised in Table 7-3. When comparing the estimated evaporation rates to the actual evaporation rate, equation (2.1) had a difference of - 21.0 and 32.2 %, while the ACI (1999) nomograph had a difference of -3.29 and 39.6 %. The difference is notably smaller than the difference found for the low bleed concrete in Section 6.3.2. As previously discussed, the cause of the difference in

evaporation rates is that equation (2.1), and the nomograph, estimates the evaporation of water on the surface of the concrete. However, equation (2.1) and the nomograph provided a rough estimate of the actual evaporation rates for the SCC.

Table 7-3: Average evaporation rate of the climatic conditions

Conditions	ERS-1	ERS-2
Equation (2.1) evaporation rate, kg/m^2/h	0.0743	0.431
ACI nomograph evaporation rate, kg/m^2/h	0.091	0.455
Actual evaporation rate, kg/m^2/h	0.107	0.379

Figure 7-1 shows the cumulative evaporation of the SCC at the two evaporation rates. A notable increase in the cumulative evaporation of the concrete can be seen when increasing the evaporation rate from ERS-1 to ERS-2.

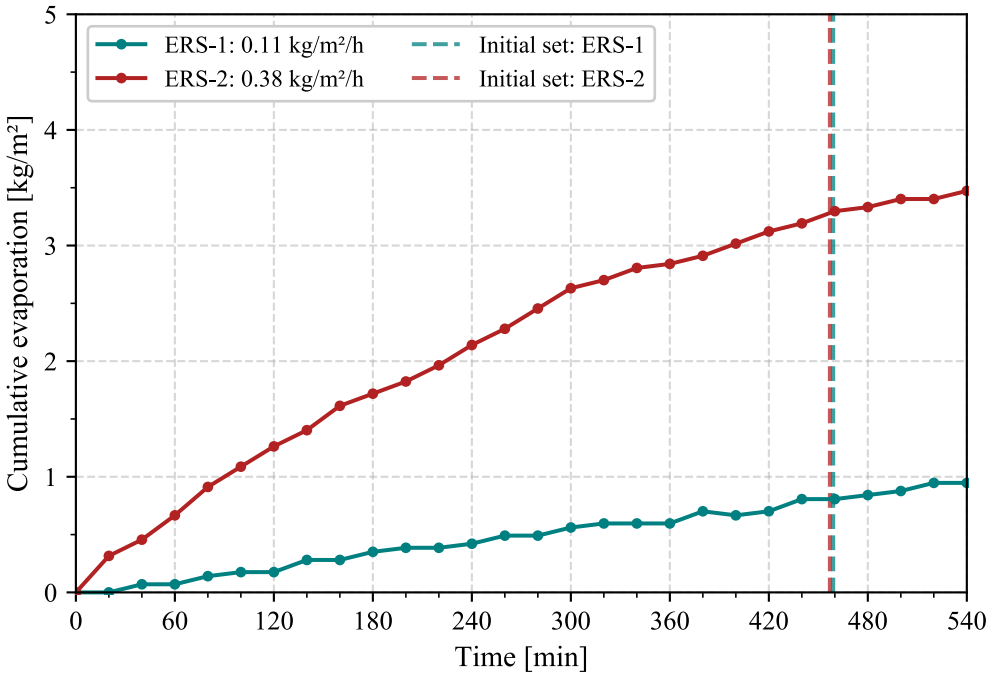

Figure 7-1: The cumulative evaporation of the SCC

7.4 CAPILLARY PRESSURE AND PLASTIC SHRINKAGE CRACKING

The negative CP build-up curve envelopes and PS crack growth of the SCC at the two evaporation rates are illustrated in Figure 7-2. Each curve envelope was determined from all

the CP build-ups obtained during each evaporation rate. The individual CP measurements and final PS cracks for each evaporation test can be found in Appendix D. The figure also shows when the concrete reached the initial setting time of 511 minutes in each test. The variability in the setting times was due to the different starting times of each test. In addition, the figure shows that an increase in the negative CP build-up rate resulted in earlier cavitation of the tensiometers, ERS-2 cavitated after 260 minutes whereas ERS-1 cavitated at 470 minutes. The noise seen in the CP measurements of ERS-2 is possibly due to the cycles of the dehumidifier in the MCC and the SCC, allowing movement.

When comparing the negative CP build-up of ERS-1: 0.11 kg/m^2/h to ERS-2: 0.38 kg/m^2/h. It can be seen that as the evaporation rate increased, the negative CP build-up rate increased significantly to a more linear curve. The findings correlate with the literature from Slowik *et al.* (2014), as the evaporation rate increase the rate of the negative CP build-up in the concrete increase.

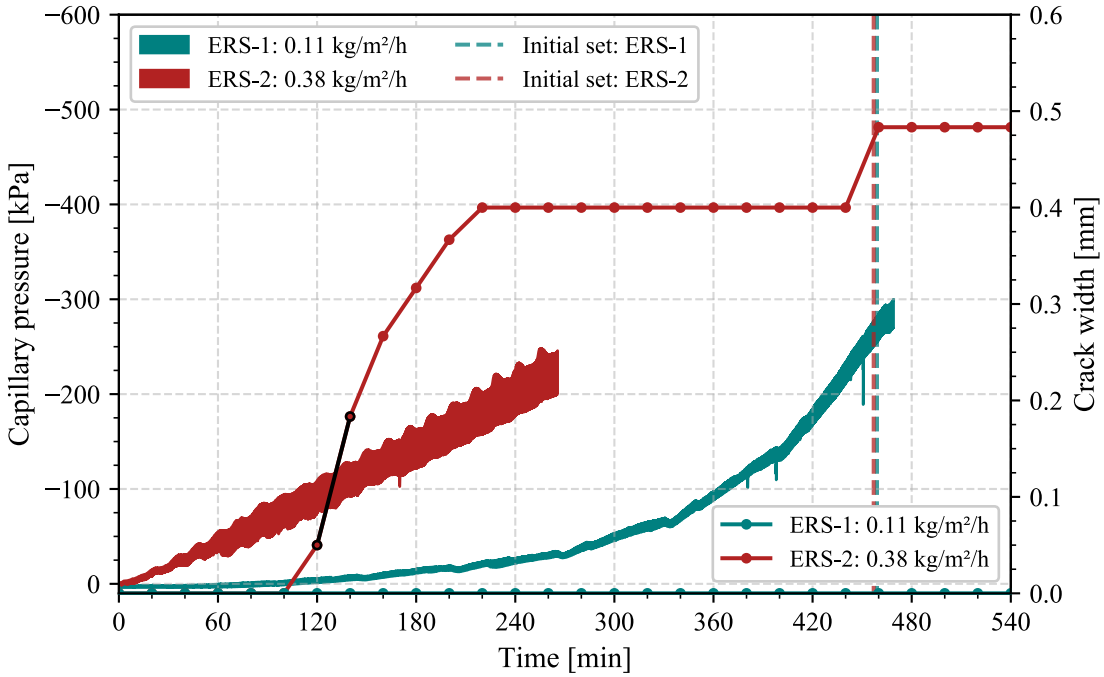

Figure 7-2: The negative CP envelopes and crack growth of the SCC at the two evaporation rates

According to Schmidt and Slowik (2009) and Leonovich (2018), finer particles produce smaller menisci between the particles, resulting in higher negative CP values. This occurrence is seen when comparing the CP envelope findings for the SCC in Figure 7-2 with the CP envelope finding for the low bleed concrete shown in Figure 6-3 at similar evaporation rates. The negative CP build-up of the SCC obtained at ERS-2: 0.38 kg/m^2/h has a significantly higher

build-up rate than that of the ERL-3: 0.31 kg/m^2/h. At 245 minutes, ERS-2 had a negative CP value of -201 kPa, whereas ERL-3 had a CP value of -52.2 kPa. This emphasises the effect of finer particles such as silica fume and fly ash on the negative CP build-up in concrete at similar evaporation rates.

Figure 7-2 shows that no PS crack has formed at an evaporation rate ERS-1: 0.11 kg/m^2/h as the negative CP builds up in the SCC, verifying that a no crack negative CP build-up curve exists for the SCC. Another important aspect shown in the figure is the notable increase in the PS crack growth as the evaporation rate increased from ERS-1 to ERS-2: 0.38 kg/m^2/h. The figure shows that the onset of the crack growth occurred at an early point in time; after that, the crack growth started to stabilise and slightly increased at initial set. This is in agreement with the findings from Combrinck and Boshoff (2013); when the concrete is exposed to an evaporation rate, the crack onset will occur before or at the initial setting time and continue to widen and stabilise towards the final set. The average PS cracking findings for the SCC can be found in Appendix D.

In Figure 7-2, a slightly pressure drop can be below the negative CP envelope of ERS-2. This pressure drop can clearly be seen in the individual negative CP build-up curves shown in Appendix D (Figure D.1). The individual CP measurements show that the pressure drop occurred between the PS cracking onset and stabilisation. According to Holt and Leivo (2004) and Slowik *et al.* (2008), pressure drops in the negative CP build-up of the concrete either occurs with air entry or by wetting the surface of the concrete. Therfore, the pressure drop might have been caused by some air entry or water movement within the SCC as a crack formed.

The average CP values before cracks occurred, at the onset of the cracks and at the initial setting time are shown in Table 7-4. The findings show that PS cracking for the specimens exposed to ERS-2: 0.38 kg/m^2/h occurred at a CP value between -78.7 and -89.4 kPa. This corresponds with the findings from Slowik *et al.* (2014), which states PS cracking will occur when a critical CP is reached.

Table 7-4: Average CPs of the SCC at the two evaporation rates

Conditions	**ERS-1**	**ERS-2**
CP before cracks, kPa	-	-78.7
CP at the onset of cracks, kPa	-	-89.4
CP at the initial setting time, kPa	-268	Sensor cavitation

The CP drying times obtained for the SCC at the two evaporation rates are presented in Table 7-5. The findings from Kwak and Ha (2006) stated that the drying time would occur earlier in time when the bleeding remains constant, and the evaporation rate is increased. The same phenomenon was seen in CP drying time results when the evaporation rate increased.

Table 7-5: Drying time of the SCC at different evaporation rates

Conditions	ERS-1	ERS-2
CP drying time, min	75.6	3.12

The findings also showed that the pressure-time area under each curve (between the CP drying time and initial set) increased, as the negative CP build-up rate increased with the increase in the evaporation rate. Therefore, the findings are in agreement with the pressure-time area term discussed in Chapter 3, which showed that as the rate of the negative CP build-up increased, the pressure-time area would increase.

The negative CP build-up of ERS-1 will be used as the no crack negative CP build-up curve in the empirical model to aid in preventing PS cracking in the SCC. It should be noted that it is not known whether ERS-1 is the true no cracking negative CP build-up curve and might be conservative. However, ERS-1 will be sufficient for evaluating the model.

7.5 PROPERTIES TO VERIFY PLASTIC SHRINKAGE CRACKING CHARACTERISATION

The VMC, internal and surface temperature, and plastic settlement are presented and discussed in this section.

7.5.1 Volumetric Moisture Content

The VMC measurements for the SCC were not evaluated because the inconsistent data made it challenging to calibrate. A probable cause for the inconsistency in the data is that the SCC had a lower viscosity than the low bleed concrete, allowing movement and making the sensor placement difficult.

7.5.2 Concrete Temperature

The average internal and surface temperature for the SCC specimens is illustrated in Figure 7-3. The figure clearly shows how air temperature affects concrete temperature and the correlation between the internal and surface temperature of the SCC. The internal and surface temperatures of the concrete in ERS-1 and ERS-2 followed more or less the same temperature path, with the surface temperature slightly higher than the internal temperature in both cases.

When comparing the internal and surface temperature of ERS-1 and ERS-2, the concrete temperature at ERS-2 initially decreased with the higher evaporation rate to about 100 minutes, where the temperature started to rise at a constant rate. After 320 minutes, the concrete temperature at ERS-2 exponentially increased as the concrete reached the initial set time. While the concrete temperature at the lower evaporation rate ERS-1 slightly decreased and slowly increased as the concrete stiffened towards the initial setting time.

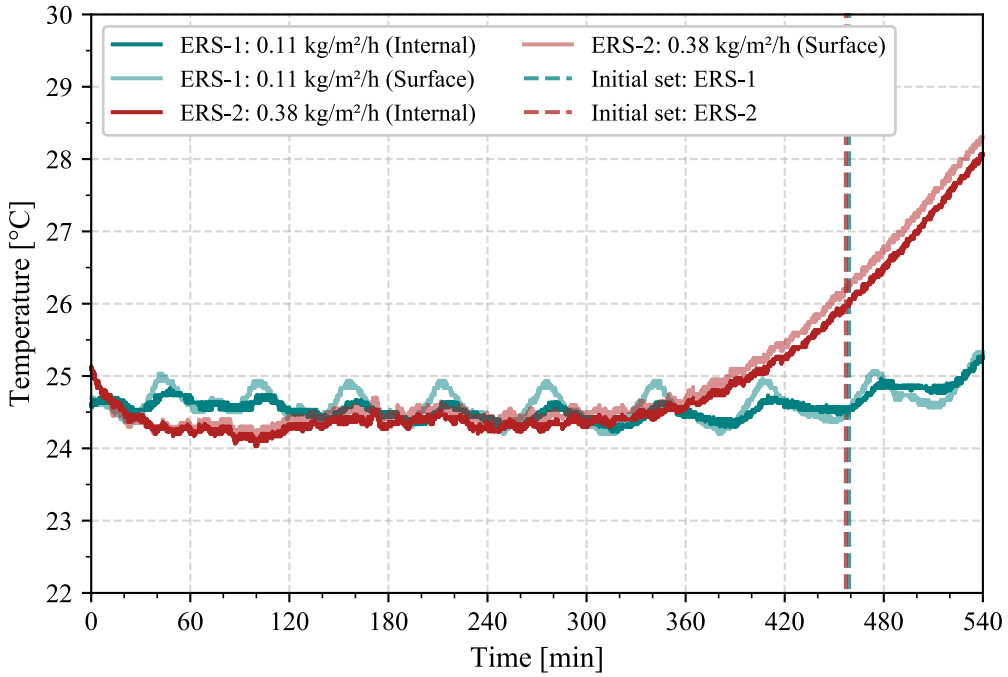

Figure 7-3: The concrete temperature of the SCC at different evaporation rates

Table 7-6 summarises the concrete temperature before cracking, at the cracking onset, at the initial set and after the test duration. No notable change in concrete temperature were noticed between the temperature before cracking and the temperature at the cracking onset. The internal and surface temperature of the concrete in ERS-1 obtained a similar temperature at the initial setting time and after 9 hours. However, in ERS-2, a difference of 8.08 and 4.98 % was observed between the internal and surface temperature of the concrete. The higher air temperature increased the surface temperature of the concrete, which was expected. When comparing the internal and surface temperature of ERS-1 with the air temperature, the concrete temperature was found to be 0.2 °C higher. The cause for this might be due to the heat generated from cement hydration within the concrete.

Table 7-6: The concrete temperature of the SCC

Conditions	ERS-1		ERS-2	
	Internal	Surface	Internal	Surface
Temperature before crack, °C	-	-	24.3	26.0
Temperature at the onset of cracks, °C	-	-	24.3	26.3
Temperature at the initial setting time, °C	24.6	24.6	26.0	28.1
Temperature after 9 hours (540 minutes), °C	25.3	25.3	28.1	29.5

Thus, the results show that the concrete temperature is influenced by the air temperature and the heat generated from cement hydration.

7.5.3 Plastic Settlement

Figure 7-4 presents the plastic settlement for the SCC at the two evaporation rates. The large initial settlements seen in the graph were possibly caused by the high sensitivity of the laser, which records the slightest movements. Another plausible cause is the lower viscosity of the SCC (compared to the low bleed concrete), and as the concrete started to stiffen, the recorded measurements became more constant. It should be noted that the plastic settlement specimens and the PS cracking specimens had different concrete depth. Therefore, the CP and temperature results were not compared to the plastic settlement results.

The figure shows that the concrete exposed to the higher evaporation rate in ERS-2 had more settlement than the concrete exposed to the evaporation rate in ERS-1. Therefore, the findings are in agreement with the findings from Sayahi *et al.* (2020), plastic settlement is related to the volume reduction in concrete.

Sayahi *et al.* (2020) recognised that when the concrete reaches initial set, the concrete moves from the constant rate period to the falling rate period, where the concrete bleeds at a lower rate, resulting in the concrete settling at a more constant rate. A similar phenomenon was seen with the SCC. Figure 7-4 shows that as the concrete matured and reached initial set, the settlement the concrete in ERS-1 and ERS-2 occurred at more constant rate. However, no bleeding was found for the SCC, showing that the increase in the plastic settlement was mainly due to the evaporation on the concrete.

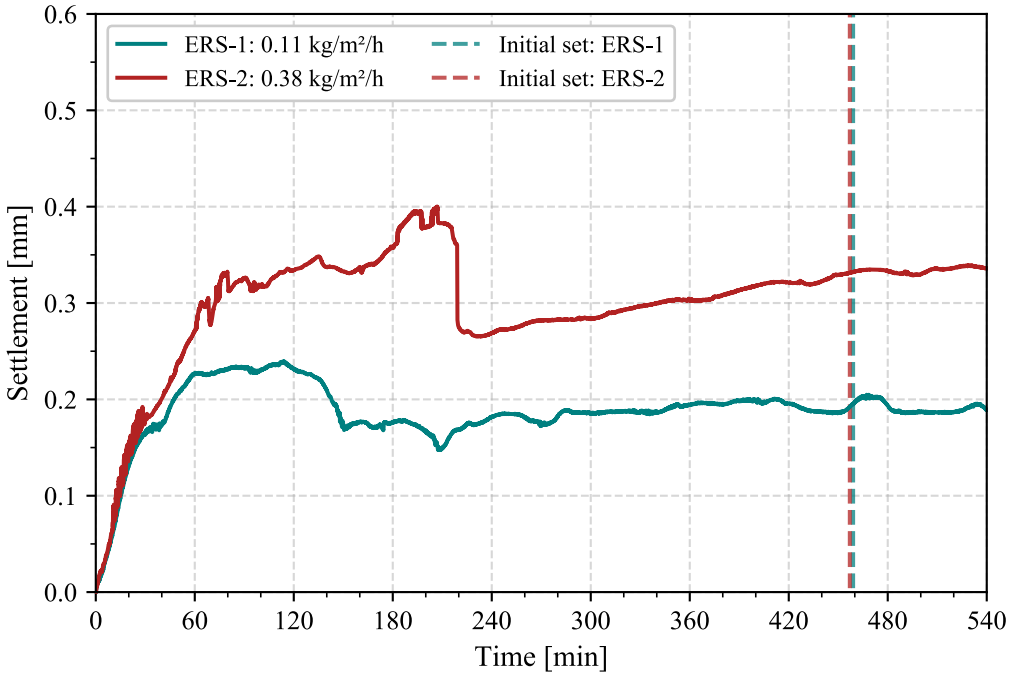

Figure 7-4: The plastic settlement at different evaporation rates

The plastic settlement at initial set and after 9 hours are shown in Table 7-7. It can be seen that the plastic settlement at initial set and after the 9 hours increased by 55.3 and 77.3 % by increasing the evaporation rate from 0.11 to 0.38 kg/m^2/h.

Table 7-7: The plastic settlement at the two evaporation rates

Conditions	**ERS-1**	**ERS-2**
Settlement at initial setting time, mm	0.195	0.303
Settlement after 9 hours, mm	0.189	0.336

7.6 CONCLUDING SUMMARY

In this chapter, the PS characteristics for the SCC were determined to obtain the required model parameter to verify the empirical model. The conclusion drawn from this chapter are grouped as the relationship between the PS cracking characteristic for the SCC and the evaporation and the required model parameters for the No Cracking CP Boundary Model.

7.6.1 Relationship between Plastic Shrinkage and the Evaporation Rate

- The findings showed that as the evaporation rate increased, the negative CP build-up rate and the PS crack width on the concrete would increase.
- The increase in finer particles such as silica fume and fly ash significantly increased the negative CP pressure build-up.
- It was found that the CP drying time decreased in time as the evaporation rate increased.
- The pressure-time increased with the increase in the negative CP build-up rate.
- The increase in evaporation rate increased the internal and surface temperature of the concrete. No notable change in the concrete temperature was observed when PS cracking occurred.
- The plastic settlement results showed that the increase in the evaporation rate increased the total amount of settlement.

7.6.2 Model Parameters Required for the Empirical Model

- The initial setting time of 511 minutes for the SCC obtained from the Penetration Resistance Test Method will be used in the model.
- The results proved that a negative CP build-up where no PS cracking will occur exists at the evaporation rate of ERS-1: 0.11 kg/m^2/h. Therefore, ERS-1 will be used in the no cracking CP boundary model for the SCC.

8 MODEL VERIFICATION PHASE

8.1 INTRODUCTION

Three model tests were conducted to verify the proposed No Cracking Capillary Pressure (CP) Boundary Model. The three tests evaluate the performance of the model with previous and live CP measurements. The model is verified to establish whether the model can provide guidance in preventing Plastic Shrinkage (PS) cracking in concrete mixtures. The three tests consisted of evaluating the model with:

- the low bleed CP results from the PS cracking characterisation phase
- Model Test A: the low bleed concrete at three different evaporation rates
- Model Test B: the Self-Compacting Concrete (SCC) at two distinct evaporation rates

In this chapter, the previous low bleed concrete CP results for the model tests are presented and covered. The findings for Model Tests A and B are discussed, followed by the model limitation and calibration needed for the model.

8.2 PREVIOUS LOW BLEED CONCRETE CAPILARY PRESSURE RESULTS

Table 8-1 provides the three model parameters and the average crack width of the low bleed concrete for the six evaporation tests. The calculated negative CP build-up area and calculated critical pressure limit are also shown in the table. The findings show that the negative CP build-up area increased as the evaporation increased. As the negative CP build-up area increased after the no crack negative CP build-up area (ERL-2), the average crack width in the concrete also increased. The reason for the occurrence is that the higher the evaporation rate, the higher the negative CP build-up in the concrete. The higher the amount of PS within the concrete, the more severe the PS cracking on the concrete surface will be when the concrete is restrained.

The findings show that the calculated critical pressure limit increased as the negative CP build-up area increased. When comparing the critical pressure limit of ERL-4: 0.62 $kg/m^2/h$ and ERL-5: 0.64 $kg/m^2/h$, it can be seen that ERL-5 had a higher evaporation rate and a lower calculated critical pressure limit. It is plausible that some of the CP build-ups of the concrete exposed to ERL-5 had a lower negative CP build-up rate. This results in the calculation of a lower critical pressure limit and therefore having to apply a lower, no cracking CP boundary. The empirical model was developed to calculate a lower critical pressure limit as the negative CP build-up rate decreases (increase in the evaporation rate) or a higher critical pressure limit when the negative CP build-up rate increases in the concrete. The critical pressure limit

equation, therefore, performs correctly in determining when to apply the no cracking CP boundary.

Table 8-1: The previous average CP results and model results for the low bleed concrete

Conditions	ERL-1	ERL-2	ERL-3	ERL-4	ERL-5	ERL-6
Actual evaporation rate, $kg/m^2/h$	0.06	0.15	0.31	0.62	0.64	0.84
CP drying time, min	234	133	87.9	54.7	67.8	20.5
Initial setting time, min	239	239	245	242	239	233
CP build-up area, kPa.min	-2.570	-634.8	-2317	-7335	-8130	-12140
Calculate critical pressure limit, kPa	-	-	-3.81	-3.20	-3.29	-2.95
Average crack width, mm	0	0	0.32	1.23	1.23	1.47

Figure 8-1 shows the regression line for plotting the negative CP build-up area against the evaporation rate. The figure shows that the evaporation rate increases as the negative CP build-up area increases. A strong linear relationship can be seen between the negative CP build-up area and the evaporation rate with an R^2-value of 0.982.

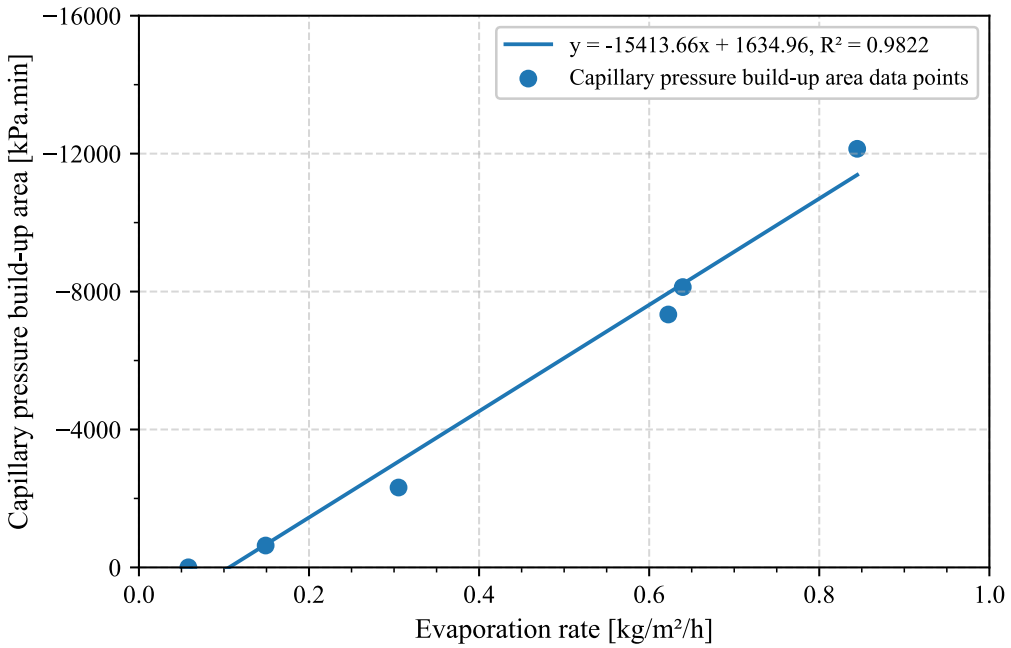

Figure 8-1: The negative CP build-up area versus the Evaporation rate

At the same time, Figure 8-2 shows the regression line for plotting the average crack width and no cracking CP boundary (that will have to be applied) against the negative CP build-up. The R^2-value of 0.953 shows a strong correlation between the average crack width and the negative CP build-up area of the concrete. A similar correlation between the no cracking CP boundary and the negative CP build-up area is seen. As the negative CP build-up area of the concrete increase, the average crack width increases while the no cracking CP boundary decreases.

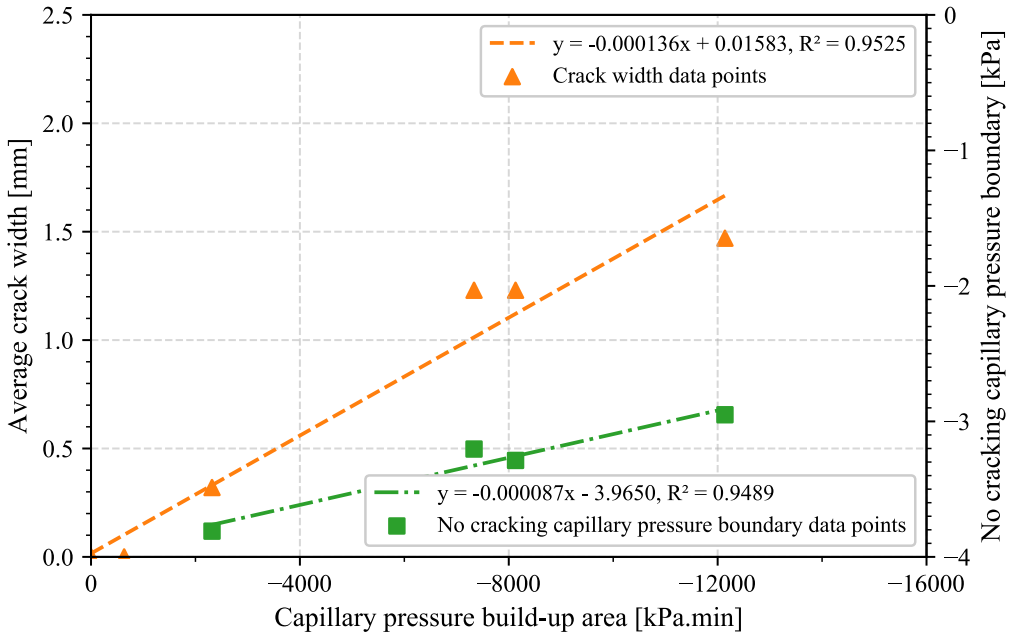

Figure 8-2: Average crack width and no cracking CP boundary versus the negative CP curve area

When considering the strong correlation between the plotted parameters. It can be argued that the two graphs can be utilised to predict the average PS crack width and the required no cracking CP boundary for preventing these PS cracks in the low bleed concrete. While only requiring the measured evaporation rate of the low bleed concrete.

8.3 MODEL TEST A: LOW BLEED CONCRETE

The results for testing the No Cracking CP Boundary Model with the low bleed concrete are provided and discussed in this section. By examining how applying the model, affected the following properties of the concrete, namely the climatic conditions, evaporation rate, CP and PS cracking, Volumetric Moisture Content (VMC) and concrete temperature.

8.3.1 Climatic Conditions

Table 8-2 presents the climatic conditions of the three low bleed concrete model tests. The Standard Deviation (SD) for each climatic condition is also shown in brackets in the table. The

three different model tests for the low bleed concrete will be referred to as Test A-1 to Test A-3 throughout the study.

Table 8-2: Climatic conditions for Model Test A with the SD in brackets

Conditions	Test A-1	Test A-2	Test A-3
Relative humidity, %	33.6 (1.42)	31.6 (4.61)	20.5 (1.99)
Concrete surface temperature, °C	25.2 (1.53)	23.3 (0.549)	22.2 (1.99)
Air temperature, °C	33.8 (1.67)	29.3 (0.829)	29.4 (1.18)
Wind velocity, km/h	2.81 (0.364)	4.73 (0.195)	18.4 (0.458)

8.3.2 Evaporation Rates

The cumulative evaporation from the concrete during Model Test A is shown in Figure 8-3. Solid lines represent the actual evaporation, whereas dashed dot lines showed the evaporation when water was added when the no cracking CP boundary was reached.

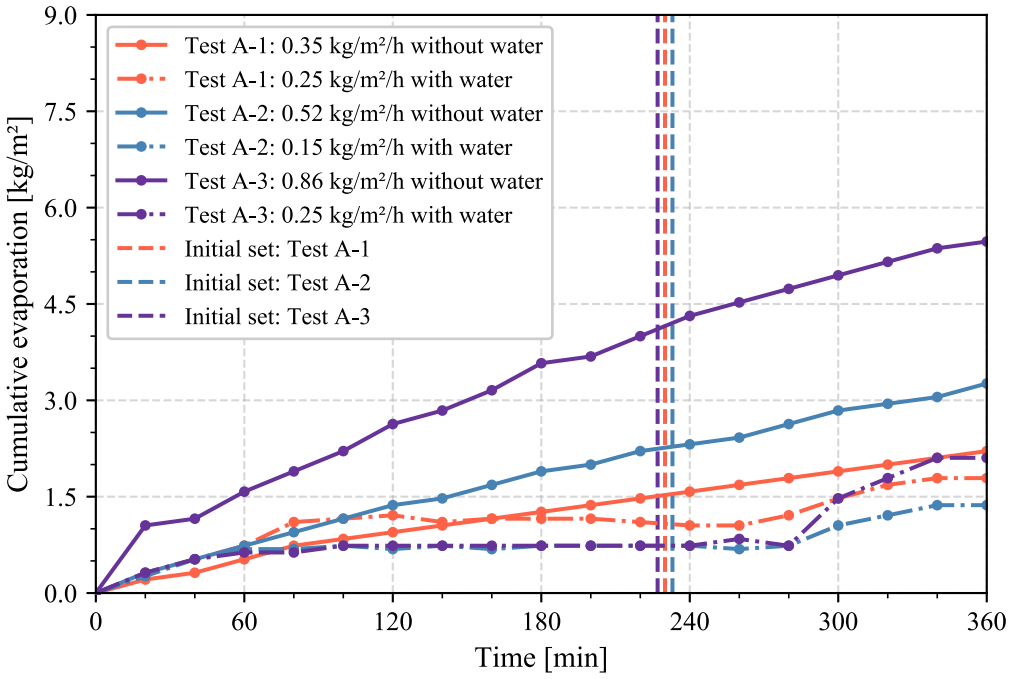

Figure 8-3: Cumulative evaporation during the Model Test A

The different evaporation rates and the total added water obtained during Model Test A are shown in Table 8-3. Figure 8-3 and Table 8-3 indicates that by adding water when the no cracking CP boundary was reached, the evaporation rate decreased significantly by 0.140, 0.371 and 0.253 kg/m^2/h. The results showed that when adding water to the surface of the concrete, the evaporation ceased for the duration that the boundary was applied. The graph shows that when the boundary was removed, and no water was further added to the concrete, the evaporation increased again.

Table 8-3: Total evaporation and water addition for Model Test A

Conditions	Test A-1	Test A-2	Test A-3
Actual total evaporation, kg/m^2	2.10	3.12	5.16
Total measured evaporation with the addition of water, kg/m^2	1.26	0.897	1.75
Total water added, kg/m^2	0.514	1.13	2.63

8.3.3 Capillary Pressure and Plastic Shrinkage Cracking

Figure 8-4 to Figure 8-6 show the negative CP build-up envelopes found by applying the model at three distinctive evaporation rates. The individual CP measurements and final PS cracks for each test can be found in Appendix C. The graph shows the CP and cracks width measurements over time. The figures also show when the concrete reached the initial setting time of 283 minutes in each test. The variability in the setting times was due to the different starting times of each test. The low bleed concrete was only sprayed with water for up to 280 minutes to observe the negative CP behaviour of the concrete after the added water.

The figure shows that as the evaporation rate increased, the no cracking CP boundary increased from -5.08 to -2.96 kPa. This confirms that the model correctly calculated the critical pressure limits as the evaporation rate increased. It can also be seen that all the calculated critical pressure limits were lower than the critical CPs between -14.32 and -12.46 kPa from Table 6-6.

All the Model Test A tests show that no PS cracks formed for the time that water was added when the no cracking CP boundary was reached. However, when no water was added after 280 minutes, only the specimens of Model Test A-3 started forming PS cracks. The cracks can be seen in Appendix C (Figure C.4).

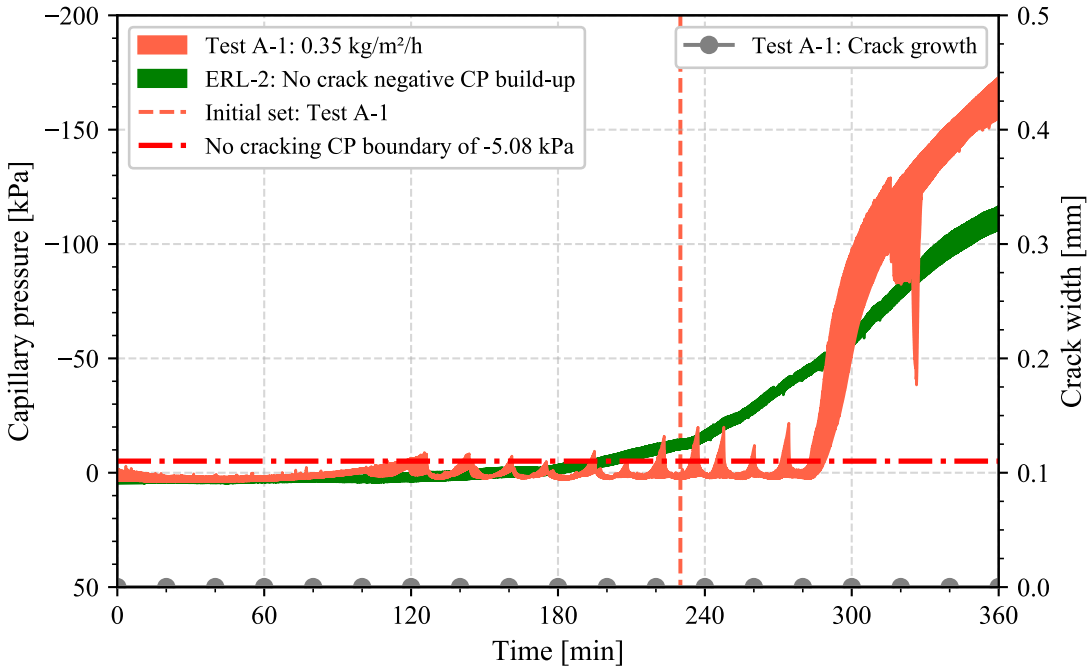

Figure 8-4: Negative CP build-up envelope and crack width for Model Test A-1

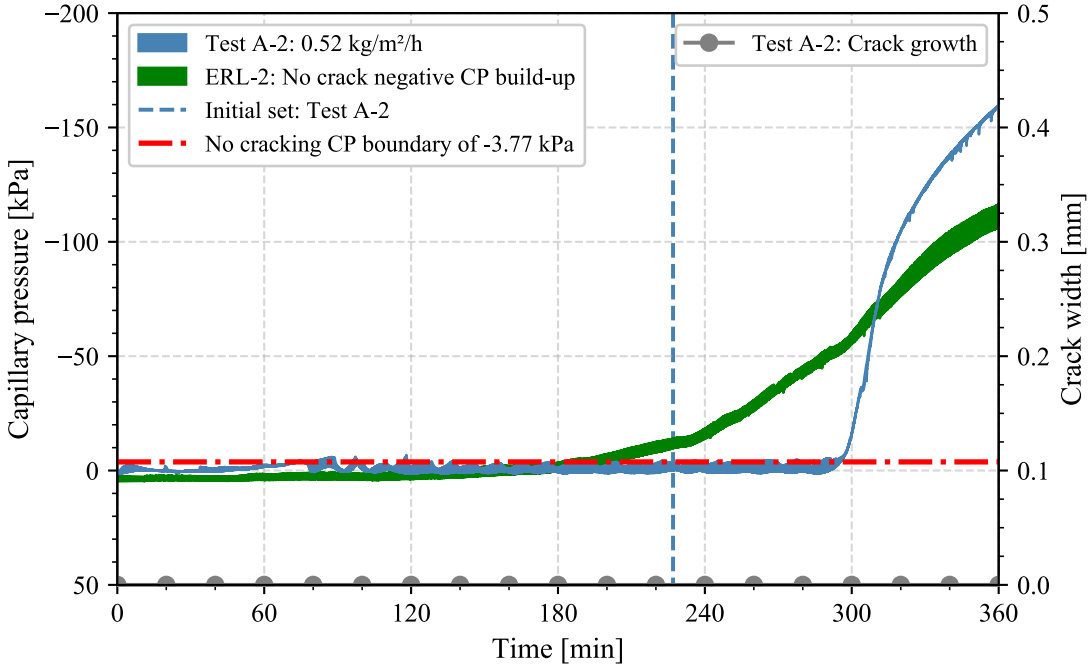

Figure 8-5: Negative CP build-up envelope and crack width for Model Test A-2

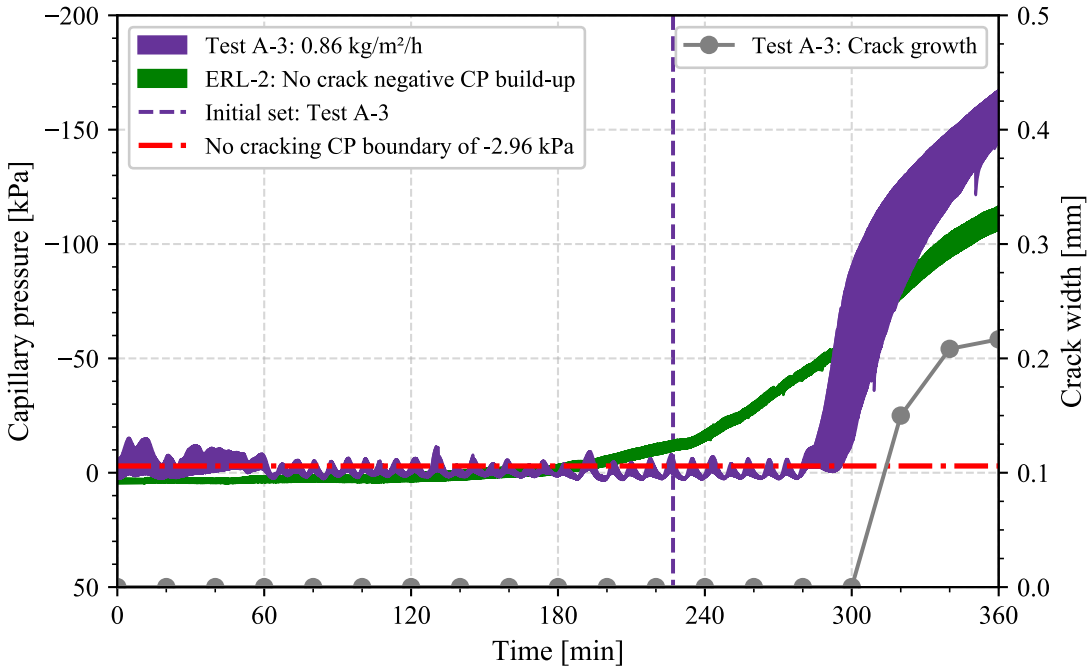

Figure 8-6: Negative CP build-up envelope and crack width for Model Test A-3

The findings during each of the tests in Model Test A are summarised in Table 8-4. The table presents the drying time and CP before and at the onset of cracking. The calculated critical pressure limit and the average crack width found during each test are also presented in the table. The findings show that as the evaporation rate increased, the drying time decreased for the model, which is in agreement with the findings from Kwak and Ha (2006). Kwak and Ha (2006) stated that when the bleeding remains constant, the evaporation rate is increased, resulting in the drying time occurring earlier in time.

When comparing the three Model Test A graphs with each other, all of the model tests followed more or less the same CP curve when no water was added, and only the Model Test A-3: 0.86 kg/m^2/h cracked. This occurrence might be because of an earlier event. The figure shows that at the start of the Model Test A-3, the CP passed the no cracking CP boundary, and water had to be added to reduce the negative CP in the concrete. The sudden negative CP build-up in the concrete could have damaged the concrete from the start of the test.

The graphs also show that after 280 minutes, the negative CP build-up in the concrete had similar rates. A plausible reason for the negative CP build-up being the same in all the Model Test A tests after 280 minutes is that at that point, the negative CP build-up was no longer dependent on the evaporation rate and only dependent on the hydration of the cement. Indicating that PS cracking is not dependent on the CP in the concrete after a certain point in time. Another reason might be that the concrete surface and the inner concrete in which the

sensors were placed are now at different stages. An alternative possibility is that the negative CP build-up due to the cement hydration in the concrete is greater than that of the build-up caused by the evaporation rate.

Table 8-4: Model results found for Model Test A

Conditions	Test A-1	Test A-2	Test A-3
CP drying time for the model, min	95.3	49.3	14.0
CP before the cracks, kPa	-	-	-186
CP at the onset of cracks, kPa	-	-	-240
Critical pressure limit, kPa	-5.08	-3.71	-2.96
Average crack width after 6 hours, mm	0	0	0.22

The findings confirmed that by using the No Cracking CP Boundary Model, PS cracking can be prevented, by maintaining the negative CP build-up below the no cracking CP boundary.

8.3.4 Volumetric Moisture Content

The VMC for three tests of Model Test A is shown in Figure 8-7. The graph illustrates the effect of the different evaporation rates on VMC envelopes of the concrete. The large envelope of Test A-2: 0.52 kg/m^2/h is due to two of the three sensors not being placed correctly in the concrete. The most representable sensor measurements between the two faulty sensors were used in the figure.

The figure shows that as water was added when the no cracking CP boundary was reached, the VMC ceased to decrease. After ceasing the addition of water, the VMC decreased with the ongoing evaporation as expected.

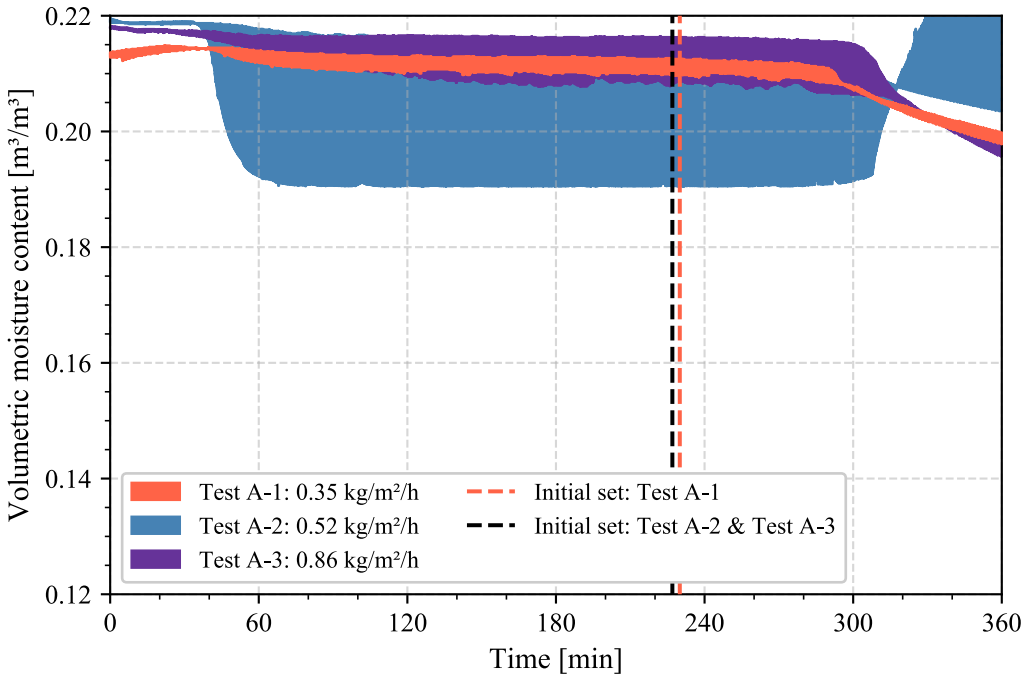

Figure 8-7: VMC envelopes of the concrete in Model Test A

8.3.5 Concrete Temperature

The average internal and surface temperature for Model Test A is shown in Figure 8-8. The internal and surface temperatures are represented with the solid and transparent colours for each evaporation rate.

The graph shows that each time water was added to the surface of the concrete, the surface temperature of the concrete was reduced and then suddenly increased again. After ceasing the addition of water at 280 minutes, the surface temperature increased significantly.

The effect of adding water to the surface of the concrete could only be noticed on the internal temperature at the high evaporation rate at Test A-3: 0.86 kg/m^2/h. The reason for this can be that more water had to be added (2.63 kg/m^2) to the concrete exposed to a higher evaporation rate in Test A-3.

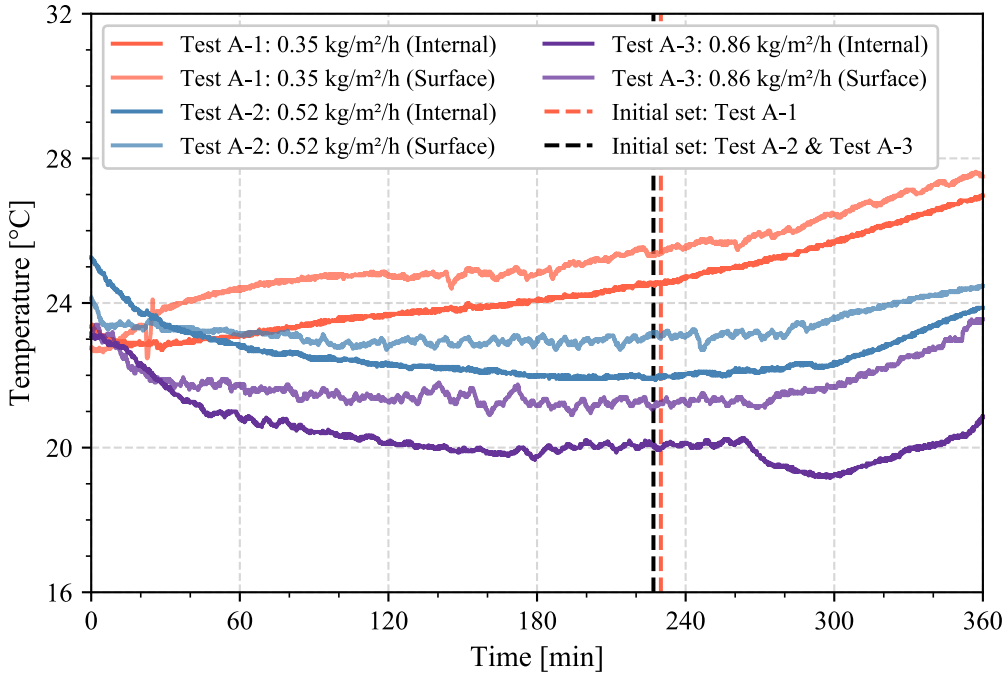

Figure 8-8: Internal and Surface Temperature for Model Test A

8.4 MODEL TEST B: SELF-COMPACTING CONCRETE

This section presents and discusses the findings of the No Cracking CP Boundary Model tested with the SCC mixture. The following concrete properties are presented: climatic conditions, evaporation rate, CP, PS cracking, and concrete temperature found during the model test.

8.4.1 Climatic Conditions

The climatic conditions of the SCC model tests are shown in Table 8-5. The SD for each climatic condition is also shown in brackets in the table. The two evaporation rates used in the SCC model tests are referred to as Test B-1 and Test B-2 throughout the study.

Table 8-5: Climatic conditions for Model Test B with SD in brackets

Conditions	Test B-1	Test B-2
Relative humidity, %	29.6 (4.56)	19.5 (2.86)
Concrete surface temperature, °C	25.3 (1.77)	22.4 (1.07)
Air temperature, °C	32.1 (0.988)	29.8 (0.893)
Wind velocity, km/h	7.24 (0.327)	15.9 (0.355)

8.4.2 Evaporation Rates

Figure 8-9 presents the cumulative evaporation rate obtained from evaporation rates in Test B-1 and Test B-2. The actual evaporation is represented by solid lines, whereas the dashed dot lines are the evaporation when water was added as the no cracking CP boundary was reached. Lastly, the estimated evaporation is illustrated with a fine dotted line.

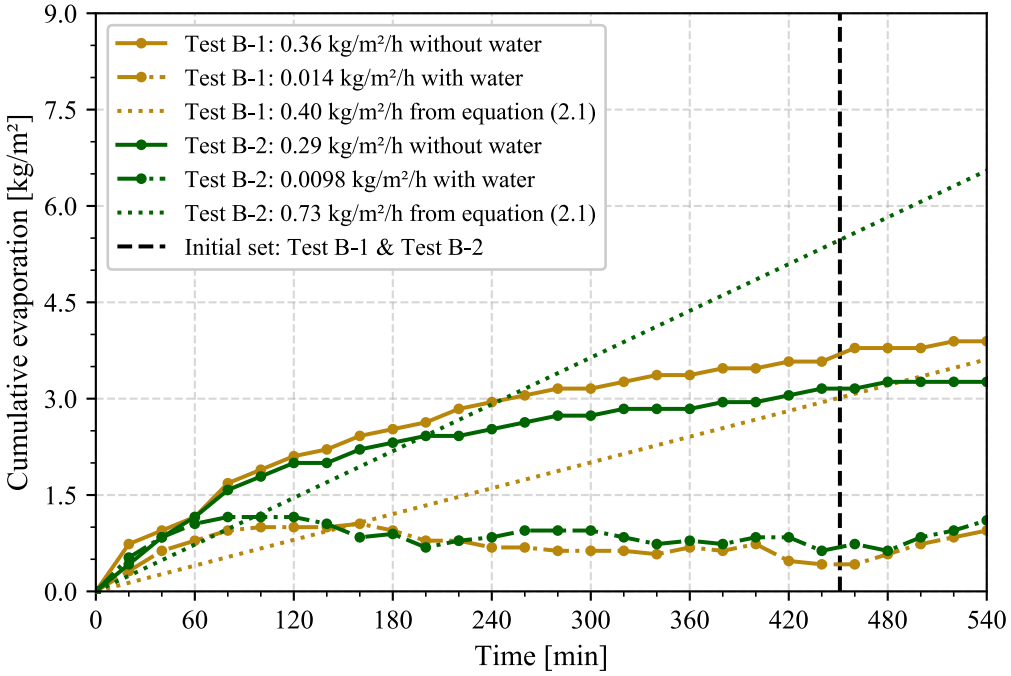

Figure 8-9: Cumulative evaporation during the Model Test B

The total amount of evaporation, total measured evaporation with the additions of water and the total amount of water added are summarised in Table 8-6. In the graph and in Table 8-6, the cumulative evaporation for Model Tests B-1 and B-2 obtained similar evaporation rates. The low evaporation rate of the actual measurement in Test B is possibly due to when water was added to the surface of the PS cracking specimens; some of the water may have fallen on the evaporation specimens. Therefore, it was decided that equation (2.1) would be used to estimate the evaporation rate to have an approximate of what the evaporation rate should be. An evaporation rate of 0.73 kg/m^2/h was estimated; therefore, it was decided that an evaporation rate of >0.70 kg/m^2/h would be used as the evaporation rate in Test B-2.

The addition of water to the concrete surface significantly reduced the cumulative amount of evaporation in Test B-1 and Test B-2. Test B-1 was reduced by -70 %, and Test B-2 was reduced by -98.6 %.

Table 8-6: Total evaporation and water addition for Model Test B

Conditions	Test B-1	Test B-2
Actual total evaporation, kg/m^2	3.23	2.65 (>6.30)
Total measured evaporation with the addition of water, kg/m^2	0.13	0.088
Total water added, kg/m^2	2.50	3.64

8.4.3 Capillary Pressure and Plastic Shrinkage Cracking

The negative CP build-up envelopes and PS crack width for the SCC in Test B-1 and Test B-2 are shown in Figure 8-10 and Figure 8-11, respectively. The figure shows the CP and crack width measurements over time. The individual CP measurements and final PS cracks of each Model Test are shown in Appendix D. The figures also show when the concrete reached the initial setting time of 511 minutes in each test. It should be noted that the SCC surface was only sprayed with water for up to 480 minutes to observe the negative CP behaviour of the concrete after the added water.

The figures show that as the evaporation rate increased in Test B-1: 0.36 kg/m^2/h to Test B-2: >0.70 kg/m^2/h, the applied no cracking CP boundary reduced from -57.3 to -53.4 kPa. When comparing the calculated critical pressure limits from Model Test B to the critical CP between -78.7 and -79.4 kPa founds for ERS-2: 0.38 kg/m^2/h from Table 7-4. It can be seen that the calculated critical pressure limits are significantly lower. Confirming that the empirical model performs correctly, as the evaporation rate increases, a low critical pressure limit is calculated at which the boundaries will have to be applied. The figures show that by adding water to the concrete surface, the negative CP build-up was effectively delayed by applying the boundary to obtain approximately the same pressure-time area as the no crack negative CP build-up curve.

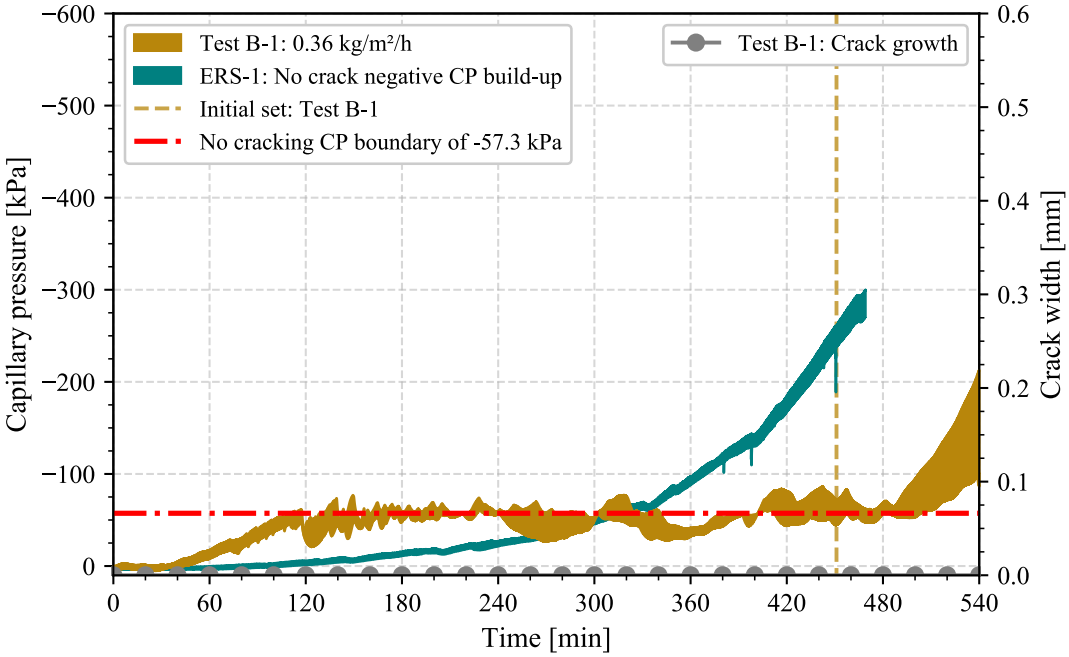

Figure 8-10: Negative CP build-up envelope and crack width for Model Test B-1

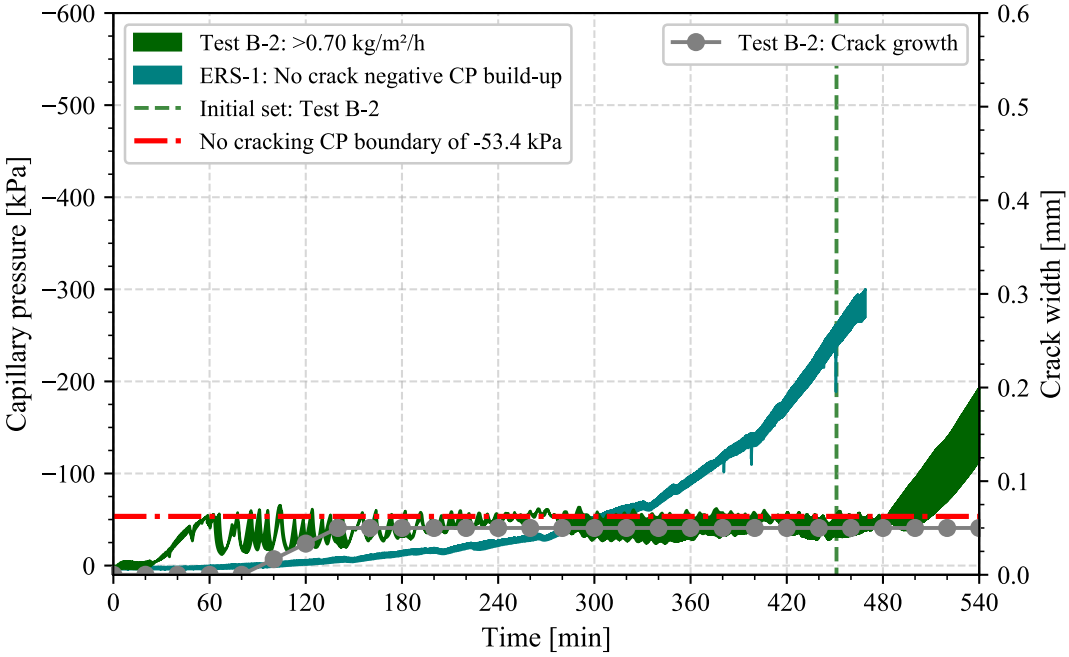

Figure 8-11: Negative CP build-up envelope and crack width for Model Test B-2

No PS cracks formed on the concrete surface in Test B-1: 0.36 kg/m^2/h when the negative CP build-up was maintained below the no cracking CP boundary. Figure 8-11 shows that PS cracks formed in the concrete even after applying the no cracking CP boundary. During Test B-2:

>0.70 kg/m^2/h, only one of the three specimens cracked on one side. The crack can be seen in Appendix D (Figure D.4). However, Figure 8-11 shows that relieving the negative CP build-up when the no cracking CP boundary was reached helped to prevent further cracks growth in the concrete. Therefore, confirming that the No Crack CP Boundary Model helps to prevent and reduce PS cracking in SCC.

Another important aspect to notice in the figure is that after the water was added to the surface of the concrete, the CP in Test B-1: 0.36 kg/m^2/h and Test B-2: >0.70 kg/m^2/h had a similar negative CP build-up rate between 480 and 540 minutes. A plausible reason for this occurrence is that after the initial set, that negative CP build-up is no longer dependent on the evaporation rate and more dependent on the hydration of the cement, as previously mentioned in Model Test A. Implying that before initial set, the negative CP build-up is dependent on the evaporation rate and after initial set, the build-up is caused by the hydration in the cement.

When comparing the calculated critical pressure limit of Model Tests, A and B. Model Test A had a critical pressure limit range between -5.08 to -2.96 kPa. While Model Test B had a critical pressure limit range between -57.3 to -53.4 kPa. This shows that the empirical model calculates the critical pressure limit relevant concrete mixture and evaporation rate.

The CP drying times for the SCC are shown in Table 8-7. The results show that the drying time of Test B-2 occurred 11 minutes earlier than Test B-1, which is as expected. Kwak and Ha (2006) stated that the drying time would occur earlier in time when the bleeding remains constant and the evaporation rate increases. The literature and findings are, therefore, in agreement.

Table 8-7: Model results found for Model Test B

Conditions	Test B-1	Test B-2
CP drying time for the model, min	37	26

The model helped to prevent and reduce PS cracks in the SCC by applying the no cracking CP boundary.

8.4.4 Concrete Temperature

Figure 8-12 illustrates how the average internal and surface temperature of the SCC were affected by the two evaporation rates in Model Test B. The internal and surface temperature of Test B-1: 0.36 kg/m^2/h were not affected when water was added to the surface of the concrete. A similar phenomenon was noticed with the concrete temperature in Test A-1: 0.35 kg/m^2/h.

Test B-2: >0.70 kg/m^2/h shows that the addition of water influences the internal and surface temperature of the SCC. The internal temperature was reduced and maintained between 20 and 22 °C, and the surface temperature between 21 and 23 °C. When the addition ceased, the concrete temperature increased significantly.

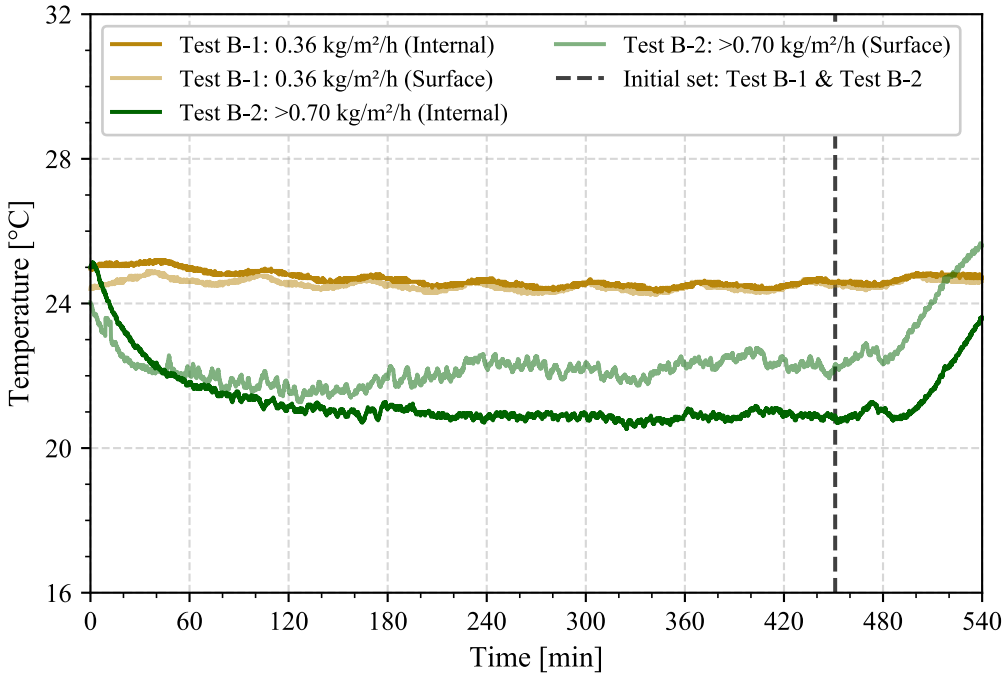

Figure 8-12: Internal and Surface Temperature for Model Test B

8.5 OBSERVATIONS, LIMITATIONS AND CALIBRATION

The following observations and limitations found during the model verification phase and the required calibrations are discussed in this section.

8.5.1 Observations

- The model uses the rate of the negative CP build-up of the concrete. Therefore, a sudden change in the negative CP build-up will affect the no cracking CP boundary for the concrete.

8.5.2 Limitations

- The empirical model is limited to the time between the drying time and the initial set time of the concrete and the area of the no crack negative CP build-up curve.
- The model can currently only be used for the low bleed concrete at a temperature range of 29 - 34 °C and for the SCC at a temperature range of 29 - 32 °C.

- Early cavitation of the tensiometers. When the sensor cavitate early, the negative CP build-up will not intersect the initial setting time, making it difficult to calculate the pressure-time area between the drying time and initial set.

8.5.3 Calibration

- The results of Model Test A showed that PS cracking occurred at high evaporation rates when the addition of water was ceased after 280 minutes. Therefore, it is recommended that water be added to maintain negative CP build-up below the no cracking CP boundary throughout the test (for the duration that the concrete is exposed to an evaporation rate) or up until the concrete has reached the final setting time.
- In the findings for Model Test B, it was seen that a PS crack occurred even after the boundary was applied to the concrete. Meaning that the no crack negative CP build-up area was the boundary for PS cracking; any negative CP build-up greater than the boundary area would result in cracking. Therefore, the model could be calibrated accordingly to effectively help prevent PS cracking by applying a safety factor of 1.5 to the no crack negative CP build-up curve area, which would calculate a lower critical pressure limit.
- The model can be further improved by determining the true no cracking negative CP build-up curve for the concrete mix as the current no cracking negative CP build-up curves might have been too conservative.

8.6 CONCLUDING SUMMARY

The performance of the No Cracking CP Boundary Model was tested in this chapter with previous results and in real-time with low bleed concrete and SCC. The following conclusions were drawn from the findings:

- A strong linear relationship was found between the evaporation rate and the negative CP build-up area and the average crack width, the negative CP build-up area and the no cracking CP boundary. Therefore, the model could be simplified for on-site usage by utilising these relationships.
- The model was shown to help prevent PS cracking in fresh concrete while the negative CP build-up was maintained below the no cracking CP boundary in Model Test A. Model Test A showed that when the negative CP was left to build up after the initial set, PS cracking still occurred at a high evaporation rate. Therefore, the model was calibrated, maintaining the negative CP build-up below the no cracking CP boundary for the duration that the concrete is exposed to an evaporation rate.

- The findings from Model Test B showed that the model effectively helped prevent PS cracking in Test B-1. In Test B-2, one of the three specimens cracked slightly and maintaining the negative CP build-up below the no cracking CP boundary prevented further crack growth. Due to the cracking of one specimen, the model was calibrated by adding a safety factor of 1.5 (or greater) to the no crack negative CP build-up area; a lower boundary would be applied, reducing the risk of PS cracking.
- The finding of Model Test A at the different evaporation rates showed that after maintaining the negative CP build-up below the no cracking CP boundary, the negative CP build-up rate was similar. The findings suggest that the negative CP build-up is no longer driven by the evaporation rate but by the cement hydration after the initial set. The same phenomenon was noticed with Model Test B.
- The model verification findings showed a significant difference in the critical pressure limits calculated for the low bleed concrete and SCC. The model calculated critical pressure limits relevant to the concrete mixture and evaporation rate. It was also found that the critical pressure limit in both Model Tests was calculated below the range of critical CP where cracking occurred (in the previous phase).

Therefore, the findings proved that the No Cracking CP Boundary Model could aid in preventing PS cracking in fresh concrete with the required calibrations.

9 CONCLUSIONS AND RECOMMENDATIONS

9.1 CONCLUSIONS

The Plastic Shrinkage (PS) cracking characteristics of concrete mixtures were studied, focusing on the Capillary Pressure (CP) mechanism in fresh concrete. The study aimed to develop a model that uses live in-situ CP measurements in fresh concrete to control the CP build-up to prevent plastic shrinkage cracking at any evaporation rate. The following conclusions can be drawn based on the finding obtained throughout the study:

- The PS and PS cracking characteristics of the low bleed and Self-Compacting Concrete (SCC) showed that as the evaporation rate increased: the CP build-up rate, PS crack width, concrete temperature, and the plastic settlement would increase.
- A negative CP build-up curve exists for both concrete mixtures where no PS cracking will occur. It was seen that before the initial set, the negative CP build-up was dependent on the evaporation rate, and after the initial set, the CP was more dependent on the hydration of the cement in the concrete.
- The Model Tests findings showed that the No Cracking CP Model calculated a critical pressure limit relevant to the concrete mixture and evaporation rate. In addition, it was seen that the calculated critical pressure limits were lower than the range of critical CPs where cracking occurred.
- Tensiometers measured high negative CP values in concrete before cavitation. The tensiometers proved to be very responsive to the slightest change in pressure and were helpful in monitoring the negative CP behaviour in the low bleed concrete and SCC. The tensiometers were used to monitor the negative CP when the empirical model was tested, which prevented PS cracking in concrete.
- An empirical model known as the No Cracking CP Boundary Model was proposed. The model helped to prevent and reduce PS cracking in a low bleed concrete and a SCC mixture. After calibrating the model by adding the safety factor and maintaining the boundary for the duration of the concrete exposed to an evaporation rate, the model can effectively aid in preventing PS cracking in fresh concrete.

Therefore, the conclusions drawn confirmed the two hypotheses of the study:

1. A negative CP build-up in concrete over time does exist, where no PS cracks will form.

2. PS cracks can be prevented by maintaining a similar or lower pressure-time area as the negative CP build-up where no crack will form.

9.2 RECOMMENDATIONS

Some pitfalls were found during the study, and the following advice is recommended for future studies:

- The modified ASTM C1579 mould should be verified whether it is representable for evaluating the cracking risk of real concrete members such as concrete pavements, bridge decks and floor slabs.
- The No Cracking CP Boundary Model can be improved by coding a program to store the CP measurement for the required time steps. The program can provide a more precise estimate of when the no cracking CP boundary should be applied.
- Testing whether adding curing compounds to fresh concrete when the model locates the critical pressure limit will help prevent PS cracking.
- The model has been validated with low bleed concrete and SCC. In contrast, more research is needed for this model with other concrete mixtures and with different specimen heights.
- Testing the model with two identical specimens in the same evaporation conditions and only apply the no cracking CP boundary on one of the specimens. This can help establish the appropriateness of applying the no cracking CP boundary to concrete.
- Investigating how the No Cracking CP Model works fundamentally.
- The model can be refined by investigating how different cement types, cement content and w/c ratios in the concrete affect the model.
- Investigating the behaviour of the negative CP build-up after wetting the concrete at the boundary for a certain amount of time.
- Lastly, a question for future work. Does applying the no cracking CP boundary to a negative CP build-up causes the radii of the menisci to form at the same rate as that of the no crack CP build-up?

10 REFERENCES

ACI. 1999. *Hot weather concreting, ACI Manual of Concrete Practice*. Detroit: American Concrete Institute, pp 305.

Afrisam. 2021. Rapid Hard Cement - AfriSam. [online] Available at: <https://www.afrisam.co.za/products-services/cement/rapid-hard-cement> [Accessed 21 June 2021].

Aggarwal, P. Aggarwal, Y. and Gupta, S. 2008. Self-Compacting Concrete - Procedure for Mix Design. *Leonardo Electronic Journal of Practices and Technologies*, 12, pp 15-24.

ASTM. 2013. *C 1579 - Standard Test Method for Evaluating Plastic Shrinkage Cracking of Restrained Fiber Reinforced Concrete*. ASTM International. West Conshohocken.

ASTM. 2016. *C 403/C403M - Standard Test Methods for Time of Setting pf Concrete Mixtures by Penetration Resistance*. ASTM International. West Conshohocken.

Boshoff, W. and Combrinck, R. 2013. Modelling the severity of plastic shrinkage cracking in concrete. *Cement and Concrete Research*, 48, pp 34-39.

BS EN. 2005. 480-4 – *Admixtures for concrete, mortar and grout – Test methods – Part 4: Determination of bleeding of concrete*. BSI. Brussels.

Cheng, G. 1994. Early Age Behavior of Portland Cement Paste. *ACI Materials Journal*, 91, 1, pp 13-25.

Combrinck, R. 2011. *Plastic Shrinkage Cracking In Conventional And Low Volume Fibre Reinforced Concrete.* MSc Dissertation. University of Stellenbosch.

Combrinck, R. 2016. *Cracking of Plastic Concrete in Slab-Like Elements*. PhD Thesis. University of Stellenbosch.

Combrinck, R. and Boshoff, W. 2013. Typical plastic shrinkage cracking behaviour of concrete. *Magazine of Concrete Research*, 65, 8, pp.486-493.

Combrinck, R. Kayondo, M. le Roux, B. de Villiers, W. and Boshoff, W. 2019. Effect of various liquid admixtures on cracking of plastic concrete. *Construction and Building Materials*, 202, pp 139-153.

Combrinck, R. Steyl, L. and Boshoff, W. 2018. Influence of concrete depth and surface finishing on the cracking of plastic concrete. *Construction and Building Materials*, 175, pp 621-628.

Combrinck, R. Steyl, L. and Boshoff, W. 2018. Interaction between settlement and shrinkage cracking in plastic concrete. *Construction and Building Materials*, 185, pp 1-11.

Dao, V. Dux, P. Morris, P. and O'Moore, L. 2010. Plastic Shrinkage Cracking of Concrete. *Australian Journal of Structural Engineering*, 10, 3, pp 207-214.

Domone, P. and Illston, J. 2010. *Construction Materials: Their nature and behaviour*. 4th ed. Taylor & Francis Ltd. London.

Ghoddousi, P. Abbasi, A. Shahrokhinasab, E. and Abedin, M. 2019. Prediction of Plastic Shrinkage Cracking of Self-Compacting Concrete. *Advances in Civil Engineering*, 2019, pp 1-7.

Ghourchian, S. Butler, M. Krüger, M. and Mechtcherine, V. 2021. Modelling the development of capillary pressure in freshly 3D-printed concrete elements. *Cement and Concrete Research*, 145, pp 106457.

Holt, E. and Leivo, M. 2004. Cracking risks associated with early age shrinkage. *Cement and Concrete Composites*, 26, 5, pp 521-530.

Huang, L. Hua, J. Kang, M. Zhou, F. and Luo, Q. 2019. Capillary tension theory for predicting shrinkage of concrete restrained by reinforcement bar in early age. *Construction and Building Materials*, 210, pp 63-70.

Jacobsz, S. 2021. *Tensiometers – Personal correspondence*.

Kayondo, M. Combrinck, R. and Boshoff, W. 2019. *A Review of Plastic Concrete Bleeding Measurement Techniques and the Proposed use of Super Absorbent Polymers.*

Kayondo, M. Combrinck, R. and Boshoff, W. 2019. State-of-the-art review on plastic cracking of concrete. *Construction and Building Materials*, 225, pp 886-899.

Klieger, P. 1955. Effect of Atmospheric Conditions During the Bleeding Period and Time of Finishing on the Scale Resistance of Concrete. *ACI Journal Proceedings*, 52, 3, pp 309-326.

Knappett, J. and Craig, R. 2012. *Craig's soil mechanics*. 8th ed. Spon Press. New York, pp 22-23.

Kwak, H. and Ha, S. 2006 Plastic shrinkage cracking in concrete slabs. Part I: A numerical model. *Magazine of Concrete Research*, 58, 8, pp 505–516.

Kwak, H. and Ha, S. 2006. Plastic shrinkage cracking in concrete slabs. Part II: numerical experiment and prediction of occurrence. *Magazine of Concrete Research*, 58, 8, pp 517-532.

Lamond, J. and Pielert, J. 2006. *Significance of Tests and Properties of Concrete and Concrete-Making Materials. STP 169D.* ASTM International.

Leonovich, S. 2018. Modeling of Capillary Shrinkage and Cracking in Early-Age Concrete. *Science & Technique*, 17, 4, pp 265-277.

le Roux, P. F. 2020. *The Measurement of Soil-Water Retention Curves using the Tensiometer Method.* MEng Dissertation. University of Pretoria.

Lourenço, S. Gallipoli, D. Toll, D. and Evans, F. 2006. Development of a Commercial Tensiometer for Triaxial Testing of Unsaturated Soils. In: *Fourth International Conference on Unsaturated Soils*. ASCE. Reston, pp 1875-1886.

Matalkah, F. Jaradat, Y. and Soroushian, P. 2019 Plastic shrinkage cracking and bleeding of concrete prepared with alkali activated cement, *Heliyon*, 5, 4, pp e01514.

Mehta, N. and Monteiro, P. 2001. *Concrete: Microstructure, Properties and Materials*. 2nd ed. McGraw-Hill. New York.

Mehta, N. and Monteiro, P. 2006. *Concrete: Microstructure, Properties and Materials*. 3rd ed. McGraw-Hill. New York.

METER. 2021. TEROS 10 | Simple Soil Moisture Sensing | METER. [online] Available at: <https://www.metergroup.com/environment/products/teros-10/> [Accessed 29 July 2021].

Mora-Ruacho, J. Gettu, R. and Aguado, A. 2009. Influence of shrinkage-reducing admixtures on the reduction of plastic shrinkage cracking in concrete. *Cement and Concrete Research*, 39, 3, pp 141-146.

Neville, A. 1995. *Properties of concrete*. 4th ed. Longman Group Limited. Harlow.

Neville, A. 2012. *Properties of concrete*. 5th ed. Pearson Education. Harlow.

Otieno, M. Alexander, M. and Beushausen, H. 2010. Corrosion in cracked and uncracked concrete – influence of crack width, concrete quality and crack reopening. *Magazine of Concrete Research*, 62, 6, pp 393-404.

Qi, C., 2003. *Quantitative assessment of plastic shrinkage cracking and its impact on the corrosion of steel reinforcement.* PhD Thesis. Purdue University.

Qi, C. Weiss, J. and Olek, J. 2003. Characterization of plastic shrinkage cracking in fiber reinforced concrete using image analysis and a modified Weibull function. *Materials and Structures*, 36, 6, pp 386-395.

Raviv, M. and Lieth, J. 2008. *Soilless Culture*. Amsterdam: Elsevier Science, pp 147-151.

SA, J. 2021. Atmos: SKYWATCH. [online] Shop.skywatch.ch. Available at: <https://shop.skywatch.ch/atmos-b6c102p12i1.html> [Accessed 29 May 2021].

SANS 50196-3. 2006. *Method of testing cement Part 3: Determination of setting times and soundness*. 2nd ed. SABS Standards Division. Pretoria.

SANS 1083. 2017. *Aggregates from natural sources - Aggregate for concrete*. 2.5th ed. SABS Standards Division. Pretoria.

Sayahi, F. Emborg, M. Hedlund, H. and Cwirzen, A. 2019. Plastic Shrinkage Cracking of Self-compacting Concrete: Influence of Capillary Pressure and Dormant Period. *Nordic Concrete Research*, 60, 1, pp 67-88.

Sayahi, F. Emborg, M. Hedlund, H. and Cwirzen, A. 2020. Effect of Admixtures on Mechanism of Plastic Shrinkage Cracking in Self-Compacting Concrete. *ACI Materials Journal*, 117, 5, pp 51-60.

Sayahi, F. Emborg, M. Hedlund, H. and Löfgren, L. 2016. Plastic shrinkage cracking in self-compacting concrete: a parametric study. In: *In Proceedings of International Rilem Conference on Materials, Systems and Structures in Civil Engineering*. Paris, France: Rilem Publications, pp 609–619.

Sayahi, F. Emborg, M. Hedlund, H. Cwirzen, A. and Stelmarczyk, M. 2021. The severity of plastic shrinkage cracking in concrete: a new model. Magazine of Concrete Research, 73, 6, pp 315-324.

Schmidt, M. and Slowik, V. 2009 Capillary shrinkage cracking and its prevention by controlled concrete curing, *Proceedings of the 2nd International RILEM Workshop on Concrete Durability and Service Life Planning – ConcreteLife'09*, 1, pp 8.

Schmidt, M. and Slowik, V. 2013. Capillary Pressure Controlled Curing in Pavement. *Proceedings of 2013 Airfield and Highway Pavement American Society of Civil Engineers*, pp 295-306.

Slowik, V. Hübner, T. Schmidt, M. and Villmann, B. 2009. Simulation of capillary shrinkage cracking in cement-like materials. *Cement and Concrete Composites*, 31, 7, pp 461-469.

Slowik, V. Schmidt, M. and Fritzsch, R. 2008. Capillary pressure in fresh cement-based materials and identification of the air entry value. *Cement and Concrete Composites*, 30, 7, pp 557-565.

Slowik, V. Schmidt, M. Kässler, D. and Eiserbeck, M. 2014. Capillary Pressure Monitoring in Plastic Concrete for Controlling Early-Age Shrinkage Cracking. *Transportation Research Record: Journal of the Transportation Research Board*, 2441, 1, pp 1-5.

Soutsos, M. and Domone, P. 2017. *Construction materials: their nature and behaviour*. 5th ed. CRC Press. Roca Raton.

Steyl, L. 2016. *Plastic Cracking of Concrete and the Effect of Depth.* MEng Dissertation. University of Stellenbosch.

TE Connectivity. 2021. MS54XX Miniature SMD Pressure Sensor. [online] Available at: <https://www.te.com/commerce/DocumentDelivery/DDEController?Action=showdoc&DocId=Data+Sheet%7FMS54XX%7FB3%7Fpdf%7FEnglish%7FENG_DS_MS54XX_B3.pdf%7FCAT-BLPS0028> [Accessed 13 July 2021].

Toll, D. Lourenço, S. and Mendes, J. 2013. Advances in suction measurements using high suction tensiometers. *Engineering Geology*, 165, pp 29-37.

Topçu, İ. and Elgün, V. 2004. Influence of concrete properties on bleeding and evaporation. *Cement and Concrete Research*, 34, 2, pp 275-281.

Turcry, P. and Loukili, A. 2006. Evaluation of Plastic Shrinkage Cracking of Self-Consolidating Concrete. *ACI Materials Journal*, 103, 4, pp 272-279.

Uno, P. 1998. Plastic Shrinkage Cracking and Evaporation Formulae. *ACI Materials Journal*, 95, 4, pp 365-375.

Van Dijk, J. and Boardman, V. R. 1971. Plastic Shrinkage Cracking of Concrete. Proceedings, *RILEM International Symposium on Concrete and Reinforced Concrete in Hot Countries*, pp 225-239.

Wittmann, F. 1976. On the action of capillary pressure in fresh concrete. *Cement and Concrete Research*, 6, 1, pp 49-56.

Zhu, W. Wei, J. Li, F. Zhang, T. Chen, Y. Hu, J. and Yu, Q. 2016. Understanding restraint effect of coarse aggregate on the drying shrinkage of self-compacting concrete. *Construction and Building Materials*, 114, pp.458-463.

APPENDIX A:

TENSIOMETERS AND VOLUMETRIC MOISTURE CONTENT SENSORS

A.1 TENSIOMETER CALIBRATION PROCEDURES

As mentioned, the tensiometers were calibrated using a data acquisition system (5.7), air-water interface (4) supplying the water pressure and a pressure gauge (3.1). The tensiometers were calibrated by applying water pressure to the tensiometers at 100 kPa intervals for 2 minutes up to 800 kPa. Tensiometers were then calibrated using the average millivolt per volt reading for each pressure reading.

Figure A.1 shows the calibration curve for the tensiometers on a pressure versus millivolt per volt axis. The calibration curve equation and R^2-value for each tensiometer are also shown in the figure.

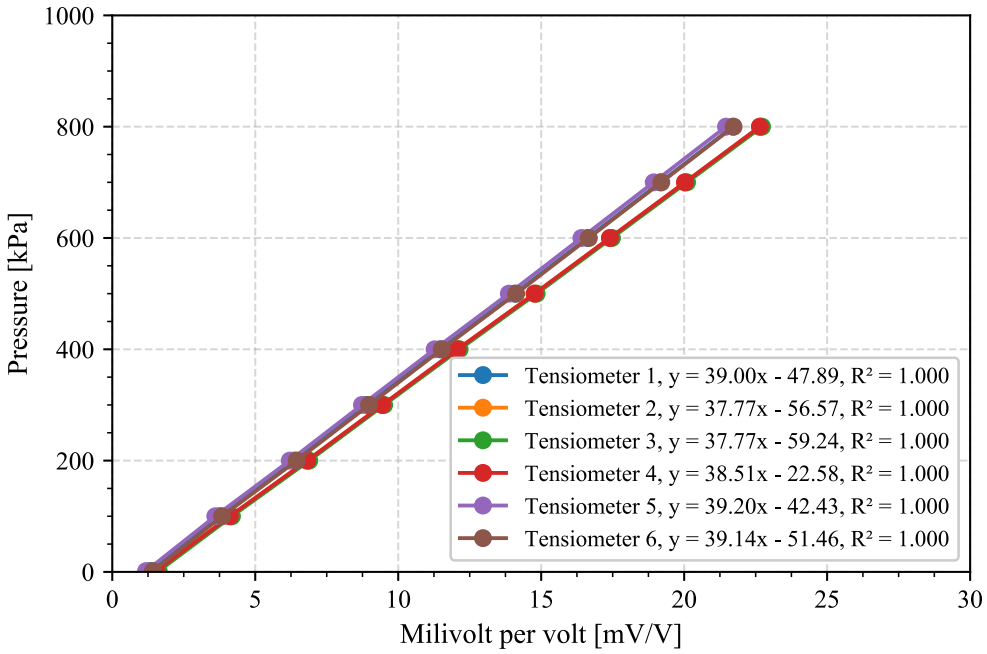

Figure A.1: The calibration curves for the tensiometers

A.2 VOLUMETRIC MOISTURE CONTENT SENSOR CALIBRATION PROCEDURES

The Volumetric Moisture Content (VMC) sensors were calibrated using the results for the first 3 hours of the measured evaporation from the concrete at the different evaporation rates. It was assumed that no cement hydration occurred within the first 3 hours after the cement and water made contact. In addition, it was also assumed that at the start of each test, the concrete was still fully saturated.

The VMC in the concrete was calculated using the measured water evaporation from the concrete at the different evaporation rates. Figure A.2 shows the calibration curves for each sensor on a VMC versus the millivolt axis. The figure also shows each VMC sensor's calibration curve equation and R^2-value.

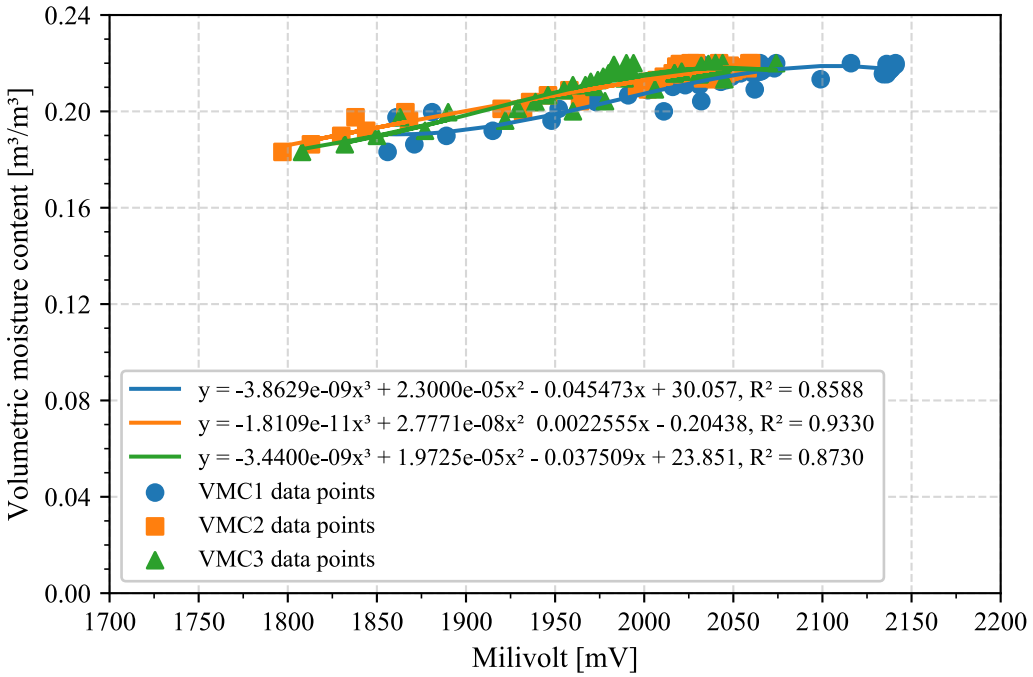

Figure A.2: The calibration curves for the VMC sensors

APPENDIX B:

CEMENT PROPERTIES

B.1 CEM I 52.5 R PROPERTIES

Table B.1: The requirements and performance of the cement (AfriSam, 2021)

Criteria	SANS 50197-1 requirements for a class 52.5 R	Typical performance
2-day strength, MPa	≥ 30	33
28-day strength, MPa	≥ 52.5	59
Initial setting time, min	≥ 60	191

Table B.2: The chemical compound in the cement (AfriSam, 2021)

Chemical compound [% by mass, ignited basis]	CEM I 52.5 R
Loss on ignition	2.98
SiO_2	20.79
P_2O_5	0.07
Al_2O_3	4.64
Fe_2O_3	2.69
CaO	65.05
MgO	1.73
K_2O	0.47
TiO_2	0.39
Na_2O	0.15
SO_3	2.99
Mn_2O_3	0.12

APPENDIX C:

LOW BLEED CONCRETE RESULTS

C.1 COMPRESSIVE STRENGTH

Table C.1: The low bleed concrete cube results

Samples	Air [g]	Water [g]	Compressive strength [MPa]
Cube 1	2481	1466	45.3
Cube 2	2466	1454	49.5
Cube 3	2472	1453	50.7
Cube 4	2472	1460	52.6
Concrete (average)	2473	1458	49.5

C.2 SETTING TIMES

Table C.2: Penetration Resistance Test Method Results

Samples	Initial setting time [min]	Final setting time [min]
Cube 1	285	442
Cube 2	281	417
Concrete mixture (Average)	283	430

Table C.3: Vicat Test Method Results

Samples	Initial setting time [min]	Final setting time [min]
Cone 1	225	345
Cone 2	235	360
Concrete mixture (Average)	230	353

C.3 PLASTIC SHRINKAGE CRACKING CHARACTERISATION PHASE: CAPILLARY PRESSURE AND FINAL PLASTIC SHRINKAGE CRACKS

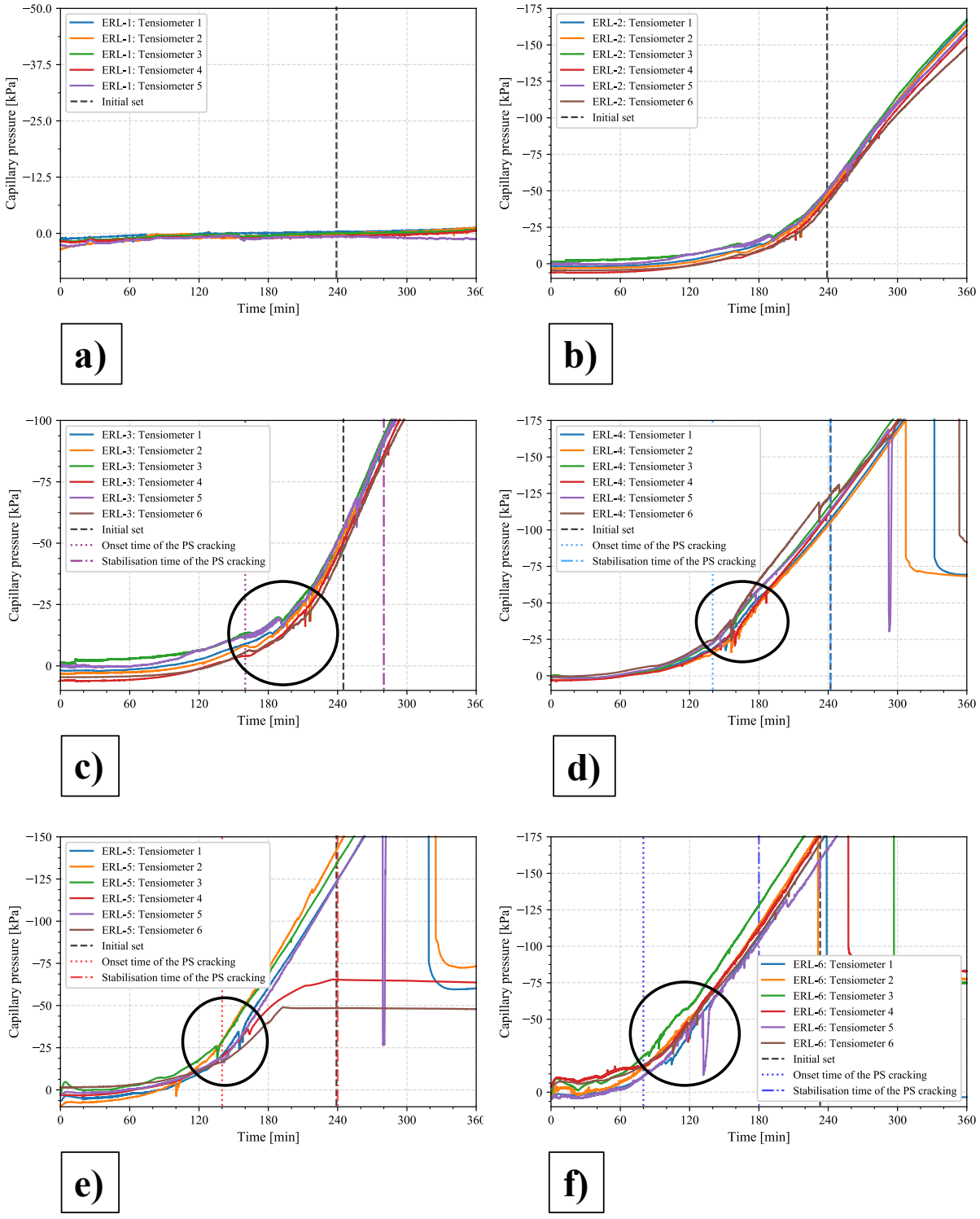

Figure C.1: Capillary pressure measurements for the six evaporation rates a) ERL-1: 0.06 kg/m^2/h, b) ERL-2: 0.15 kg/m^2/h, c) ERL-3: 0.31 kg/m^2/h, d) ERL-4: 0.62 kg/m^2/h, e) ERL-5: 0.64 kg/m^2/h and f) ERL-6: 0.84 kg/m^2/h

(With pressure drops marked with a black circle at the cracking onset)

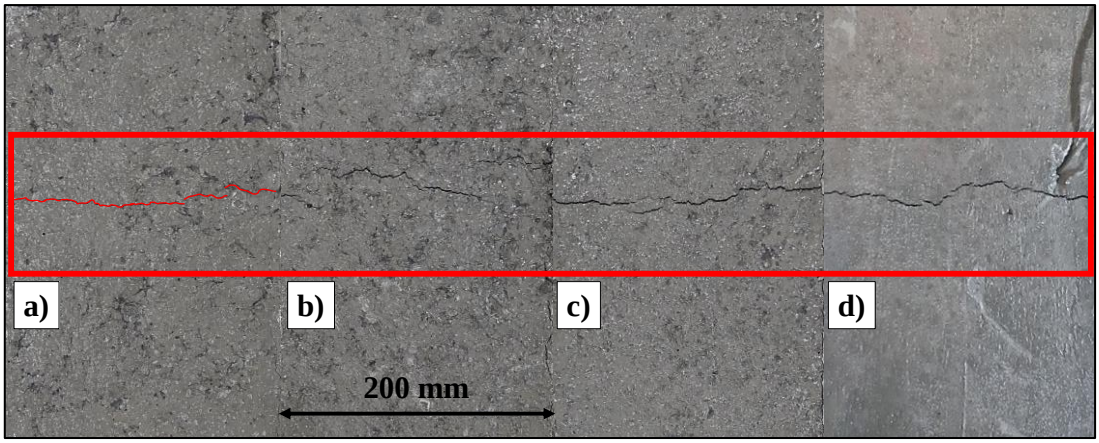

Figure C.2: Final crack width for a) ERL-3, b) ERL-4, c) ERL-5and d) ERL-6

(ERL-3 crack indicated in red)

C.4 MODEL TEST A: CAPILLARY PRESSURE AND FINAL PLASTIC SHRINKAGE CRACKS

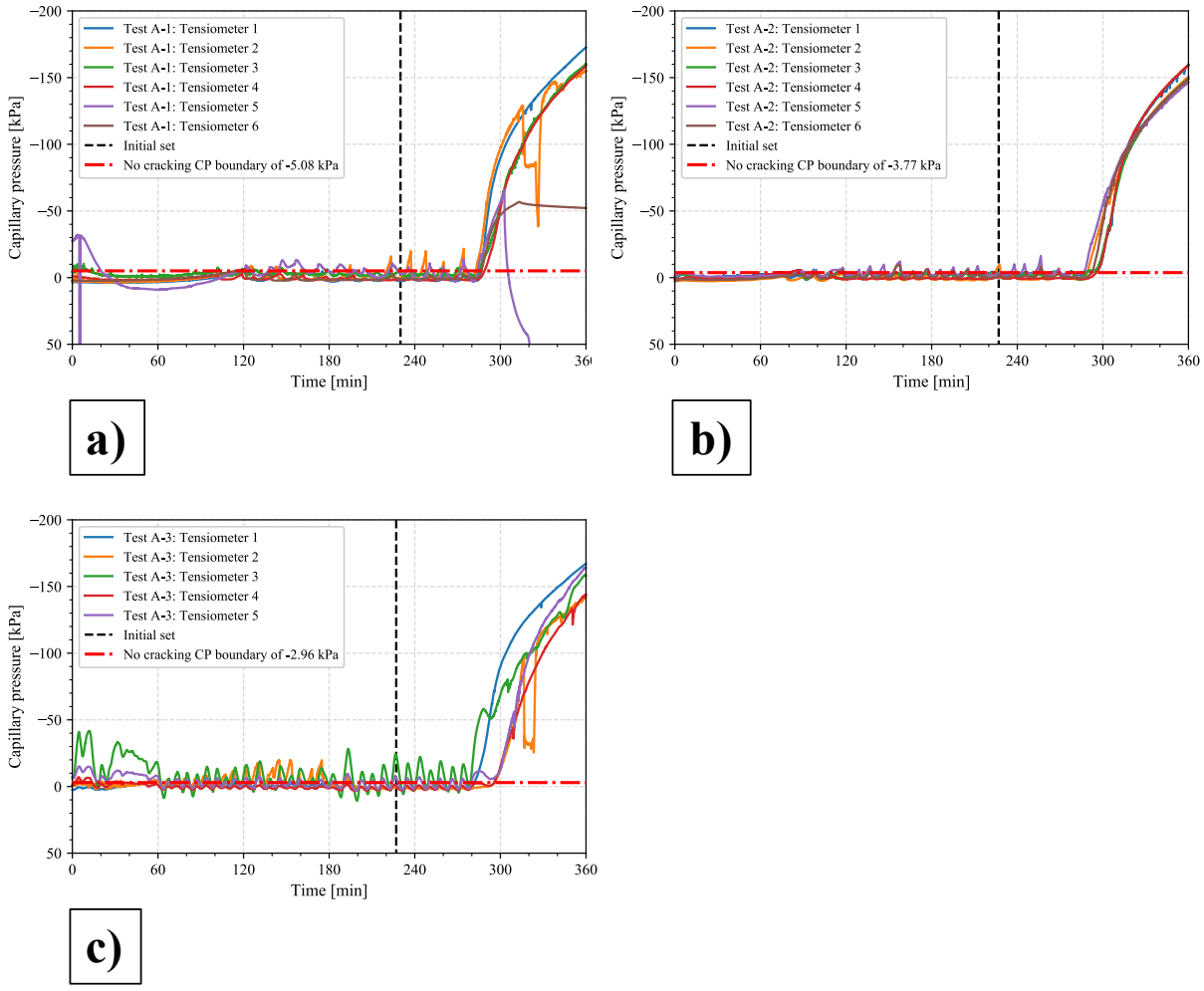

Figure C.3: Capillary pressure measurements at the three Model Tests

a) A-1: 0.35 kg/m^2/h, b) A-2: 0.52 kg/m^2/h and c) A-3: 0.86 kg/m^2/h

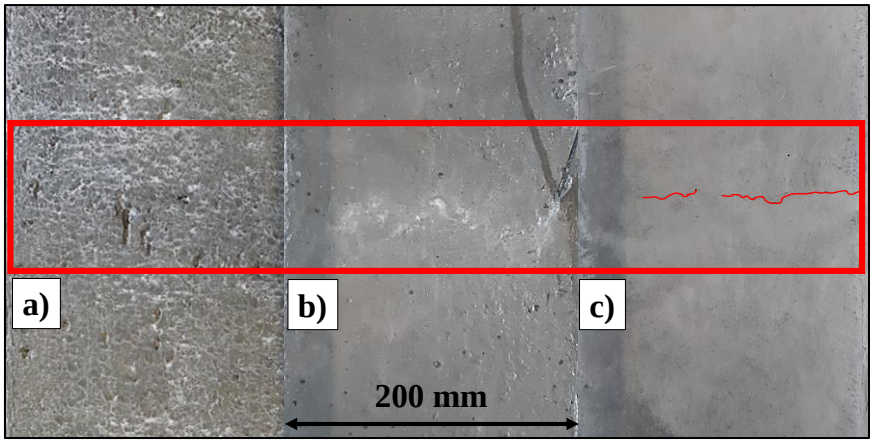

Figure C.4: Final crack width for Model Tests a) A-1, b) A-2 and c) A-3

(Only Model Test A-3 cracked, with the crack indicated in red)

APPENDIX D:

SELF-COMPACTING CONCRETE RESULTS

D.1 COMPRESSIVE STRENGTH

Table D.1: The self-compacting concrete cube results

Samples	Air [g]	Water [g]	Compressive strength [MPa]
Cube 1	2418	1431	101
Cube 2	2396	1403	101
Cube 3	2393	1400	99.1
Cube 4	2346	1374	102
Concrete (average)	2388	1402	101

D.2 SETTING TIMES

Table D.2: Penetration Resistance Test Method Results

Samples	Initial setting time [min]	Final setting time [min]
Cube 1	506	599
Cube 2	516	602
Concrete mixture (Average)	511	601

D.3 PLASTIC SHRINKAGE CRACKING CHARACTERISATION PHASE: CAPILLARY PRESSURE WITH FINAL PLASTIC SHRINKAGE CRACKS

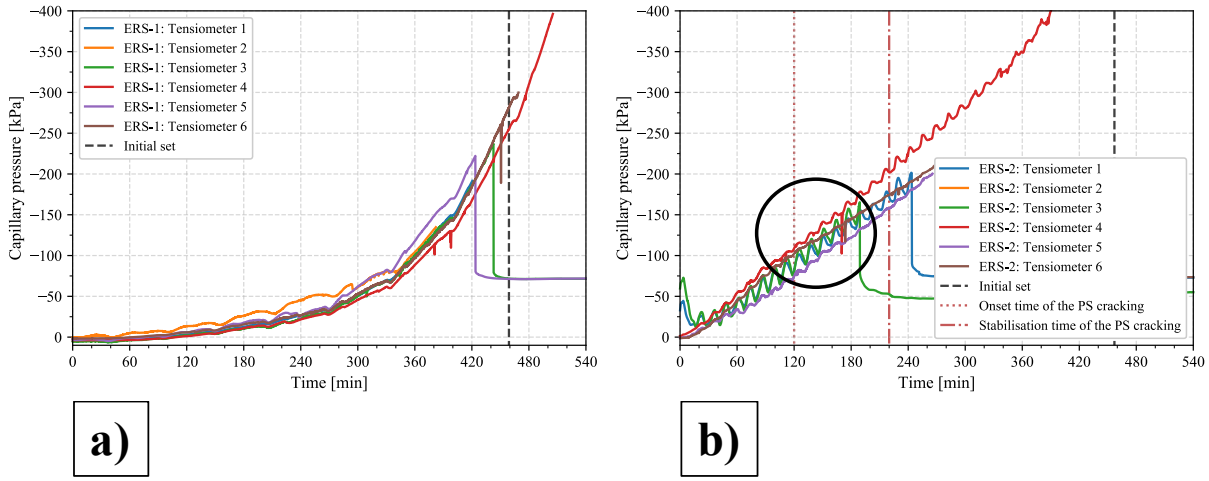

Figure D.1: Capillary pressure measurements at the two evaporation rates a) ERS-1: 0.11 kg/m^2/h and b) ERS-2: 0.38 kg/m^2/h

(With pressure drops marked with a black circle at the cracking onset)

Figure D.2: Final crack width for ERS-2, indicated in red

Table D. 3: PS cracking of the SCC at two evaporation rates

Conditions	ERS-1	ERS-2
Average onset time of PS cracks, min	-	147
Average PS crack after stabilisation time, min	-	213
Initial setting time during the test, min	459	457
Average PS crack width at onset, mm	-	0.2
Average PS crack width at stabilisation, mm	-	0.5

D.4 MODEL TEST B: CAPILLARY PRESSURE AND FINAL PLASTIC SHRINKAGE CRACKS

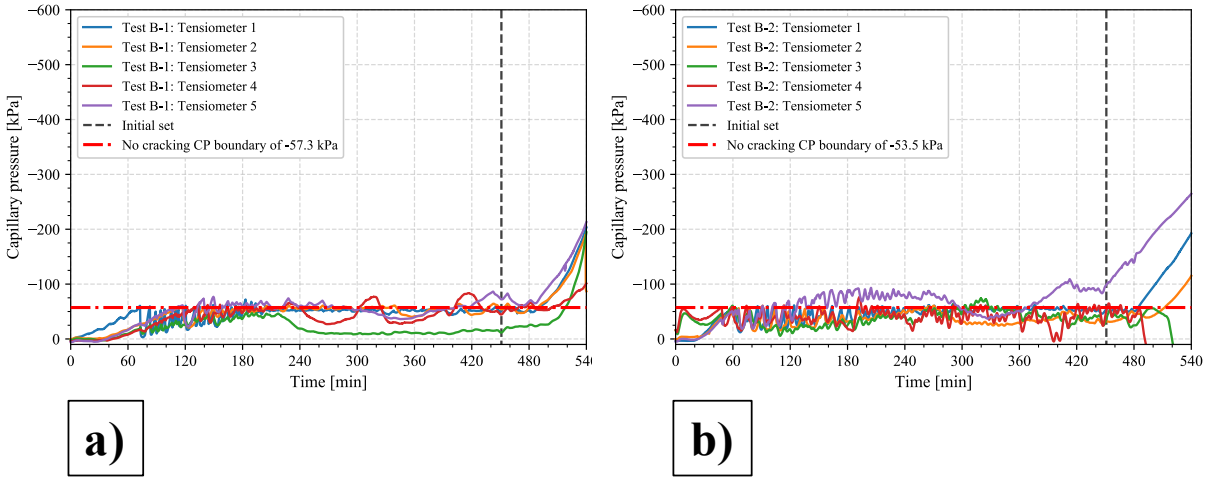

Figure D.3: Capillary pressure measurements at the two Model Tests

a) B-1: 0.36 kg/m^2/h and b) B-2: >0.70 kg/m^2/h

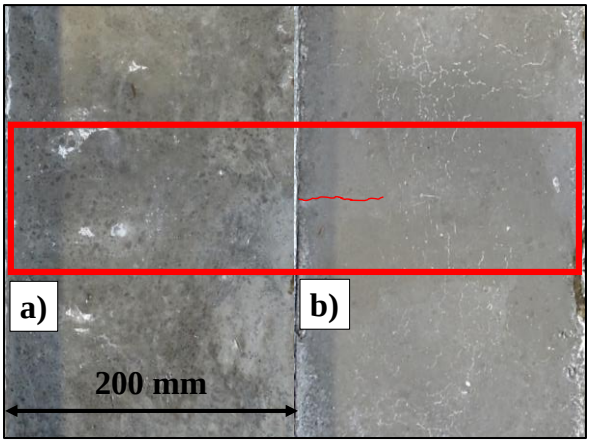

Figure D.4: Final crack width for Model Tests a) B-1 and b) B-2

(Only Model Test B-2 cracked, with the crack indicated in red)